Global and Planetary Change 210 (2022) 103717

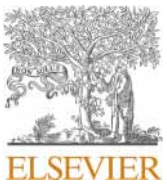

Contents lists available at ScienceDirect

Global and Planetary Change

journal homepage: www.elsevier.com/locate/gloplacha

Cyclic sediment deposition by orbital forcing in the Miocene wetland of western Amazonia? New insights from a multidisciplinary approach

Carina Hoorn [a,*], Tyler Kukla [b], Giovanni Bogotá-Angel [c], Els van Soelen [d], Catalina González-Arango [e], Frank P. Wesselingh [f,g], Hubert Vonhof [h], Pedro Val [i], Gaspar Morcote-Rios [j], Martin Roddaz [k], Elton Luiz Dantas [l], Roberto Ventura Santos [l], Jaap S. Sinninghe Damsté [d,g], Jung-Hyun Kim [m], Robert J. Morley [n,o,*]

[a] Institute for Biodiversity and Ecosystem Dynamics, University of Amsterdam, 1098 XH Amsterdam, the Netherlands
[b] Department of Geological Sciences, Stanford University, Stanford, CA 94305, United States of America
[c] Facultad del Medio Ambiente y Recursos Naturales, Universidad Distrital Francisco José Caldas, Bogotá D.C., Colombia
[d] NIOZ Royal Netherlands Institute for Sea Research, Department of Marine Microbiology and Biogeochemistry, PO Box 59, 1790 AB Den Burg, Texel, the Netherlands
[e] Departamento de Ciencias Biológicas, Universidad de los Andes, Bogotá D.C., Colombia
[f] Naturalis Biodiversity Center, P.O. Box 9517, 2300 RA Leiden, the Netherlands
[g] Department of Earth Sciences, Faculty of Geosciences, Utrecht University, P.O. Box 80.121, 3508 TA Utrecht, the Netherlands
[h] Climate Geochemistry Department, Max Planck Institute for Chemistry, Hahn-Meitner-Weg 1, 55128 Mainz, Germany
[i] Departamento de Geologia, Escola de Minas, Universidade Federal de Ouro Preto, DEGEO 58, Brazil
[j] Instituto de Ciencias Naturales, Universidad Nacional de Colombia, Bogotá D.C., Colombia
[k] Géosciences-Environnement Toulouse, Université de Toulouse; UPS (SVT-OMP); CNRS; IRD, 14 Avenue Édouard Belin, F-31400 Toulouse, France
[l] Universidade de Brasília, Instituto de Geociências, Brasília, Brazil
[m] Korea Polar Research Institute, 26 Songdomirae-ro, Yeonsu-gu, Incheon 21990, South Korea
[n] Palynova Ltd, Littleport, UK
[o] Earth Sciences Department, Royal Holloway, University of London, Egham, Surrey TW20 0EX, UK

ARTICLE INFO

Editor: Luis Palazzesi

Keywords:
Amazon, palynology
Sequence stratigraphy, geochemistry
Biomarkers
Estuarine
Marine incursions

ABSTRACT

In the Miocene, a large wetland system extended from the Andean foothills into western Amazonia. This system has no modern analogue and the driving mechanisms are not yet fully understood. Dynamic topography and Andean uplift are thought to have controlled deposition, with allocyclic base level changes driven by eustasy and orbital forcing also playing a role. In this study we investigate the presumed orbital cyclicity that controlled sediment deposition, while also assessing sediment source and biomes in the Miocene wetland. We do this by integrating lithological, palynological, malacological and geochemical data from the Los Chorros site (Amazon River, Colombia), and by placing our data in a sequence stratigraphic framework. In this sequence biostratigraphic evaluation, the Los Chorros succession is visualized to be composed of a series of flood-fill packages, with a rapid initial flood, marine-influenced conditions at the time of maximum flood, followed by a longer regressive infill phase. Based on the palynology we could differentiate local vegetation, such as palm swamps, from regional origin such as *terra firme* vegetation (non-flooded Amazonian forest) and Andean montane forest, while from sediment geochemistry we could separate local and regional sediment sources. At the times of flooding, oligotrophic and eutrophic aquatic conditions alternatively characterized the wetland, as is shown by the presence of algae, floating ferns, and mollusc assemblages, while intervening subaquatic debris points to proximal submerged lowlands. In the lower 20 m of the section, marine influences are intermittently evident and shown by short-lived maxima of mangrove pollen, foraminiferal test linings, dinoflagellate cysts, coastal mollusc species, and an episodic decline in terrestrial biomarkers. The upper 5 m of the section is characterized by floodplain forest taxa with a diversity in tropical rain forest taxa and relatively few lacustrine indicators. These marine, mangrove, and lacustrine indicators suggest that the outcrops at Los Chorros represent predominant marine-influenced lacustrine conditions during periods of sea level highstand. The sequence biostratigraphic evaluation further points to eight 41 kyr obliquity-driven depositional cycles, with rapid phases of transgression. Mangrove elements would have colonised within the timeframe of each sea level rise. Based on this relative age constraint and comparison to regional records, deposition likely took place prior to the 13.8 Myr global

* Corresponding authors.
E-mail addresses: m.c.hoorn@uva.nl (C. Hoorn), bobmorley100@gmail.com (R.J. Morley).

https://doi.org/10.1016/j.gloplacha.2021.103717
Received 6 April 2021; Received in revised form 15 November 2021; Accepted 25 November 2021
Available online 17 December 2021

sea level fall, and most likely during the period just after 14.5 Ma, between Middle Miocene Climatic Optimum (MMCO; 17–14 Ma) and Middle Miocene Climate Transition (MMCT; 14.7–13.8 Ma). Palynological evidence further suggests that to the west, surface elevation ranged from ~1000 up to ~3500 m and hosted protoparamo vegetation, the oldest yet reported and in agreement with predictions from molecular studies. In contrast, contemporaneous sites to the northeast of the wetland consisted of fluvial and cratonic formations, as shown by their Nd and Sr isotopic sediment signature. In summary, our data lead to an improved understanding of how geological and astronomical mechanisms controlled the floral and faunal distribution and controlled sediment deposition in western Amazonia during the middle Miocene. As Miocene conditions strongly contrast with modern western Amazonia, our data provide an important context for the deep time history and evolution of the modern western Amazon rainforest.

1. Introduction

A large wetland system (known as “Lake Pebas” or “Pebas System”) extended across western Amazonia from the late Oligocene to late Miocene (>23–11 Ma) and reached a maximum coverage of more than a million square kilometres during the middle Miocene (Wesselingh et al., 2001; Wesselingh et al., 2006a). Wesselingh et al. (2001) highlight that *“Lake Pebas is among the largest and longest-lived lake complexes in Phanerozoic history”,* which he compared with estuaries, and other long-lived lake systems such as the Caspian Sea, Lake Maracaibo, and the modern Amazon River varzeas.

According to Wesselingh et al. (2001), the Pebas System has no modern analogue and is unique in its longevity and areal extent, as well as the prolonged freshwater conditions and episodic (relatively short-lived) marine incursions (see also Jaramillo et al., 2017). The system hosted radiations of endemic molluscs, such as pachydontine bivalves and cochliopid gastropods, and the *Cyprideis*-dominated ostracod fauna (see Wesselingh and Ramos, 2010). It also was home to diverse fish (Lundberg et al., 1998, 2010) and reptile faunas (Riff et al., 2010; Salas-Gismondi et al., 2015). Most strikingly, the Miocene Amazonian wetland is thought to have hosted the most diverse crocodilian assemblage ever, with unique forms evolving that benefited from the rich invertebrate resources in the wetland (Scheyer et al., 2013; Salas-Gismondi et al., 2015). The Miocene wetland is often mentioned in biogeographic studies and thought to have acted as a cradle of speciation for aquatic taxa, a barrier for terrestrial taxa, but was also a permeable system, enabling biotic exchange (see for overview Hoorn et al., 2021).

The ephemeral marine influences in the Miocene Amazonian wetland are of great value for understanding the floral and faunal biogeographic history of lowland Amazonia. Although their existence remains controversial (e.g. Latrubesse et al., 2010; Gross and Piller, 2020), there is growing evidence that coastal taxa, such as mangroves, dinoflagellates and foraminifers (Hoorn, 1993, 1994a, 1994b; Hoorn, 2006; Boonstra et al., 2015; Jaramillo et al., 2017; Sá et al., 2020; Sciumbata et al., 2021), fish (Lovejoy et al., 1998; Monsch, 1998), marine related mollusc and ostracod taxa (Wesselingh and Ramos, 2010; Linhares and Ramos, 2011), and others, including marine taxa with particular ichnofabric (Gingras et al., 2002; Hovikoski et al., 2010), were able to repeatedly inhabit the heart of the Amazon for thousands to tens of thousands of years. Moreover, the isotopic composition of mollusc and foraminiferal tests (Vonhof et al., 2003) and Pacu (serrasalmid fish) teeth (Alvim et al., 2021) in the wetland deposits point at episodic oligohaline conditions, with water ranging between 0.5 and 5 practical salinity units.

Marine incursions during the Paleogene (Santos et al., 2008; Louterbach et al., 2014) and Miocene (Hoorn, 1993; Jaramillo et al., 2017; Espinosa et al., 2021) allowed fish taxa such as stingrays, anchovies, drums and hardheads to migrate, adapt and diversify in the continental environment (e.g. Lovejoy et al., 1998; Bloom and Lovejoy, 2011, 2017; Cooke et al., 2012; Fontenelle et al., 2021). More recently, Bernal et al. (2019) proposed that the incursions also permitted dispersal —and subsequent adaptation— of coastal plant taxa into Amazonia, such as *Pachira aquatica* and *Dalbergia ecastaphyllum* (among others). Furthermore, the deposits of the Miocene Amazonian wetland also provide a diverse and often nutrient-rich substrate in western Amazonia that has created a heterogenous edaphic landscape supporting high species richness today (Quesada et al., 2010, 2012; Higgins et al., 2011; Bernal et al., 2019; Tuomisto et al., 2019; Oberdorff et al., 2019).

Räsänen et al. (1998) first recognized cyclic sedimentation patterns in the Pebas Formation. This was corroborated by Wesselingh et al. (2006a) based on a lithological study of hydrocarbon exploration wells in Peru. Wesselingh et al. (2006a) proposed autocyclic processes induced by basin subsidence and allocyclic processes caused by eustasy and orbital forcing as driving mechanisms. Further study of outcrops in Peruvian Amazonia also revealed cyclic sedimentation characterized by changes in lithofacies alone (Vonhof and Kaandorp, 2010) or in combination with changes of mollusc composition and diversity (Wesselingh et al., 2006b). Such cyclic changes were also observed in the granulometry and coarsening upwards packages at the Los Chorros site in Colombia, (Vonhof and Kaandorp (2010) (Fig. 1, point 1). Previously, Vonhof et al. (2003) recognized eight coarsening-upward (CU) cycles at Los Chorros, which have an average of c. 4 m and thought to be controlled by orbital cyclicity (Vonhof and Kaandorp, 2010) — a conclusion strongly supported from the sequence biostratigraphic evaluation described in our study. Based on this local sediment succession and regional analysis of the Miocene sedimentary record, Vonhof and Kaandorp (2010) propose changes in precipitation due to precession (a 23000 year cyclicity) or obliquity (a 41000 year cyclicity) as possible driving forces.

In this study we revisit the sedimentary record at the Los Chorros site (Fig. 1, point 1) to investigate in further detail the sediment provenance and composition of local and regional biomes in the wetland system. We also analyse the lithological and palynological succession in a sequence biostratigraphic framework and revisit the hypothesis of orbital cyclicity on the Miocene Amazonian wetland. The method of sequence biostratigraphy, which is the process of identifying depositional sequences from the examination of microfossil distribution patterns, is here applied to the Los Chorros succession for the first time. The sequence biostratigraphic approach was developed to help characterize sequence stratigraphic packages in the Gulf of Mexico using foraminifera (Armentrout, 1987, 1991) and nannofossils (Shaffer, 1987, 1990) and has been expanded to include palynology by Morley (1996) and Morley et al. (2011, 2020, 2021), who developed a scheme of high frequency cycles for the Cenozoic tied to the global isotope curve. These cycles were shown to be driven by cyclic phases of Antarctic glaciation (Morley et al., 2021). Similar patterns are seen in the Los Chorros succession, and it is thought that the sequence biostratigraphic approach might facilitate and improve age estimates of the Los Chorros section which, like other Neogene Amazonian intervals, has a poor stratigraphic age constraint (Wesselingh et al., 2006a).

We compare the sequence biostratigraphic approach with an alternative palynological evaluation based on multivariate ordination techniques (see ‘material and methods’ section) to an extended palynological dataset. This enables us to identify the palynological ‘sedimentary’ cycles, but also assess biome changes. The dataset is further complemented with organic and inorganic geochemistry and mollusc analyses from selected strata. Together, these results help us better understand successive depositional environments and

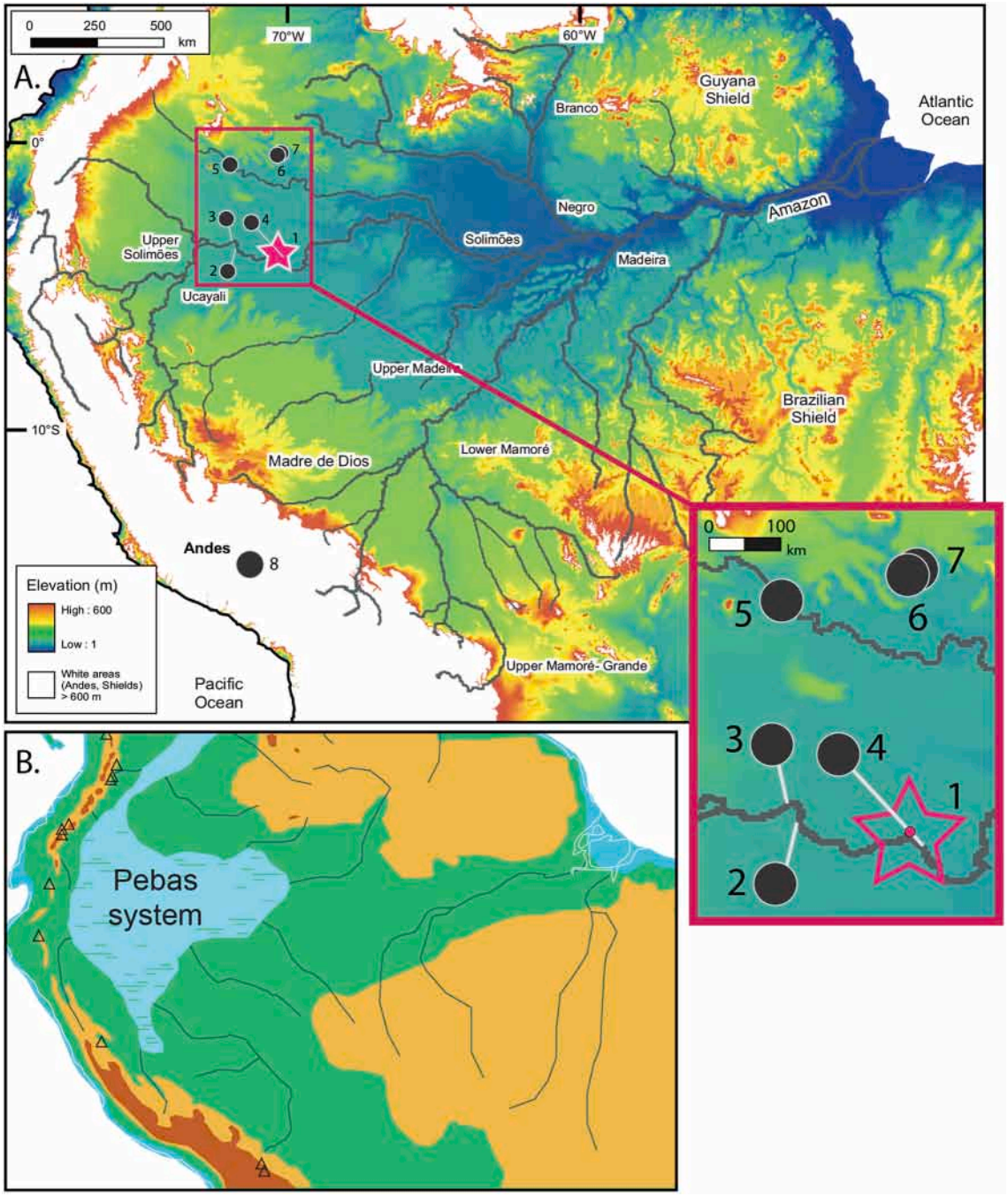

Fig. 1. a) Map with Neogene sites discussed in this work (see Appendix 1 for coordinates and references). Pink star denotes the Los Chorros site. Map colors refer to elevation with continental white regions denoting >600 m altitude (base map courtesy H. Wittman). Locations: 1 (star). Los Chorros, 2. Santa Rosa de Pichana, 3. Pebas, 4. Santa Sofia, 5. Mariñame; 6. Pira Parana; 7. Apaporis; 8. Altiplano; b) Schematic map of the Miocene Pebas System at its maximum extent based on the distribution of the Pebas, Solimões and equivalent formations (from Hoorn et al., 2010b). (For interpretation of the references to colour in this figure legend, the reader is referred to the web version of this article.)

connectivity with surrounding areas, as well as the mechanisms that drove deposition.

2. Geological setting

The geological record of the Miocene Amazonian wetland is contained within the Pebas Formation (Peru, southern Colombia), the Curaray Formation (Ecuador) and the Solimões Formation (western Brazil). These formations form part of the sedimentary infill of the Andean foreland basins, from north to south these are the Putumayo, Oriente, Marañon and Acre basins. Towards the east these sediments extend into the intracratonic Solimões and Amazonas basins. In the NE and SE, the extension of the Miocene sedimentary record is limited by the Amazon craton (see for summary Hoorn et al., 2010a, 2010b; Roddaz et al., 2010).

The Pebas Formation (Peru) was first mentioned as Pebas Beds by Gabb (1869) and Conrad (1871). However, the formation was only formally described by Seminario and Guzado (1976)), and a type location was assigned by (Sánchez Fernández et al., 1999). The formation is best documented in the Marañon Basin, where it has a thickness of ~ c.

1000 m (Hermoza, 2004; Wesselingh et al., 2006a; Roddaz et al., 2010) and was dated as Miocene (Parra et al., 2020). The best exposed outcrops of the Pebas Formation can be observed along the lower Marañon River and the Peruvian part of the Amazonas River, especially near the village of Pebas (Fig. 1, point 3; Vonhof et al., 2003) where outcrops reach up to 20 m in height and display the typical lithology and fossils as described below (Hoorn, 1994a; Sánchez Fernández et al., 1999; Zavala Carrión et al., 1999).

In Brazil, the Miocene Amazonian wetland system is represented by the Solimões Formation. This formation was first described by Moraes Rego (1930), and later validated by Caputo et al. (1971). The type location of the formation is well 2-RJ-1-AM in the Solimões Basin (Eiras et al., 1994). A recent re-evaluation of a cored section in the Acre Basin restricted the Solimões Formation to a Miocene age and a thickness of more than 2000 m. Instead, in the Solimões Basin the formation reaches just over ~500 m (see Fig. 4 in Da Silva-Caminha et al., 2020). Until now, sediment dating was based on biostratigraphy and correlation with Caribbean palynological zonations. Kern et al. (2020) compared biostratigraphic dating methods with radiometric ages derived from U/Pb in detrital zircon grains and confirm the Miocene age estimate for the Solimões Formation. Sediment provenance of the Miocene sediments in the Acre and Solimões was previously addressed by Horbe et al. (2019). These authors show that the Andes was the principal source of Amazonian Neogene sediments, but that between the Miocene and Pliocene an increase of immature mineral assemblages point at uplift in the Peruvian Eastern Cordillera.

The Pebas and Solimões formations are characterized by fossil-rich, bright blue smectite-rich mudstones, siltstones and fine-grained sandstones (Räsänen et al., 1998; Hernani, 2012; Wesselingh et al., 2006a) (Fig. 2). In outcrops, these sediments are seen as CU cycles with an average thickness of c. 4 m, and lignites (low-grade coal) or organic-rich claystones that are now considered as base of each cycle (Vonhof et al., 2003; Wesselingh et al., 2006a; Vonhof and Kaandorp, 2010). In cored sections, sandstone layers of 2 to 15 m thick are also observed, suggesting episodes of fluvial conditions (Maia et al., 1977; see overview in Hoorn et al., 2010a). Other characteristic features of the Pebas and Solimões formations are the lenticular (channel) bodies that are particularly rich in fossil remains of plants and animals (Hoorn, 1994a). Furthermore, fossil pollen, foraminifera, dinoflagellate, mollusc and geochemical records indicate that the wetland system was frequently influenced by (oligohaline) marine incursions, without full marine conditions (mesohaline or higher) ever being established (Hoorn, 1993; Hoorn et al., 1996; Vonhof et al., 2003; Boonstra et al., 2015; Jaramillo et al., 2017).

3. Material and methods

3.1. Lithology, age, and sample location

The Los Chorros outcrops are a series of up to c. 35 m high cliffs (in dry season) located in a c. 2 km stretch between the confluences of the Loreto-Yacu and Amazon and Amacayacu and Amazon rivers respectively (Fig. 1, point 1; Colombia), in the proximity of the village of Puerto Nariño. Wesselingh (1993), Hoorn (1994a) and Vonhof et al. (2003) first documented the sedimentary succession and palynological and malacological composition at this site. An overview of facies descriptions for the Los Chorros and other similar sites can be found in Hoorn (1994a). The age of the sediments was estimated at middle to late Miocene (Hoorn, 1994a) and then adjusted to 14.2 to 12.7 Myr (zone T15; Boonstra et al., 2015 sensu Jaramillo et al., 2011). Other sites that were sampled for comparison are situated at Santa Sofia (4, Fig. 1; Hoorn, 1994a), Mariñame (5, Fig. 1) (Hoorn, 1994b; Salamanca Villegas et al., 2016), and along the Pira Parana and Apaporis Rivers (Fig. 1, points 5, 6) (Hoorn, 2006; Boonstra et al., 2015; Sciumbata et al., 2021). The coordinates and reference data for all sites mentioned in this work are presented in Appendix 1; the lithology of the Los Chorros outcrops is shown in Fig. 2, with details and sample position in Appendix 2.

3.2. Palynology

3.2.1. Sporomorphs: collection, processing, and analysis

In total, 121 palynological samples were collected during the 1989 and 1991 fieldwork at the Los Chorros site (Fig. 1, point 1). Of these, 26 samples were previously analyzed and published (Hoorn, 1994a), in this study we extended the existing dataset to a total of 69 analyzed samples. From each sample 1cm^3 of material was sieved through a 250 μm mesh, and a tablet of *Lycopodium clavatum* spores was added to each sample to estimate its pollen concentration. The organic-rich clays were treated with sodium pyrophosphate ($Na_4P_2O_7{\cdot}10H_2O$) in a 10% solution with H_2O, while lignites were oxidized with Schulze mixture ($2HNO_3$, 60%: $KClO_3$, 7%). Then, bromoform with density 2.0 g/cm^3 was used to separate the inorganic fraction. The resulting organic residue was mounted in glycerine gelatin and sealed with paraffin.

All sporomorphs were included in the pollen sum. With logging at 400× magnification we aimed for a pollen sum between 100 and 400 sporomorphs (pollen and fern spores). Dinoflagellate cysts, foraminiferal test linings, *Azolla* massulae and *Botrycoccus* colonies, other algae, fungal spores, damaged and/or reworked spores and pollen were also counted. The sporomorph composition was reported as percentages; only 22% of the samples were barren or gave a sum lower than 100 sporomorphs, namely at levels 19.5, 15.4, 15.3, 6.0, 4.8, and 2.7 m. The complete palynological dataset is in Appendix 3a, the complete diagram is in 3b, and details of the palynological zonation are shown in 3c.

Results are initially plotted in diagrams using Tilia 7.6 software (Grimm, 1991) and subdivided into pollen zones based on a stratigraphical constrained cluster analysis using the total sum of squared (Fig. 3; CONISS: Grimm, 1987; Gill et al., 1993). The palynological zones correspond to the first and second orders of division of the clustering. Additionally, DCA multivariate analysis was performed on samples and sporomorph taxa to corroborate ecological grouping and zonation (Appendix 5; PAST: Hammer et al., 2001). DCA scores are plotted in the summary pollen diagram (Fig. 3).

3.2.2. Grouping of the sporomorphs

Sporomorphs were identified with the help of palynological catalogues (Hooghiemstra, 1984; Roubik and Moreno, 1991; Hoorn, 1993, 1994a, 1994b; Velásquez, 1999; Jaramillo et al., 2008, 2014; Jiménez et al., 2008; De Silva and de Assis Ribeiro dos Santos, 2008; da Silva-Caminha et al., 2010; Leal et al., 2011; D'Apolito et al., 2021). We used affinities reported for Neogene taxa in Hoorn (1993, 1994a, 1994b), Jaramillo et al. (2008, 2014), (D'Apolito (2016), D'Apolito et al. (2021)), and Sciumbata et al. (2021), but in the course of this study we also established new affinities. The ecological preferences of the identified taxa were inferred from their nearest living relatives (NLR) (Fig. 3; Appendix 3a). This information was then used to assign each taxon to a biome, following the South American synthesis of Marchant et al. (2002), and to estimate their contribution throughout the record.

Taxonomic assignments of NLR were confirmed using the Colombia Plant and Lichen Catalog (http://catalogoplantasdecolombia.unal.edu.co/es/; Bernal et al., 2015) and this allowed us to determine the biogeographical distribution of most of the taxa (i.e. Amazonia, Andes, Orinoquia, Amazon craton). In addition, the GBIF database (www.gbif.org) enabled us to establish the elevational ranges and latitudinal distribution of taxa in northern South America. For a selection of fossil taxa we plotted the elevational distribution of their modern NLR using the GBIF database (www.gbif.org) (Fig. 4, Appendix 4 with list of citations), this to support the assignment of paleoelevational range estimates. Microphotographs of these representative taxa of high elevation Andean ecosystems (including protoparamo) are shown in Fig. 5.

The pollen sum included 374 palynomorph taxa which were subdivided into eleven categories from which we derived changes in biome composition during the Miocene and across the Andes-Amazon region (see Appendix 3a for details). The categories are formed of: 1) Mangrove vegetation, which comprises pollen of three angiosperm families plus the fern spore of

Deltoidospora adriennis; 2) Tropical lowland forest (restricted), composed of forty nine tropical elements (15 families), including e.g., Apocynaceae, Malvaceae, Sapotaceae, Arecaceae, Fabaceae; 3) Tropical lowland-seasonal vegetation, composed of fifteen taxa typical from seasonal forests mainly belonging to Mimosoideae and Faboideae; 4) Montane forest, which includes four pollen types plus 19 fern spores (e.g., Cunoniaceae, Adoxaceae, Cyatheaceae, Pteridaceae); 5) Mixed high-Andean vegetation to proto-paramos, formed by five pollen types (e.g., Rosaceae) and 9 fern spores (e.g., Pteridaceae, Lycopodiaceae); 6) Tropical vegetation of wide distribution (0 to >3000 m altitude), including 126 elements, mostly composed of angiosperms occuring in diverse tropical habitats (e.g., Melastomataceae-Combretaceae, Arecaceae, Fabaceae, Euphorbiaceae, Moraceae-Urticaceae). 7) Palm swamp vegetation and associated taxa typical of tropical forested wetlands, including five taxa (e.g., Arecaceae, Euphorbiaceae, Malvaceae); 8) Freshwater vegetation of wide distribution, composed of four pollen types and fern spores such as Cyperaceae, Nymphaceae, Lygodiaceae, Pteridaceae; 9) Asteraceae, the composites, which are of wide distribution; 10) Poaceae, the grasses, which are of wide distribution; 11) Pollen and fern spores of unknown botanical affinity which add up to 123 taxa whose occurrence cannot be assigned to any specific group.

Sporomorph abundances and zonation are illustrated in the summary pollen diagram (Fig. 3), with taxa grouped based on their NLR and corresponding biome (Table 1 and Appendix 3a). The complete palynological diagrams can be found in Appendix 3b. For the comprehensive interpretation of palynological groups in comparison to other microfossils not included in the pollen sum (i.e., foraminifer linings, dinoflagellate cysts, and algal and fungal remains) and their further incorporation as part of the sequence biostratigraphic analysis, we performed a Pearson's correlation (Acton, 1959) of the relative abundances of the groups, previously smoothed by a 3-point running average (Fig. 6; PAST: Hammer et al., 2001).

3.2.3. Phytoliths

Sixteen sediment samples from Miocene sites in Colombian Amazonia were processed for phytoliths. Although, in general, the recovery was poor, some of the most productive samples came from Los Chorros (Fig. 1, point 1) and the nearby Santa Sofia site (Fig. 1, point 4). We followed the processing methodology of Piperno (2006). Samples were ground and, for each, 1 ml of sediment was mixed with 200 ml of a 50% hydrogen peroxide (H_2O_2) solution; mixing and decanting was repeated 5 times until obtaining a clear solution. Subsequently, the samples were further diluted with ethanol (2×) at 90%, and finally with distilled water (1×). Each time the samples were spun at 2000 rpm for 5 min, with the aim to remove the remaining hydrogen peroxide. Zinc chloride ($ZnCl_2$; density 2.1) was applied for density separation (spinning 5 min at 500 rpm). Then the light (phytoliths) fraction was transferred to microtubes, and the residues were mounted in microscope slides. The specimens recovered during this study are listed in Table 2 and a selection is represented in Fig. 7.

The identification, description and photography were performed with a Nikon Eclipse E 400 microscope and an Omni LW Scientific camera. The morphological terminology is based on Madella et al. (2005). For the identification we also used the reference phytolith collection from the Laboratorio de Arqueología del Instituto de Ciencias Naturales, Universidad Nacional de Colombia (ICN-MHN-FIT) and the Amazonian Poaceae phytolith (Morcote-Ríos et al., 2015) and palm (Morcote-Ríos et al., 2016) catalogues.

3.2.4. Sequence biostratigraphy

The palynological dataset was evaluated from the sequence biostratigraphic perspective following methods outlined in Morley (1996), and Morley et al. (2020) using the software 'Stratabugs' (www.stratadata.co.uk). This involved plotting palynological data as percentages in a manner that allowed the approximate differentiation of palynomorphs from *terra firme,* montane, swamp and aquatic sources, and examining their distribution in relation to lithologies, sedimentological features, the occurrence of molluscs and other criteria that may relate to lake level and salinity change. The palynological dataset was plotted using total *terra firme*-montane pollen as the pollen sum, using the taxon groupings above, but separating *Heterocolpites* pollen from the 'wide distribution' group since it displays a different pattern of abundance change to others in that group (Fig. 4). Using this approach, the pollen sum approximately captures change within the non-swamp vegetation. Taxon groups clearly derived from swamp vegetation, spores (which are unlikely to be from forest canopy elements and have different dispersal mechanisms to pollen), and algae were plotted 'outside' the *terra firme*-montane pollen sum. The representation of swamp-derived pollen, spores and algae are thus plotted in a manner whereby their spectra are not interdependent, as would be the case with taxon groups included in the sum (Chung et al., 2021). Their abundance therefore provides an approximate proxy for the abundance of the parent taxa of each group within the local pollen catchment. On the other hand, changes of *terra firme*-montane groups within the sum may reflect trends with respect to fluctuating climates. Flood-fill packages were interpreted from the succession of environments suggested from the temporal succession of pollen, spores and other microfossils from freshwater swamp and different mangrove groups, and the succession of lithologies. The resulting sequence palynostratigraphic scheme is shown in Fig. 8. The age of the succession was then evaluated based on age-restricted palynomorphs and the cyclicity pattern of the flood-fill packages by comparison with the high-resolution stable isotope studies of Holbourn et al. (2013) and Westerhold et al. (2020).

3.3. Molluscs

Mollusc data from the Los Chorros site were first reported by Wesselingh (1993) and taxonomy has been updated using Wesselingh (2006). The taxa found at Los Chorros are listed in Appendix 6. Data analyses were run on samples with >30 specimens using PAST (version 4.07: Hammer et al., 2001), for the NMDS analyses we used chord similarity (Fig. 9a and b). We compared assemblages with those reported from the Peruvian site of Santa Rosa de Pichana (Fig. 1, point 2; Wesselingh et al., 2006b). Stable isotope data from Los Chorros (Fig. 9b, 10) follow Wesselingh (1993) and Vonhof et al. (2003).

3.4. Geochemistry

3.4.1. Bulk organic geochemical analyses

Analysis of the total organic carbon weight percent (TOC wt%) and its stable carbon isotopic composition ($\delta^{13}C_{TOC}$) was performed at the NIOZ Royal Netherlands Institute for Sea Research. An aliquot (~0.3 g) of each sample was first crushed and decalcified by adding 35 ml of 4 M hydrochloric acid (HCl). Samples were then shaken overnight (12*h*), after which the sediment was rinsed with ultra-pure distilled water to remove HCl. After freeze-drying, the samples were re-weighed. An elemental analyzer (Flash EA 1112 series) was used to determine the TOC wt% and the stable carbon isotopic composition of TOC. Analyses were repeated at least in duplicate and the analytical error was on average better than 5% for TOC. Isotope ratios were calibrated to a benzoic acid standard ($\delta^{13}C_{TOC} = -28.1‰$ with respect to Vienna Pee Dee Belemnite (VPDB) calibrated on NBS-22). The analytical error was usually smaller than ±0.15‰ for $\delta^{13}C_{TOC}$. The results are listed in Appendix 7a.

3.4.2. Lipid analyses

Lipid analyses were carried out at the NIOZ Royal Netherlands Institute for Sea Research. Between 0.5 and 12 g (depending on the mass of available material) of freeze-dried and homogenized sediments were extracted using an ultrasonic bath. A solvent mixture of dichloromethane (DCM) and methanol (MeOH) (2:1, v:v) was added to each

sample before placing samples in an ultrasonic bath for 5 min. Samples were then centrifuged and solvent was decanted. This procedure was repeated 4 times, after which solvent fractions were combined and solvents were evaporated resulting in a Total Lipid Extract (TLE). Traces of water were removed using a small column (Pasteur pipette) with sodium sulfate (Na_2SO_4).

An internal standard was added to an aliquot (10–20%) of the TLE for quantification purposes. After derivatization of fatty acids and alcohols, the fraction was cleaned by dissolving it in EtOAc and eluting it over a small column with silicagel. Subsequently, lipids were analyzed using an HP Gas Chromatograph (GC) fitted with a CP-Sil 5CB fused silica capillary column (25 m, 0.32 mm i.d.) and a flame ionization detector (FID). Samples were injected on-column, with helium as the carrier gas, set at constant pressure (100 kPa). The oven was programmed starting at 70 °C, heating by 20 °C min^{-1} up to 130 °C, then by 4 °C min^{-1} up to 320 °C and kept at this temperature for 20 min. For the identification of organic compounds, GC-mass spectrometry (MS) was performed on selected samples using a ThermoFinnigan Trace GC–MS with the same type of column and oven program as used for the GC but using constant flow of the carrier gas.

Another aliquot (80–90%) of the TLE was split into three fractions of different polarity. This was done using small columns (Pasteur pipettes) with activated aluminum oxide and the following solvent mixtures as eluents: I) DCM:hexane (9:1, v:v), II) DCM:hexane (1:1, v:v) and III) DCM:MeOH (1:1), respectively. Fraction number III contained the branched and isoprenoid glyceroid dialkyl glyceroid tetraethers (GDGTs). This fraction was dissolved in a mixture of hexane:isopropanol (99:1, v:v) and filtered over a 0.45 μm PTFE filter. GDGTs were analyzed using high performance liquid chromatography-atmospheric pressure positive ion chemical ionization–mass spectrometry in selected ion monitoring mode, following the procedure described in Hopmans et al. (2000). For quantification purposes a fixed amount of a C_{46} GDGT standard was added (Huguet et al., 2006). In order to detect shifts in GDGT distributions along the sedimentary successions, the branched and isoprenoid tetraether (BIT) index (Hopmans et al., 2004), the methylation index of branched tetraethers (MBT) (Weijers et al., 2007), and the degree of cyclization (DC) (Sinninghe Damsté et al., 2009) were calculated (see Appendix 3a-b for the GDGT chemical structures and the formula of GDGT-based indexes).

3.4.3. Major and trace elements analyses

Selected samples were measured for their major and trace elements concentrations at the Service d'Analyse des Roches et Minéraux (SARM), Institut national des sciences de l'Univers (INSU) facility, Vandoeuvre-Les-Nancy, France, analytical details available on http://helium.crpg.cnrs-nancy.fr/SARM/), by Inductively Coupled Plasma Atomic Emission Spectroscopy (ICP-AES) and Inductively Coupled Plasma Mass Spectrometry (ICP-MS) after alkali fusion. Uncertainties are lower than 5% for major elements, and lower than 10% for minor and trace elements. The results are listed in Appendix 7c.

3.4.4. Strontium (Sr), Neodymium (Nd), and Samarium (Sm) isotope analyses

All analyses of Sr, Nd and Sm isotopes were carried out at the Geochronology Laboratory of the Universidade de Brasília. The preparation of bulk sediments for Sr, Nd and Sm isotope analyses followed the procedures described by Gioia and Pimentel (2000). Briefly, around 100 mg of homogenized sediments were weighed, and an internal standard was added (a mix or "spike" of Sm and Nd enriched in ^{149}Sm and ^{150}Nd). The material was then digested in a Teflon container, using different acid attacks, including HNO_3, HF and HCl.

An aliquot of each sample was used to separate Sm and Nd by ion chromatography. A first column packed with a cation resin (BIO-RAD AG 50 W-X8 200–400 mesh) was used to separate the rare earth elements (REE) from other elements, whereas a second column was used to separate Sm and Nd from other REE. The second columns are packed with LN-Spec resin (liquid resin HDEHP-270-150 mesh powdered Teflon coated with diethylexil phosphoric acid). Sr was separated from other elements by using a column packed with Eichrom Sr-Spec ion exchange resin. Isotopic analyses of Sr, Sm and Nd isotopes were carried out on a Finnigan TRITON-262 multi-collector mass spectrometer in static mode. Samples were loaded onto re-evaporation filaments of a double filament assembly.

International rock standards were used to evaluate the isotopic analyses. For $^{147}Sm/^{144}Nd$ and $^{143}Nd/^{144}Nd$ ratios standards BCR-1 and BHVO-1 were used, which generally provide uncertainties better than ±0.1% (2σ) and 0.005% (2σ), respectively (Dantas et al., 2009). $^{143}Nd/^{144}Nd$ ratios were normalized to a $^{146}Nd/^{144}Nd$ ratio of 0.7129. Nd procedure blanks were smaller than 100 pg. Nd isotope ratios are also reported as $\varepsilon_{Nd(0)}$ following DePaolo and Wasserburg (1976). For $^{87}Sr/^{86}Sr$ analyses of the NBS 987 standard yielded an average value of 0.71023 ± 8 (1σ) and uncertainties in individual analyses are better than 0.01% (2σ). The results are listed in Appendix 3a.

4. Results and interpretations

4.1. Lithology and facies

In Fig. 2 we show the lithological composition of the 27.2 m sedimentary succession observed at the Los Chorros site (see Appendix 2 for details). The section was divided into three subsections (Los Chorros A, B, and C) which we linked by following the fossil-rich marker bed at 15 m that occurred in all three sections. In general, the sediments are composed of fine-grained sandstones, sandy claystones, organic-rich claystones, and lignites (Figs. 2 and 3).

The westernmost subsection (A) includes three complete CU cycles (Fig. 2), with each cycle beginning at a lignite bed that contains plant, fish, mollusc and vertebrate fossil remains, but also marine palynomorphs. Between 8.5 and 15 m there is an alternation of fine-grained sandstone and claystone beds. At 15 m, the lignite marker bed is characterized by an irregular, lenticular base that suggests an erosive event. This incised base was subsequently filled-in with organic matter and fossil placer deposits. The succession continues with clays that are partially mottled, a feature possibly caused by burrowing of organisms (see Pebas locality, Gingras et al., 2002).

At Los Chorros B and C (Fig. 2), the two easternmost subsections, the marker bed is followed by a fine-grained sandstone interval of about 5 m thickness. This bed changes laterally into a claystone and sandstone alternation, with claystones containing varying amounts of sand. At 19.5 m, another lignite bed with marine palynomorphs occurs, which is followed by a fine-grained sandstone and claystone alteration. Towards the top, mottled clays again point at burrowing and organic activity (23.5–24.5 m and 26 to 26.5 m). The last sandy lignite was observed at 25.5 m, with the section ending at 27.6 m.

The relation between the lithology, granulometry (after Vonhof et al., 2003; Vonhof and Kaandorp, 2010) and the CU cycles is discussed in section 5.3.1 and visualized in Fig. 12.

4.2. Palynology

4.2.1. General trends in sporomorph composition

Most of the species in our palynological record are of wide distribution and can occur from lowland to highland forests. Only a limited number of palynomorphs can be confidently tied to a NLR and considered representative for a single vegetation type, such as the high Andes (Fig. 6, elevational gradient selected taxa) or the lowland tropical rainforest. The biomes are further explained inTable 1.

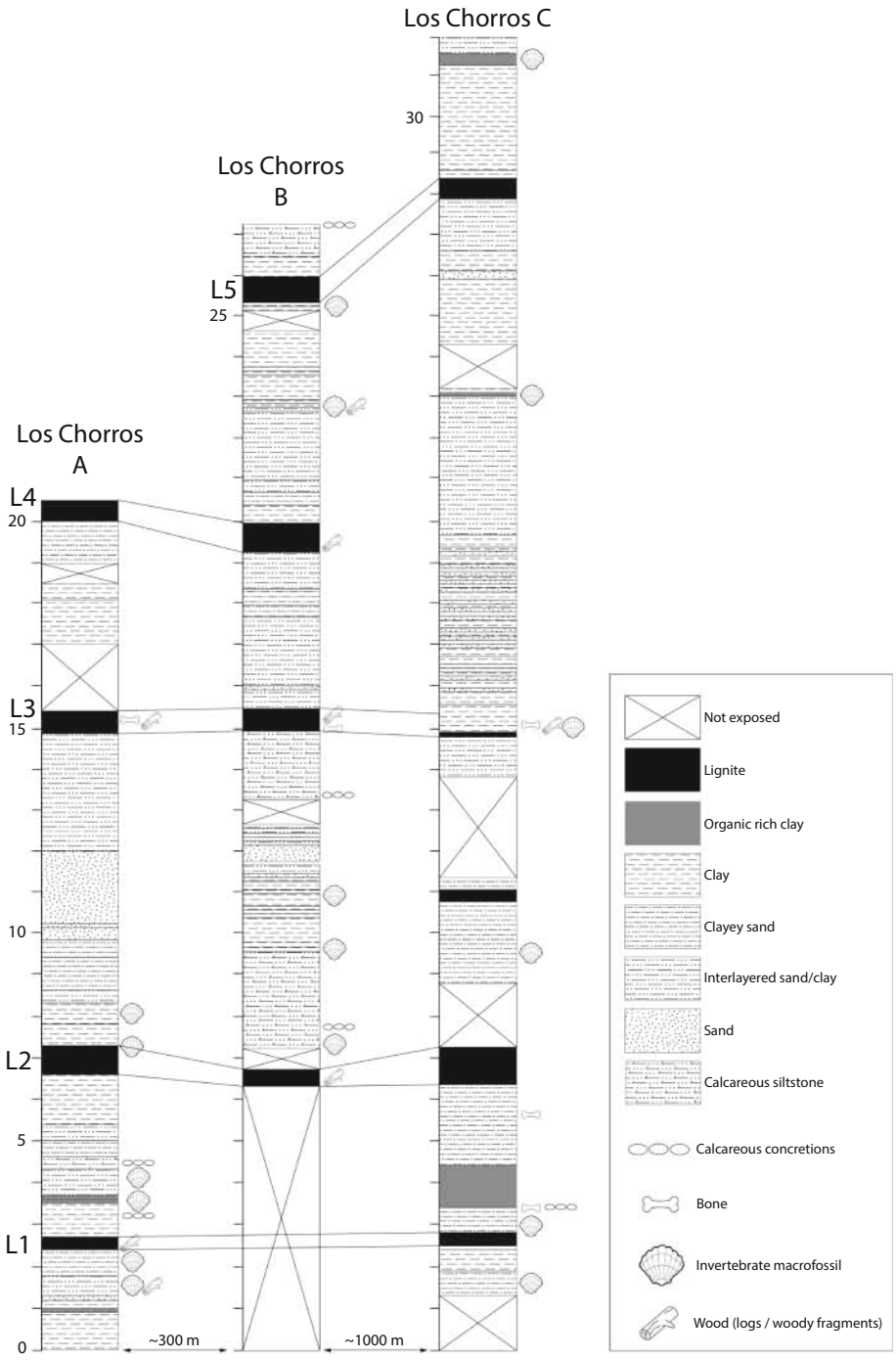

Fig. 2. Lithological columns of the outcrops at Los Chorros.

Pollen of mangrove (*Zonocostites ramonae* NLR *Rhizophora mangle*) and associated taxa are generally present in low percentages, particularly in zone 3, but can be marked by peaks in spores of the mangrove fern *Deltoidospora adriennis* (*Acrostichum*). Records of *Z. ramonae*, *Z. "costamaxilalongporatus"* (cf. *Rhizophora racemosa*), *Psilastephanocolporites schneideri*, and *Zonocostites* sp. (other *Rhizophora* spp.) mostly correspond with occurrences of foraminiferal test linings, and/or dinoflagellate cysts. Together, mangrove pollen and marine palynomorphs exhibit a certain periodicity with peaks at 2.7–3.5 m, 9.9–10 m, 19.8–20 m, and around 23.4 m. Exceptions occur at 8.8 m where only foraminiferal test linings occur, at 15 m, 11.7 m and 4.5 m only dinoflagellate cysts, and at 16.7 m with only *Z. ramonae* (Fig. 3c, Appendix 3a,b).

Palm swamp forest (mainly formed of Mauritiinae) and tropical lowland forest (including seasonal forest), all seem to have coexisted. In addition, taxa from tropical montane forests (1000 to >3200–3500 m elevation) often prevail when swamp and lowland forest taxa occur in

Table 1
Biomes or vegetation types and their main characteristics. These biomes form the basis for the grouping in the palynological diagrams (Fig. 3 and Appendix 3a).

Biome/vegetation types types	Ecology and key taxa	References	Pollen catalog reference
Mangrove vegetation	Areas occurring along the coast and riparian areas under continuous sea influence. There, trees and shrubs are mostly evergreen and show morphological adaptations to swallow intertidal environments reflecting a saline gradient from brackish water to sea water. *Rhizophora*, *Avicennia*, *Laguncularia*, *Conocarpus*, *Pellieciera, Acrostichum*	Lindeman (1953), Lacerda et al. (2001)	Willard et al. (2004), De Silva and de Assis Ribeiro dos Santos (2008)
Tropical lowland forest	Also named as Amazonian rainforest, includes a variety of forest communities developed from 0 to ~1000 m altitude influenced by warm mean annual temperatures (MAT) of ~27 oC, minimum annual precipitation 1500–1800 mm with a short dry season, annual floods, changes in drainage patterns, and soil quality. *Acalypha*, *Cecropia*, *Croton*, *Eugenia*, *Tapirira*, *Virola*, Bignoniaceae, Melastomataceae, Mimosoideae, Moraceae, Palmae, Rubiaceae, Sapindaceae	Duivenvoorden and Lips (1995), Mommersteeg (1998), Burn et al. (2010)	Roubik and Moreno (1991), Jiménez et al. (2008), Leal et al. (2011), Fontes et al. (2019)
Tropical lowland seasonal vegetation	These are regions occurring at a maximum of 500 m altitude, with warm temperature and a bimodal precipitation pattern (800–2500 mm mean annual precipitation). Its vegetation varies from grassy treeless areas to woodlands controlled by annual floods and soil quality, especially along the drainage systems. *Tracchypogon*, *Axonopus*, *Byrsonima*, *Curatella*, *Borreria*, *Clitoria*, *Miconia*, *Pavonia*, *Sida*, *Tibouchina*, *Watheria*, *Palicourea*, *Anacardium*, *Bursera*, Amaranthaceae, Asteraceae	Leal et al. (2011), Romero-Ruiz et al. (2012)	Leal et al. (2011)
Tropical montane forest	In areas from ~1000 m till 3200–3500 m altitude where the Upper Forest Line (UFL) occurs (MAT 9.5 oC). In general, two main types are distinguished. The lower montane forest or subandean forest (~1000 to 2300-2500 m) experiences MAT between 22 and 13 oC and includes species not resistant to night frost. In the upper montane forest or Andean forest (2300–2500 to 3200-3500 m) MAT range from 16 to 9 oC and night frost tolerating species develop. *Cecropia*, *Inga*, *Clusia*, *Croton*, *Hyeronima*, *Alchornea*, *Hedyosmum*, *Morella*, *Quercus*, *Podocarpus*, *Weinmannia*, *Ilex*, *Vallea*, *Gaiadendron*, *Myrsine*, *Faboideae*, Melastomataceae, Moraceae, Palmae, Rosaceae	Mommersteeg (1998), Van't Veer and Hooghiemstra (2000)	Hooghiemstra (1984), Bogotá et al. (1996), Velásquez (1999), Bogotá (2002)
High Andean vegetation	Called Páramo in the Northern Andes and Puna in the Central Andes, develop above the UFL till the permanent presence of snow and a MAT ranging from 9 to 0 oC. On the first 200–300 m altitude shrubs are common which are followed by grasses and herbaceous vegetation along the next 700 m altitude. The uppermost zones, influenced by harsh conditions, are dominated by incomplete vegetation cover. In this regions taxa like *Polylepis*, *Calceolaria*, *Lycopodium*, although characteristic, can also develop in certain sectors of the tropical montane forest. *Symplocos*, *Weinmannia*, *Berberis*, *Hypericum*, *Polylepis*, *Acaena*, *Aragoa*, *Valeriana*, *Lysipomia*, *Draba*, *Huperzia*, *Cyathea*, Asteraceae, Poaceae, Melstomataceae, Ericaceae	Van't Veer and Hooghiemstra (2000), Flantua et al. (2014), Bernal et al. (2015)	Murillo & Bless (1974), Murillo & Bless (1978), Hooghiemstra (1984), Velásquez (1999), Bogotá et al. (1996) Contreras et al. (2006)
Tropical vegetation (wide distribution)	Includes taxa present in different tropical ecosystems. Some can be present and more abundant either in the tropical lowland forest, the tropical montane forest or even in the savannas. *Alchornea*, *Drymaria*, *Hedyosmum*, *Podocarpus*, *Peperomia*, *Monnina*, *Macrolobium*, *Psychotria*, Melastomataceae-Combretaceae, Moraceae-Urticaceae, Myrtaceae among many others	Marchant et al. (2002), Flantua et al. (2014), Bernal et al. (2015)	Hooghiemstra (1984), Roubik and Moreno (1991), Velásquez (1999), Leal et al. (2011)
Palm swamp (tropical lowland forest)	Wetlands occurring at maximum 1000 m altitude where *Maurita* and *Mauritiella* dominate. These wetlands correspond to Morichales present in the valleys of the Orinoquia (Guyana shield and east savannas of Venezuela and Colombia) and in the Brazilian Cerrado, while Canaguchales develop in the Amazonian basin extending to deltas of Orinoco and Amazonas. This distinction reflects variations in floristic composition and structure, as well as geomorphologies and environmental conditions such as type of water (origin and chemical composition), water regimen, seasonality, and processes related to organic matter accumulation and nutrient flow. *Mauritia*, *Euterpe*, *Eichornea*, *Typha*, *Utricularia*	Rangel-Ch (2008), González-B & Rial (2013),	Roubik and Moreno (1991), Jiménez et al. (2008), Leal et al. (2011)
Freshwater vegetation (wide distribution)	Continental wetlands, permanently to seasonally inundated, associated to lakes, rivers to marshes. *Typha*, *Rumex*, *Ludwigia*, *Bidens*, *Polygonum*, *Potamogeton*, *Plantago*, *Eichorna*, *Sagitaria*, *Azolla*, and a myriad of *Cyperaceae*.	Ramsar Convention on Wetlands (2018); Van't Veer and Hooghiemstra (2000), Guzmán, (2012)	Hooghiemstra (1984), Velásquez, (1990), Roubik and Moreno (1991)Leal et al. (2011)
Asteraceae and Poaceae	Together with Cyperaceae and associated herbs of freshwater communities these taxa can abound throughout a variety of environments like estuaries, lagoons, seasonally inundated tropical savannas, and open Andean vegetation.	Van't Veer and Hooghiemstra (2000); Burn et al. (2010), Piedade et al. (2010); Rangel-Ch, (2010).	Hooghiemstra (1984), Velásquez (1990), Roubik and Moreno (1991)Leal et al. (2011)
Unknown affinity and ecology	This includes taxa include sporomorphs whose botanical affinity cannot be determined and therefore its occurrence to any community.		

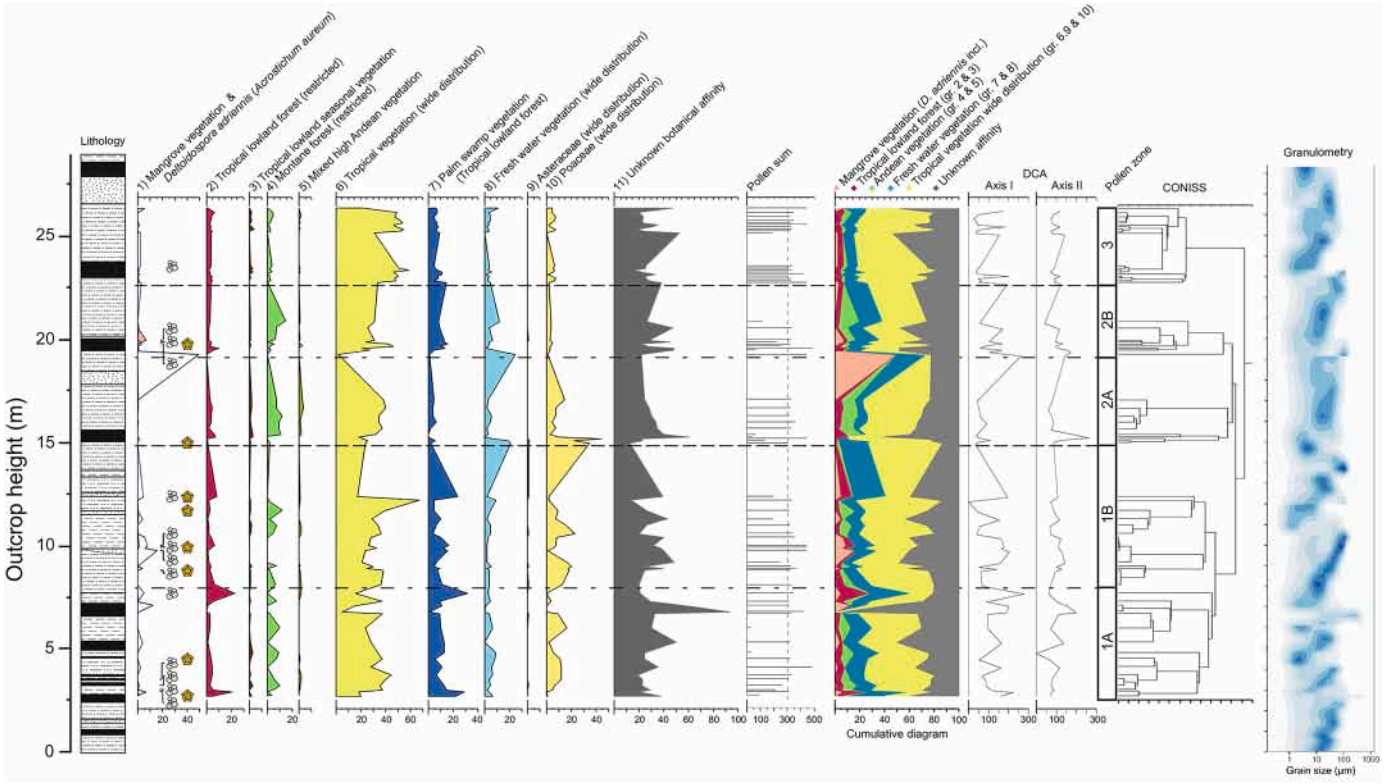

Fig. 3. Summary palynological diagram with biome representation across the Los Chorros section. The cumulative diagram shows the main contrasting biomes including taxa with wide tropical distribution and unknown affinity (see Table 1 for description); Detrended Correspondence Analysis of the Palynological data. The granulometric variation of the sediments in the Los Chorros section is after Vonhof and Kaandorp (2010). Occurrences of foraminifers and cysts are plotted next to the mangrove (*Zonocostites*) record.

low numbers. This suggests an increase in sediment input from the (high) Andes into the depositional system. Tropical montane vegetation is mostly reflected by *Siltaria "weinmaniensis"* (cf. *Weinmannia*), with some *Retitricolporites "sambucoides"* (cf. *Sambucus*) and *Echitricolporites "microspinosus"* (Brunelliaceae?), *Psilastephanocolpites "nerteroides"* (cf. *Nertera*), *Ephedripites* (aff.) *renzonii* (*Ephedra*) and a myriad of ferns principally with affinity to *Cyathea*, *Thelypteris*, and *Pleopeltis*. Fern spores with affinity to *Huperzia*, *Jamesonia* and *Cystopteris*, but particularly with the pollen type *Byttneripollis rugulatus* (*Polylepis-Acaena*) and/or *Retimonocolpites* "*margocolpatus*" (cf. *Puya*), *Retitricolpites* "*brassicoides*" (cf. Brassicaceae?), *Perfotricolpites* "*pseudocalceolarius*" (cf. *Calceolaria*?), *Psilatricolporites* "*miniclethroides*" (cf. *Clethra*), indicate the existence of high elevation Andean ecosystems and protoparamos developing above 3200–3500 m above sea level.

Poaceae attain high percentages in zone 1 but decline in zones 2 and 3. The transition from zone 2 to 3 marks a subtle turnover event, close to a major sequence biostratigraphic surface (see below). Above this level, the proportion of angiosperm pollen versus spore taxa increases and the proportion of Andean taxa slightly diminishes (Fig. 3; Appendix 3a,b). Our sequence biostratigraphic evaluation (see below) suggests that the source of the Poaceae is situated in the local floodplains.

Palynomorphs representative of palm swamp vegetation and widely distributed freshwater communities are regularly recorded. *Botryococcus* massulae and algal remains of *Spirogyra*, *Pediastrum* and *Cosmarium* are important contributors in zones 1a and 2a. *Azolla*, a floating fern and indicator of eutrophication, occurs throughout, but dominates in opposite intervals from *Botryococcus* (the latter being typical for oligotrophic environments). Fungal spores and charcoal fragments >40 µm are common (Appendix 3a,b). Remarkably, fungal spores are abundant within pollen zone 2a but specially, *Gelasinospora*, a fire indicator is recorded at 10.6 and 16.7 m. Other fire indicators, such as charcoal fragments, are abundant in the pollen zone 1a and zone 2a.

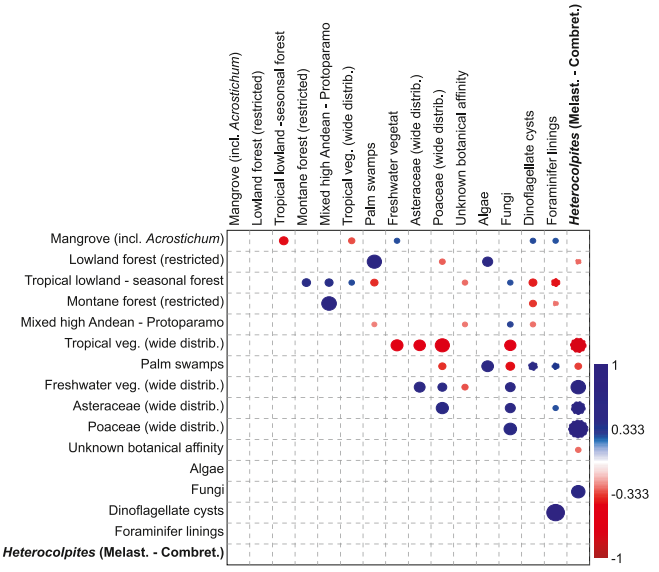

Fig. 4. Correlation between pairs of ecological groups, smoothed (3-point running average). Significant Pearson (*r*) correlation coefficients (*p*-values <0.05) are shown in blue for positive correlation and red for negative correlation. The size of the dot denotes the strength of the correlation. (For interpretation of the references to colour in this figure legend, the reader is referred to the web version of this article.)

4.2.2. Zonation and ecological reconstruction

Based on a CONISS analysis of Los Chorros sporomorph data, the record can be divided into three main pollen zones, with zones 1 and 2 each being subdivided into 2 subzones.

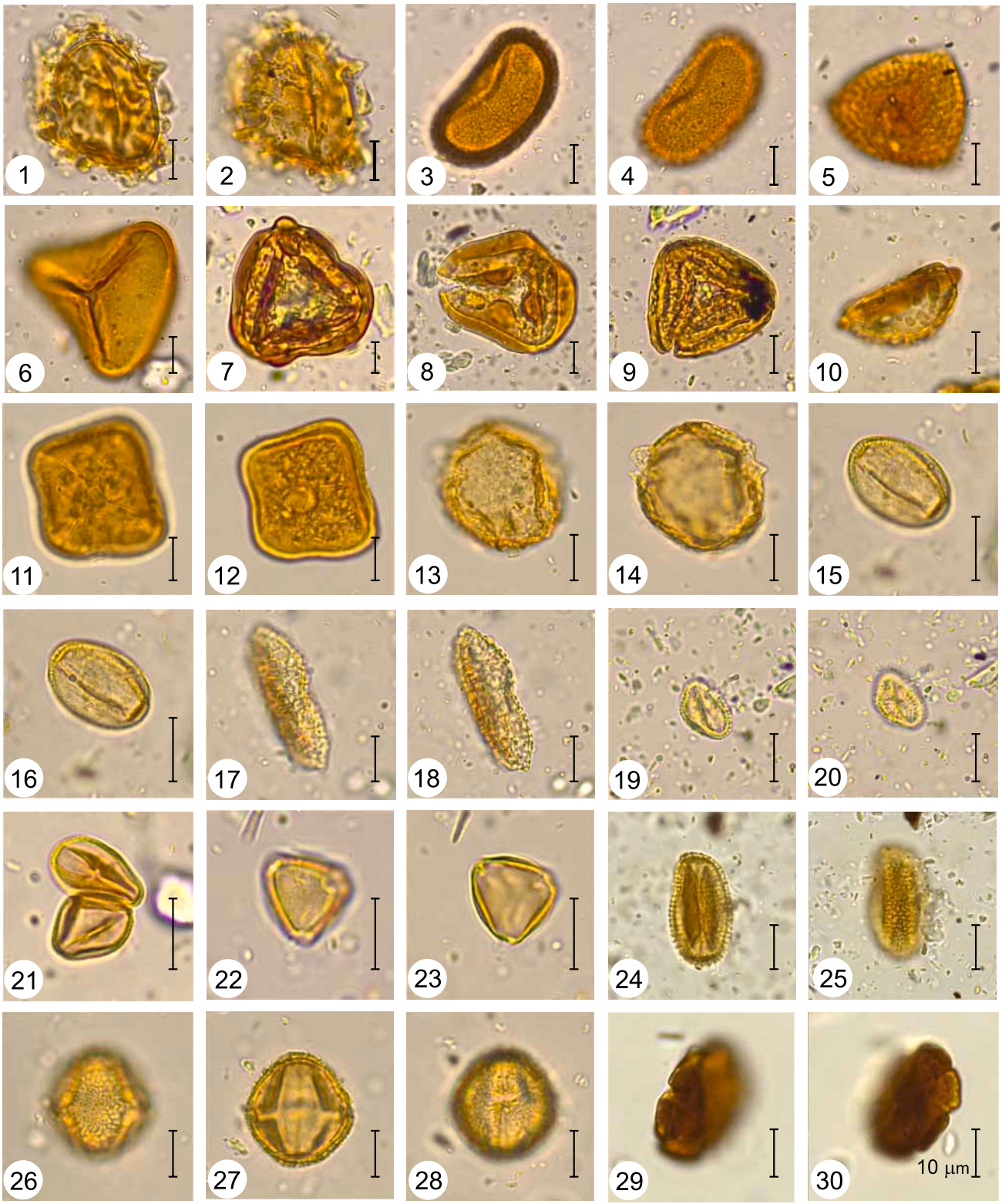

Fig. 5. Selected fossil pollen and spores taxa found in Los Chorros outcrops whose Nearest Living Relatives (NLR) develop on the high Andean forest and proto-paramos. Photographs were taken at 100× magnification. Species in "" corresponds to informal name. Information in parenthesis includes NLR, sample number and England Finder (EF) coordinate. The scale bars represent 10 µm.1–2) *Perinomonoletes* aff *Cystopteris* (Ch84, EF: G34/4), 3–4) *Perinomonoletes* aff *Thelypteris* (Ch47, EF: P16), 5) *Hamulatisporis* aff *Huperzia polycarpos* (Ch86, EF: S31/4), 6) *Cyathidites typicus* Graham 1988 (*Cyathea*; Ch86, EF: O27/3), 7–8) *Psilatriletes* aff *peruanus* Hoorn 1994 (*Jamesonia*; Ch86, EF: P19/2; Ch115–91, EF: S33/4), 9–10) *Polypodiaceoisporites* aff *Pteris* (Ch85, EF: N26/2–4; Ch 84, EF: P22/2), 11–12) *Tetraletes* aff *Sphagnum* (Ch8, EF: Q34/4), 13–14) *Byttneripollis rugulatus* D'Apolito 2016 (*Polylepis - Acaena*; Ch8, EF: O32/4), 15–16) *Perfotricolpites* "*pseudocalceolarius*" (*Calceolaria*; Ch64, EF: H25/3), 17–18) *Retimonocolpites* "*perreticulatus*" (*Puya*; Ch88, EF: H27/4), 19–20) *Retitricolporites* "*sambucoides*" (*Sambucus*; Ch86, EF: F21/4-F22/3), 21–23) *Siltaria* "*weinmanniensis*" (*Weinmannia*; Ch23, EF: G28/4; Ch88, EF: K31*2), 24–25) *Retitricolpites* "*brassicoides*" (Brassicaceae; Ch 86, EF: D24/4-D25/3), 28–28) *Echitricolporites* "*microspinosus*" (Brunelliaceae; Ch8, EF: W25-W26), 29–30) *Stephanocolpites* "*nerteroides*" (*Nertera*; Ch12, EF: C22/4).

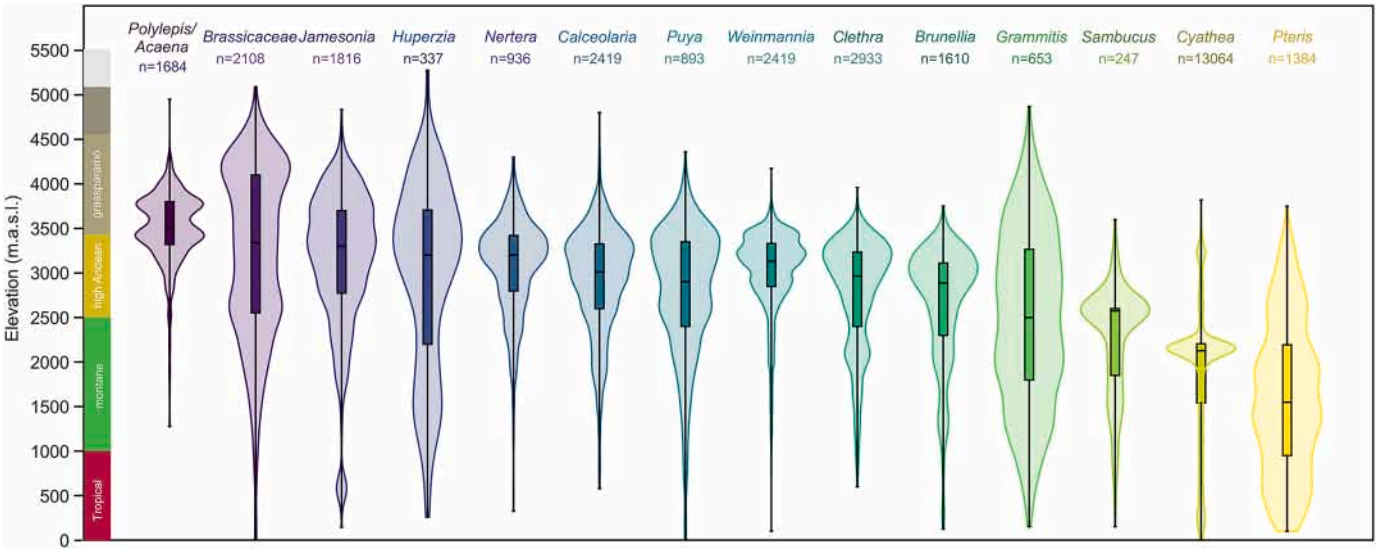

Fig. 6. Nearest living relatives (NLR) of Andean high montane/protoparamo taxa found in Los Chorros section. The elevation distribution of each genera was built using all the available specimens for Colombia, Ecuador and Northern Peru in the GBIF database (www.gbif.org) (The complete list of downloaded observations in Appendix 4).

Table 2
Phytolith data from three Miocene sites along the Amazon River.

Phytolith shape	Poaceae subfamily, genus, species
Los Chorros 42	
Trapezoidal, concave base	Anomochlooideae, Bambusoideae, Chloridoideae, Oryzoideae y Panicoideae
Trapezoidal, flat base	Bambusoideae, Chloridoideae, Oryzoideae and Panicoideae
Bilobed, convex edges	Anomochlooideae, Aristidoideae, Chloridoideae and Panicoideae
Silicified buliformes	Anomochlooideae, Bambusoideae, Chloridoideae, Ehrhartoideae, Oryzoideae and Panicoideae
Suborbicular-rectangular forms	Exclusive for the genus *Pharus* (Pharoideae)
Santa Sofia 3–91	
Buliform cells	Panicoideae, Bambusoideae, Ehrhartoideae and Oryzoideae (e.g. *Guadua, Gynerium, Homolepis, Ichnanthus, Leptochloa, Olyra Panicum, Pariana, Paspalum, Steinchisma, Streptogyna* and *Urochloa*)
Ring-shaped	***Selysia prunifera* (Cucurbitaceae)**
Santa Sofia 46	
Trapezoidal with flat base	Bambusoideae, Chloridoideae, Oryzoideae and Panicoideae

4.2.2.1. Zone 1 (2.7 to 12.4 m). This zone is subdivided into zone 1a (2.7 to 7.7 m) and zone 1b (8.1 to 12.4 m) and contains episodic occurrences of *Zonocostites ramonae* (*Rhizophora mangle*), *Z. "costamaxilalongporatus"* (cf. *R. racemosa*), *Zonocostites* sp. (*Rhizophora* sp.), and *Psilastephanocolporites schneideri* (other Rhizophoraceae; <2%), together with the presence of *Deltoidospora adriennis* (the pioneer swamp fern *Acrostichum aureum*), indicating estuarine conditions with some mangrove vegetation (0.2%). High proportions of *D. adriennis* might indicate that disturbed and open brackish habitats with mangroves occurred along three intervals, two of them in co-occurrence with foraminiferal test linings and/or dinoflagellate cysts, at 3.2 and 9.9 m.

A diverse lowland forest existed in the periphery of the site of deposition (43 taxa; 4.8% average). The most characteristic pollen types in this zone are *Echidiporites barbeitoi* (an extinct Mauritiinae), *Proxaperties tertiaria* (*Crematosperma*), *Bombacacidites lorenteae* (*Bombax*) and *Retitrescolpites irregularis* (*Amanoa*), followed by *Psilamonocolpites rinconii* (cf. *Oenocarpus-Prestoea*), *Clavainaperturites clavatus* (cf. *Sandwithia*), and *Retimonocolpites absyae* (*Virola*). Some of these elements are typically from freshwater wetlands often occurring in the transition from fully inundated to *terra firme* habitats (Urrego, 2018).

Pollen of tropical lowland-seasonal vegetation (12 taxa) is also common in this zone. The main components are *Psilatricolporites* "*costalalongporatus*" (cf. *Byrsonima*), together with taxa belonging to Faboideae, Mimosoideae, and Rubiaceae together with a continuous presence of *Striatricolporites* "*striamicroreticulatus*" (Anacardiaceae-Burseraceae-Rosaceae), and *Striatricolporites* "*burseriformis*" (Burseraceae).

Montane forest taxa (1000–3500 m) are frequent and account for 3.5%. They relate to *Siltaria* "*weinmaniensis*" (cf. *Weinmannia*), *Retitricolporites* "*sambucoides*" (cf. *Sambucus*), with some occurrences of *Echitricolporites* "*microspinosus*" (cf. Brunelliaceae) and *Psilastephanocolpites* "*nerteroides*" (cf. *Nertera*), and abundant ferns with affinity to *Cyathea*, *Dennstaedtia*, *Dicksonia*, and *Thelypteris*. The presence of 14 characteristic taxa (0.5% average) of high elevation forests and open Andean treeless areas (protoparamos) point at a high Andean sediment source situated between >3200–3500 m. This sporomorph assemblage is formed by *Byttneripollis rugulatus* (*Polylepis-Acaena*), *Psilatricolporites* "*miniclethroides*" (cf. *Clethra*), *Retitricolpites* "*brassicoides*" (Brassicaceae?) together with *Foveotriletes ornatus* (*Huperzia*), *Perinomonoletes* aff. *Cystopteris*, *Psilatriletes* aff. *Peruanus* (*Jamesonia*), *Polypodiaceoisporites*? "*proximoverrucatus*, *P. pseudopsilatus*, *P.*? *fossulatus* (all from different species of *Pteris*), *Grammitidites* (*Grammitis*) and *Tetraletes* aff. *Sphagnum*.

Abundant records of *Grimsdalea magnaclavata* (Mauritiinae), *Mauritiidites franciscoi* (*Lepidocaryum-Mauritia*) and *Psilamonocolpites amazonicus* (aff. *Euterpe*) indicate the presence of tropical lowland palm swamps, which

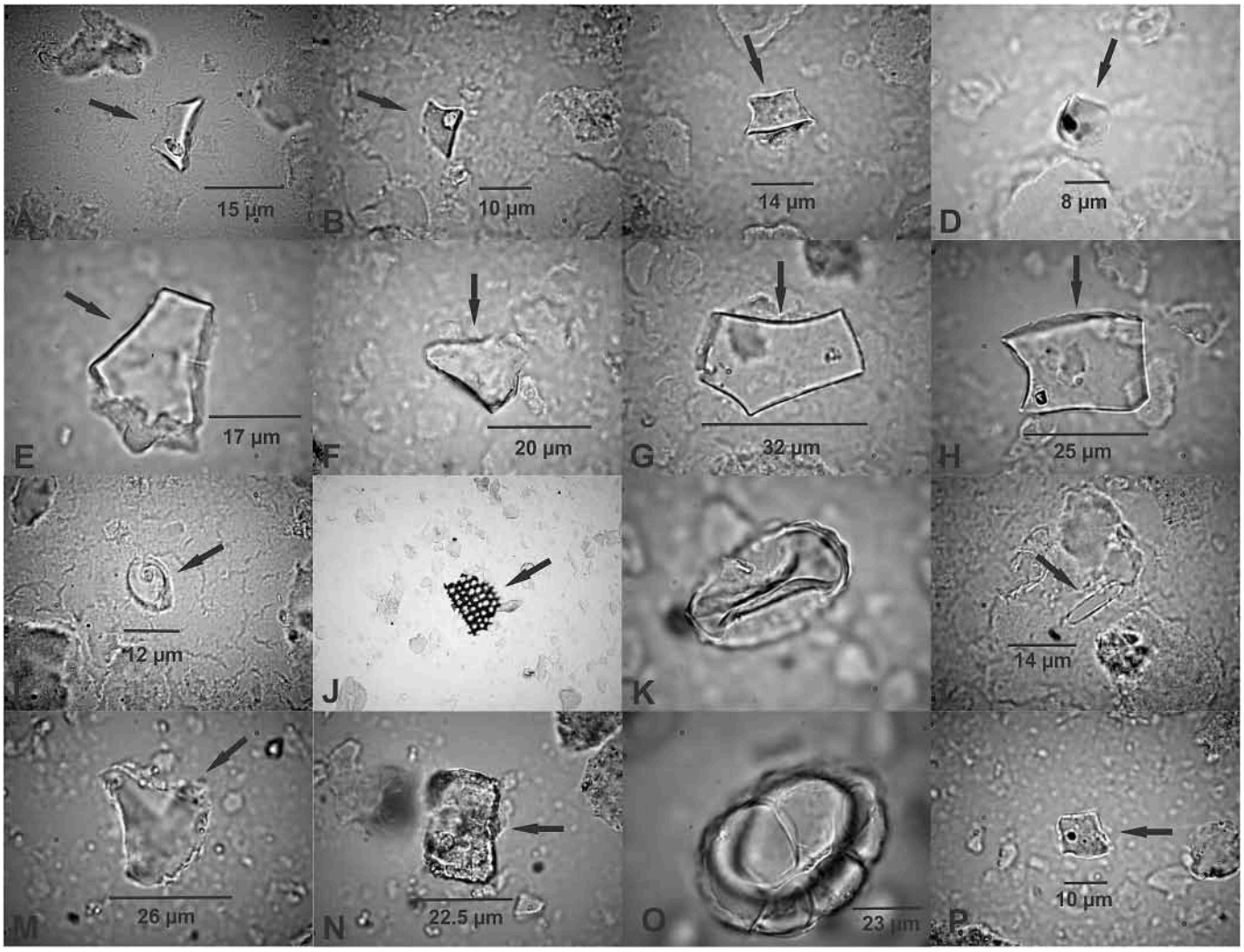

Fig. 7. Phytoliths. Los Chorros 42: A. Poaceae indet. (trapezoidal, concave base). Long. base: 15.6 µm; Central height: 5.8 µm; B. Poaceae indet. (trapezoidal flat base); Long. base: 10.7 µm; C. Poaceae indet. (trapezoidal flat base): Long. base: 14.7 µm; Long. height: 6.8 µm; D. Poaceae indet. Phytolith fragment bilobe with convex end: (100×); E. Poaceae indet. Buliform cell; Main length: 34.3 µm; F. Poaceae indet. Main length: 20.5 µm, G. *Pharus* sp. (Poaceae) (Suborbicular-rectangular); Main length: 32 µm; width: 21.5 µm; H. *Pharus* sp. (Poaceae). Main length: 25 µ; width: 22 µm; I. indet. Morphotype; Main length: 11.7 µm; J. Leave matter: (10×); K. Fossil pollen grain (100×); L. Diatom (40×); Santa Sofía 3–91: M. Poaceae indet. Buliform cell; Main length: 25.4 µm; N. Poaceae indet. Buliform cell. Main length: 22.5 µm; O. *Selysia prunifera* (Cucurbitaceae). "Ringed" form. External diameter: 47 µm; Santa Sofía 46. P. Poaceae indet. (trapezoidal flat base); Long. base: 9.8 µm.

co-occurred at the same horizons as mangrove pollen. Although more dominant, *Grimsdalea magnaclavata* often alternates with *Mauritiidites franciscoi* (*Lepidocaryum-Mauritia*) and this may suggest either changes in local ecological conditions (e.g. edaphic or hydrological), or the competition for similar biological niches among the two species. Notably, *Bombacacidites* aff. *Baculatus* (*Pachira aquatica*) occurred mostly at the beginning and end of the zone while *Echiperiporites akanthos* (*Sagittaria-Echinodorus*) was most common in the middle part. *Botryococcus* and *Azolla* are particularly abundant in the lower part of the zone.

Subzones 1a and 1b are characterized by fully developed palm swamps. However, some differences can be established between both, principally based on the higher pollen concentrations, higher abundances of *Psilatriletes* (*Cyathea*) and algal remains (*Botryococcus*, *Azolla*), and the sustained presence of charcoal along the subzone 1a, whilst in subzone 1b pollen concentrations are lower, *Heterocolpites* (Melastomataceae-Combretaceae), *Monoporopollenites* (Poaceae) and *Echitricolporites* (Asteraceae) are more abundant, as well as dinoflagellate cysts and foraminiferal test linings. These differences indicate a more disturbed subzone 1a, with frequent fires and more stagnant and eutrophic waters. Subzone 1b, on the other hand, has more marine influence and is characterized by more pioneer plants.

4.2.2.2. Zone 2 (15 to 20.9 m). This zone is subdivided into zone 2a (15 to 17.1 m) and zone 2b (19.3 to 20.9 m). Here, mangrove vegetation is scarce (0.79%), but *Deltoidospora adriennis* (*Acrostichum*) reaches its maximum at 19.3 m. More diverse mangrove establishment occurs at 16.7–17.1 m, reflected by *Zonocostites ramonae* (*Rhizophora mangle*), *Z.* "*costamaxilalongporatus*" (cf. *R. racemosa*), and *Lanagiopollis crassa* (*Pelliciera*), and at 19.8–20.9 m, where *Z. ramonae* co-occurs with foraminiferal test linings and dinoflagellate cysts; *Retitricolporites* aff. *Avicennia* only occurs sporadically.

The representation of the tropical lowland forest diminishes in this zone (31 taxa; 3.7% average), with *Clavainaperturites clavatus* (cf. *Sandwithia*), *Psilamonocolpites rinconii* (*Oenocarpus-Prestoea*), *Proxaperties tertiaria* (*Crematosperma*), *Striatricolporites* "*microestriatus*" (cf. *Tapirira*), and *Echidiporites barbeitoi* (Mauritiinae) being the principal contributors. Most of the taxa belong to Apocynaceae (11), Malvaceae (7), and Fabaceae (3) and Arecaceae (3), including *Margocolporites carinae* (*Rauvolfia*), *Psilabrevitricolporites* aff. *Lacmellea*, *Bombacacidites lorenteae* (*Bombax*), *Byttneripollis ruedae* (*Byttneria*), *Striatricolporites* aff. *Crudia*, *Striatricolporites* aff. *Dicymbe*, *Trichotomosulcites* aff *amazonicus*, *Trichotomosulcites* aff. *Bactris*, together with *Retimonocolpites absyae* (*Virola*), *Retitricolporites* "*Warszewiczia*" type.

Tropical lowland seasonal vegetation taxa slightly increase (1%), but species richness is reduced (9 taxa). *Striatricolporites* "*striamicroreticulatus*" (Anacardiaceae-Burseraceae-Rosaceae) constantly occur, together with presences of Faboideae and Caesalpinioideae and Rubiaceae taxa such as *Retitriporites* aff. *Alibertia-Duroia*, *Retitricolporites* "*microhomobrocatus*" (cf. *Platypodium-Machaerium*), *Retitricolporites* aff. *Tachigali*, and *Siltaria* "*operculatus*" (cf. *Zornia*).

The transportation from montane forest pollen into the wetland slightly increases (15 taxa; 5.3%). The main contributors being *Siltaria* "*weinmaniensis*" (cf. *Weinmannia*), *Retitricolporites* "*sambucoides*" (cf. *Sambucus*), and diverse *Cyathea*; *Ephedripites* aff. *Renzonii* (*Ephedra*) is also registered. The influence of the high Andean regions (>3200–3500 m) attain 1.4% (11 taxa) and is supported by occurrences of three taxa, particularly *Byttneripollis rugulatus* (*Polylepis-Acaena*). Representative ferns spores belonging to *Pteris* and particularly *Foveotriltetes ornatus* (*Huperzia*) occur in the middle of the zone.

A decrease in palm swamp vegetation (5.9%) suggests drying of the environment, particularly at the beginning of the zone (15.20–15.70 m). *Grimsdalea magnaclavata* still dominates, followed by lower values of *Psilamonocolpites amazonicus* (*Euterpe*) and *Mauritiidites franciscoi* (*Lepidocaryum-Mauritia*).

Overall, zone 2 is characterized by the highest values of high Andean vegetation in the record, with almost no marine influence, indicating an enhanced transport mechanism from the mountain source areas to the site. Subzones 2a and 2b can be differentiated based on the high pollen concentrations, frequent elements of Andean forests and protoparamo, abundant fungal spores, and very reduced palm swamp representation in subzone 2a, while subzone 2b is characterized by the increase of palm swamp taxa and freshwater algae, and the decrease of *Heterocolpites* spp. (Melastomataceae-Combretaceae) percentages indicating an increase of local representation of plant communities vs. allochthonous Andean elements.

4.2.2.3. Zone 3 (22.8 to 26.4 m). This zone is characterized by the lowest percentages of mangrove taxa and high-altitude elements. Mangrove vegetation slightly diminishes (0.15%), *Zonocostites ramonae* (*Rhizophora mangle*) mostly occur in the beginning of the zone, while other related taxa are scarce, except for *Deltoidospora adriennis* (*Acrostichum aureum*). Foraminiferal test linings are registered only once in the lower part of the zone. This indicates that brackish or tidally influenced conditions were not fully established.

Pollen and spores from montane forest decrease (16 taxa; 2.28%) but are still represented by diverse *Cyathea* followed by *Kuylisporites waterbolkii* (*Cnemidaria horrida)*, *Perinomonoletes* aff. (*Thelypteris*) with some *Siltaria* "*weinmaniensis*" (cf. *Weinmannia*) and *Retitricolporites* "*sambucoides*" (cf. *Sambucus*). The contribution from high Andean regions (>3200–3500 m) is also reduced (0.14%), with some representation of *Psilatricolporites* "*miniclethroides*" (cf. *Clethra*), *Retimonocolpites* "*margocolpatus*" (cf. *Puya*), *Perfotricolpites* "*pseudocalceolarius*" (cf. *Calceolaria*) together with the ferns *Pteris* aff. Spores (*Polypodiaceoisporites*), *Hamulatisporis* aff. *Huperzia polycarpos*, *Perinomonoletes* aff. *Cystopteris*, suggesting a weakening of the Andean drainages.

Pollen from tropical lowland forests include 32 taxa (3.7%). The main contributors are: *Bombacacidites lorenteae* (*Bombax*), *Clavainaperturites clavatus* (cf. *Sandwithia*), *Psilamonocolpites rinconii* (*Oenocarpus-Prestoea*), *Retimonocolpites absyae* (*Virola*), and *Proxapertites tertiaria* (*Crematosperma*). The most representative families are Apocynaceae and Malvaceae (6 each), Sapotaceae (4), and Arecaceae (3). Other less frequent elements are *Ctenolophonidites* cf. *suigeneris* (*Aspidosperma-Geissospermum*), *Bombacacidites muinaneorum* (*Bombacopsis*), *Trichotomosulcites* aff. *amazonicus*, *Tetracolporopollenites transversalis*, and *Echidiporites barbeitoi.*

Indicators of the tropical lowland-seasonal vegetation (9 taxa; 3.3%) include *Striatricolporites* "*striamicroreticulatus*" (Anacardiaceae-Burseraceae-Rosaceae), *Striatricolporites* "*burseriformis*" (Burseraceae) and the occasional input of *Retitriporites* aff. *Alibertia-Duroia*, *Retitricolporites* "*microhomobrocatus*" (cf. *Platypodium-Machaerium*), *Siltaria* "*operculatus*" (cf. *Zornia*), *Retitricolporites* aff. *Connarus* and *Psilatricolporites* "*costalalongporatus*" (cf. *Byrsonima*) among others.

The palm swamp vegetation is represented by common and abundant *Psilamonocolpites amazonicus* (*Euterpe*) and *Grimsdalea magnaclavata*, followed by *Mauritiidites franciscoi* (*Lepidocaryum-Mauritia*) and *Bombacacidites* aff. *baculatus* (*P. aquatica*). Higher values of these taxa up to 23.4 m suggest a reduction of the once extended swamp area.

4.2.3. Phytoliths as an indicator of local vegetation

At the Los Chorros and the Santa Sofia sites (Fig 1, points 1, 4) 43 phytolith specimens and at least 14 different phytolith morphotypes were found (Fig. 7). Except for one, these all belong to subfamilies of the Poaceae such as Anomochlooideae, Aristidoideae, Bambusoideae, Chloridoideae, Ehrhartoideae, Oryzoideae and Panicoideae (Table 2). These subfamilies are typical for the tropical lowlands (up to 1000 m), although some extend up to 4300 m altitude (see for distribution Kirschner and Hoorn, 2020). In addition, the presence of buliform cells points at the presence of species belonging to either *Guadua, Gynerium*, *Homolepis, Ichnanthus*, *Leptochloa*, *Olyra, Panicum, Pariana, Paspalum, Steinchisma, Streptogyna* or *Urochloa*. These taxa range from forest to open habitat (Watson and Dallwitz, 1992). To obtain more precise ecological information from the phytoliths, further study will be needed.

Interestingly, two phytolith types have parent plants that grow in the rainforest. One belongs to *Pharus* (Pharoideae, Poaceae), a genus that in Colombian Amazonia is represented by *P. latifolius,* and *P. virescens* which follows the C_3 photosynthetic pathway and grows in the understory of the tropical forest (Giraldo-Cañas, 2013). The other specimen of interest is *Selysia prunifera* (Cucurbitaceae), a liana that mainly occurs between 0 and 500 m and is associated with tropical forests that extend between Costa Rica and Amazonia. *Selysia prunifera* and *Pharus* both seem to point at the presence of tropical rainforest in the proximity of the wetland deposits. This agrees with the *terra firme* forest in the periphery of the wetland, based on sporomorph composition (see above).

4.2.4. Sequence biostratigraphic evaluation

The sequence biostratigraphic evaluation identifies each of the eight CU cycles observed in the granulometric analysis of Vonhof et al. (2003) and Vonhof and Kaandorp (2010) and which are interpreted as flood-fill packages (Fig. 8). Each cycle is reflected in the vegetation as two ecological successional phases, the first coinciding with the flood phase, and the second with the fill phase of the cycle. During the flood phase, eustatic changes promote the formation of new coastlines landward, and observed vegetation responses are thus related to the colonization of these new coastal habitats and are organised in a succession except for some cycles. Pioneer salt-tolerant species such as *Acrostichum* (*Deltoidospora adriennis*), Amaranthaceae and abundant fern spores occur at the base, indicating first stages of ecological succession, characterized by species tolerant to salty unconsolidated substrates and high light availability (González et al., 2008). This is typically followed by abundant pollen derived from obligate or facultative mangrove taxa which are associated with the presence of common foraminiferal test linings derived from monoserial and rotaliid foraminifera. The mangrove elements include the stilt-rooted mangrove *Rhizophora* (*Zonocostites ramonae*), pencil-rooted *Avicennia* (*Retitricolporites* sp.) and *Pelliciera* (*Lanagiopollis crassa*), *Pachira aquatica* (*Bombacacidites* aff *baculatus*) together with *Hibiscus* or *Thespesia* (*Echiperiporites estelae*) and *Oenocarpus* type (*Psilamonocolpites rinconii*). The chitinous test linings coincide with the horizon of greatest mangrove representation.

During the fill phase, sedimentary processes are modulated by the evolution of drainages, extensive floodplains, and the response of vegetation to fluvial dynamics. At the base of this phase, plant succession is generally dominated by pollen from open herbaceous species (Poaceae) and spores from freshwater algae and ferns, associated with fringing river channels and the accretion of new substrates (Urrego, 2018). Terra firme forests develop while depending on ocasional connections with rivers,

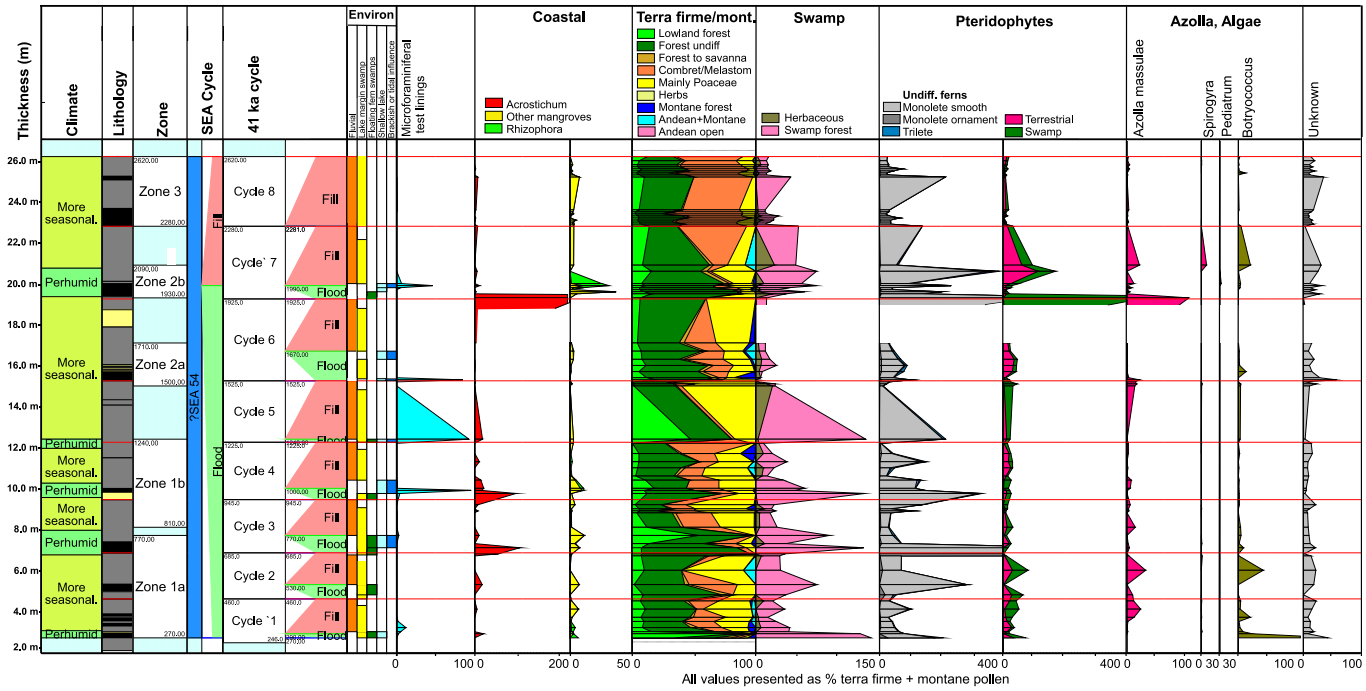

Fig. 8. Los Chorros sequence biostratigraphy presented using a 'pollen sum' of total 'terra firme + montane' pollen, with foraminiferal test linings, mangrove pollen, swamp forest pollen, spores, fern massulae, algae and indeterminate pollen presented 'outside' this sum, with scales all as % terra firme + montane pollen. The succession is divided into flood-fill packages, and the whole succession is thought to correlate to Cycle SEA54 of Morley et al. (2021). Palynological zones based on CONISS are shown together with probable trends in regional climate and local depositional environment.

Table 3
Lithological and palynological characterisation of depositional cycles.

Cycle	Lithology	Flood phase	Fill phase	Climate
Cycle 8	Lignite with large wood fragments and molluscs followed by rhythmically laminated sandy mudstone and a thin lignite bed.	Not well characterized	Not well characterized, *Euterpe* swamps.	Mainly seasonal climates, but pattern obscured by large sample gap. Common *Heterocolpites* spp. may reflect the presence of Combretaceae in deciduous forest.
Cycle 7	Lignite at base with wood fragments and molluscs, followed by burrowed sand-mudstone intercalations (heterolithics?), a bone bed and weathered sandy mudstone above.	Initially a freshwater lake with *Acrostichum* and the floating ferns *Ceratopteris* and *Azolla*, followed by mangroves with *Rhizophora*.	Swamps with parent plant of *Grimsdalea magnaclavata* and *Euterpe* present throughout, fern swamps well developed in early stage, with some lacustrine development with *Botryococcus*.	Strong perhumid climate during flood phase, and probably more seasonal during fill phase.
Cycle 6	Lignite at base with shell bed and abundant wood, followed by sandy mudstone with bivalve bed at base, overlain by sands and mudstones with ripple marks	Freshwater swamps poorly developed but well-developed mangrove swamps present at time of maximum flood	Poorly characterized due to sample gap.	Mainly probable seasonal climates but little evidence for changing climates, due to large sample gap.
Cycle 5	Sand at base, followed by silty and sandy bioturbated mudstones.	Swamp forest with *Grimsdalea, Mauritia* and *Euterpe* and ferns together with minor mangroves.	Poorly characterized due to sample gap.	Perhumid during flood phase, and more probable more seasonal climate during fill phase.
Cycle 4	Lignite and mollusc bed over erosional surface, followed by mudstone with molluscs and sand-shale laminations (heterolithics?) showing bioturbation,	Swamp forest with *Grimsdalea* and *Mauritia*, with common ferns, including *Acrostichum*, followed by a pulse of mangroves.	Minor swamp forest with *Grimsdalea* and possible grass swamps.	Weak perhumid climate during flood phase, and probable more seasonal climate during fill phase.
Cycle 3	Lignite at base with wood fragments, followed by mollusc bed, calcareous concretions (caliche?) in mudstone and sandy mudstone above.	Swamp forest dominated by *Grimsdalea magnaclavata* with subordinate *Mauritia* and *Euterpe* with abundant ferns with *Acrostichum* and some mangroves	Minor swamp forest with *Grimsdalea magnaclavata* and possible grass swamps.	Strongly perhumid climate during flood phase, and probable more seasonal climate during fill phase.
Cycle 2	Lignite at base, grading up to mudstone.	Swamp forest *with Grimsdalea magnaclavata*, *Mauritia* and *Euterpe*, and subordinate mangroves	Swamp forest with *Grimsdalea,* ferns and possible grass swamp. Lacustrine facies with *Botryococcus*.	Weak perhumid climate during flood phase, and probable more seasonal climate during fill phase.
Cycle 1	Lignite at base with wood fragments and burrows, grading to silty mudstone with thin lignite horizons and concretions.	Extensive swamp forest dominated by *Grimsdalea magnaclavata*, and ferns, including the climbing fern *Lygodium microphyllum,* lacustrine facies with *Botryococcus* followed by weakly developed mangroves at time of maximum flood.	Possible grass swamps.	Weak perhumid climate during flood phase, and probable more seasonal climate during fill phase.

while large areas of swamps establish on more clayish substrates. Typically, swamp palm forests are dominated by *Mauritia-Lepidocaryum* (*Mauritiidites franciscoi* group), *Euterpe* (*Psilamonocolpites amazonicus*), and an extinct mauritioid palm which produced the fossil pollen type *Grimsdalea magnaclavata* (Bogotá-Ángel et al., 2021).

As indicated above, pollen from montane sources is more common in zone 2a, which approximately coincides with the maximum flood of cycle 6. This could be explained by the Neves effect (Chaloner and Muir, 1968) whereby in a large water body, the representation of upland taxa increases with distances from the shoreline, and testifies to the great expanse of the Pebas lakes at the time of maximum flood. Increased values of montane taxa also occur during the flood phase of Cycle 1.

Obligate swamp elements are of limited occurrence within the upper part of each cycle, although freshwater algae, such as *Botryococcus, Pediastrum* and *Spirogyra* are variously present in low numbers. It is also likely that Poaceae marshes may have been present at the time of deposition of the upper part of cycles 1–7, and within cycle 8. Molluscs are mostly associated with the lignite, or the interval immediately following, sometimes forming actual shell beds.

Within the restraints of the sample set, the eight cycles are mostly also paralleled by assemblage changes which suggest fluctuating climates, from perhumid during the flood phase, suggested by the dominance of the lowland perhumid forest group, to slightly more seasonal during the fill phase, where forest elements characteristic of forest to savanna vegetation is regularly present in low frequencies (Fig. 8). *Heterocolpites* spp. are particularly characteristic of the fill phase. Although Combretaceae and Melastomataceae can occur in a wide variety of environments from high mountains to mangroves, their abundance here suggests a local source, either from *terra firme* vegetation or from swamps. However, the palynomorph groupings cross-plot shows a negative correlation with palm swamps, fungi and algae (Fig. 4, Appendix 5b), suggesting a source away from wet lake margin settings, and a mainly *terra firme* source. It is suggested that the *Heterocolpites* spp. were mainly produced by members of the family Combretaceae from seasonal forests, supporting the suggestion that the 'fill' phase for each cycle was characterized by more seasonal climates. Details of the vegetation present during the flood and fill stage of each cycle, and also suggestions of climate change, are presented in Table 3and Appendix 8.

The palynological zones suggested from CONISS, discussed above coincide closely with the scheme of flood-fill cycles, but do not identify all the cycles (Fig. 3). Zone 1a coincides with Cycles 1, 2 and the Cycle 3 flood phase, with zone 1b corresponding to the Cycle 3 fill phase and Cycles 3 and 4. Zone 2a corresponds to the Cycle 6 flood, during which time freshwater swamps were suppressed compared to earlier cycles. Zone 2b coincides with the Cycle 7 flood, which is the most pronounced flood within the Los Chorros succession, and Zone 3 with Cycle 8, which does not have a 'flood' phase, and during which time swamps with *Euterpe* predominated. (Appendix 8).

4.3. Mollusc results and ecological interpretations

In total 63 mollusc taxa were encountered and are listed in Appendix 6. The fauna is dominated by representatives of a few families, viz. Cochliopidae, Corbulidae and freshwater Cerithioidea. Two assemblages are evident (Fig. 9a). Assemblage 1 (samples F16, F18, F19, F23, F24, F27A, F27C) is dominated by *Tryonia nuttalli/scalarioides* (68%) with common *Aylacostoma browni* (8%) and *Dyris ortoni* (8%). Further characteristic taxa are *Toxosoma grande* and *Anadontites capax/batesi*. This assemblage contains an admixture of fluvial taxa (pearly freshwater mussels and freshwater cerithoideans) and some Pebasian endemics. The assemblage has similarities with the tall-*Dyris* assemblage from Santa Rosa de Pichana (Wesselingh et al., 2006b) that represents early transgressive outer deltaic settings to shallow lacustrine settings. Assemblage 2 (samples F12, F13, F15, F22, F26, F31, F41, F42, F52) is dominated by often well-preserved Pebasian endemic cochliopid and pachydontine species. Most common are *Pachydon trigonalis* (45%), *Onobops communis* (11%) and *Toxosoma contortum* (9%). Characteristic species of this assemblage are smaller endemic cochliopid species (including *Dyris huberti*, *D. elongatus*, *D. romeroi, Sioliella* spp.) and endemic pachydontine bivalve species. The assemblage has the general composition on genus level and fine preservation in common with the small *Dyris* assemblage described by Wesselingh et al. (2006b). The latter assemblage represents clear water below the storm wave base in late transgressive settings of the Miocene Amazonian wetland. The very rare occurrence of marine species (*Nassarius wesselinghi*, *Melongena woodwardi*) in samples F41 and F42 indicates slightly elevated salinities (possibly oligohaline: Vonhof et al., 1998, 2003). In several of the samples (including F41) the faunas are dominated by minute-sized specimens of common species such as *Pachydon trigonalis* and *Onobops ventricosus*. In some instances, fine strings with juvenile paired bivalves in butterfly orientation were observed. This implies the occurrence of (seasonal) anoxia. These levels might correspond to maximum flooding phases. Sample F21 is an atypical admixture of Assemblage 1 fluvial type and Assemblage 2 lacustrine type taxa with the common occurrence of the cerithoidean *Charadreon glabrum*.

The stable isotope data provide information on the water chemistry

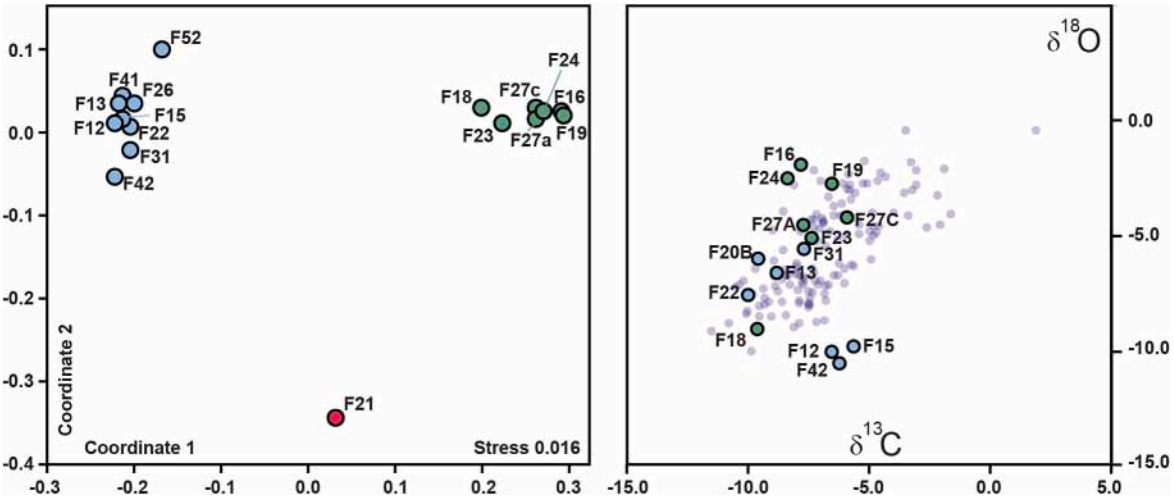

Fig. 9. (A) NMDS (chord) ordination of mollusc samples. (B) Stable oxygen and carbon ratios for Los Chorros mollusc samples. Colors correspond to assemblages in fig. (A). Light gray ratios in background from Pebas Formation molluscs Santa Rosa de Pichana (Wesselingh et al., 2006b).

(Figs. 9b and 10). Oxygen, and especially carbon, isotope ratios are very negative and correspond reasonably well to ratios measured from Santa Rosa de Pichana (Wesselingh et al., 2006b). The two Los Chorros clusters have similar $\delta^{13}C$ ratios, but cluster I has higher $\delta^{18}O$ ratios (range − 2 to −5‰) than cluster II (range − 5 to −11‰). In summary, the very low $\delta^{18}O$ values identified in lacustrine species is incompatible with brackish water, and instead points to freshwater conditions. Furthermore, $\delta^{13}C$ ratios are relatively high and similar to those reported from depositional cycles in Santa Rosa de Pichana (Wesselingh et al., 2006b), pointing to long residence times in the waters (Vonhof et al., 1998). As yet, there is no clear indication of possibly increased salinities in the isotope data of Assemblage 2. All stable isotope data in principle support freshwater conditions, whether the higher $\delta^{18}O$ values in one cluster mean slightly more marine influence or more evaporation in the freshwater system is impossible to determine based on these data alone.

4.4. Geochemistry

4.4.1. Bulk organic geochemical parameters

Total organic carbon (TOC) generally varies between 0.3 and 7 wt%, except for the lignite layers where TOC exceeds 15 wt%. The carbon isotopic composition of TOC ($\delta^{13}C_{TOC}$) ranges from −25 to −30‰, consistent with a C_3-dominated landscape, with no major excursions in the section (Fig. 10a,b).

4.4.2. Lipid biomarkers

Biomarker lipid concentrations were only quantifiable in the lignites where TOC exceeded 8 wt% (see Appendix 7a). In these beds, fatty acids were the most abundant lipids, of which C_{28} and C_{30} were dominant. Concentrations of the sum of long chain fatty acids (C_{26}-C_{34}) range from 0.3 to 1.3 mg/g TOC. In addition to hopanoids, friedelin (~7–131 μg/g) and tetrahymanol (~9–128 μg/g) were detected in variable concentrations in the ranges of ~0.007–0.131 μg/g TOC and ~ 0.009–0.128 μg/g TOC, respectively.

GDGTs were quantifiable in most samples (Appendix 7b, A1). GDGT concentrations range from 0.2–30 μg/g TOC for crenarchaeol (Fig. 10c) and 8–250 μg/g TOC for the sum of all branched GDGTs (Fig. 10d). The BIT index varies between 0.4 and 1.0 (Fig 10e), MBT between 0.8 and 0.9, and DC between 0.1 and 0.3. Neither GDGT concentrations nor calculated indices show systematic variation with stratigraphic height (Fig. 10).

4.4.3. Major and trace element geochemistry

Concentrations for major and trace elements of selected samples are given in Appendix 7c. SiO_2 is the dominant constituent of most of the selected samples, with values ranging from 57.14 to 66.01%. The exceptions are samples CH 37P (31.28% SiO2) and CH 13 (7.12%), which have high loss on ignition (LOI) values (54 and 83%, respectively). The Al/Si atomic ratios of analyzed sediments range from 0.22 to 0.31 (mean = 0.26). While sparse measurements for major and trace elements ($n = 7$) make robust correlations difficult, we note no correlation with Hf and Zr values (slope not significantly different from zero; $P = 0.26$ and $R^2 = 0.25$ for each due to close correlation between Hf and Zr).

The Chemical Index of Alteration (CIA) (Nesbitt and Young, 1982) which measures the degree of weathering of feldspars relative to unaltered protoliths, is presented in Appendix 3c. Overall CIA values range from 49 to 86, with a mean of 77.

Appendix 7c reports the REE concentrations measured in the sediment samples by ICP-MS after alkali fusion (see also plot in Appendix 7b). The Nd and Sm concentrations of samples that were determined both by ICP-MS and TIMS are within 10% of each other. The abundances are normalized to Post Archean Australian Shales (PAAS) (Taylor and McLennan, 1985; McLennan, 2001) and presented Appendix 7b, A2 together with the Eu/Eu*, in which Eu/Eu* = EuN/(SmN × GdN)1/2

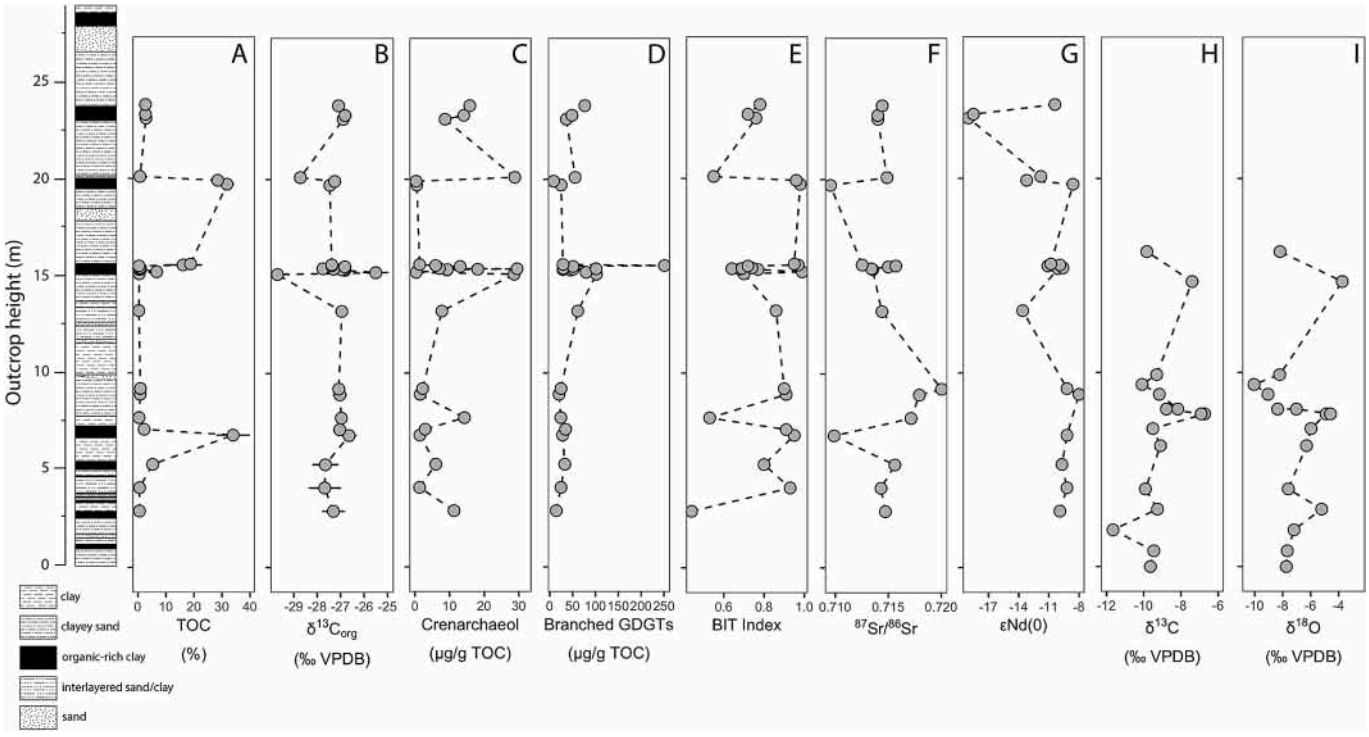

Fig. 10. Composite lithological column of the Los Chorros section. **a)** Total organic carbon weight percent; **b)** Carbon isotope composition of organic carbon; **c)** crenarchaeol concentrations in TOC; **d)** branched GDGT concentrations in TOC; **e)** the BIT index; **f)** The $^{87}Sr/^{86}Sr$ isotope ratio; **g)** Neodymium isotope ratio; **h)** carbon isotopes of mollusc shells; and **i)** oxygen isotopes of mollusc shells.

where N refers to the chondrite value (Condie, 1993).

Compared with PAAS, the Los Chorros sediments have slightly lower Eu anomalies (higher Eu/Eu* values, 0.68–0.73) and, except for two lignite samples, yield a narrow, flat REE pattern. Cr/Th, Zr/Sc and Th/Sc values are also presented in Appendix 7c with PAAS values for reference. Cr/Th values (4.28–5.82), Th/Sc values (0.67–0.86), and Zr/Sc values (6.74–22.56) of Los Chorros sediments are comparable to upper continental crust (UCC). The Al/Si atomic ratio is not well correlated with Eu/Eu* ($P = 0.19$; $R^2 = 0.31$), Th/Sc ($P = 0.82$; $R^2 = 0.01$), nor Cr/Th ($P = 0.06$; $R^2 = 0.53$). The Al/Si ratio is weakly negatively correlated with Zr/Sc ($P = 0.013$, $R^2 = 0.74$), but this result is sensitive to the sample size of the regression.

4.4.4. Nd—Sr isotope chemistry: Andean and cratonic sediment sources

Sr and Nd isotope ratios at Los Chorros cluster near the range of the high Andean Plateau (Altiplano) values presented in Roddaz et al. (2005) in western Amazonian sediments (Fig. 11) (compiled from Pinto, 2003, thesis). Generally, Los Chorros Sr and Nd isotope ratios indicate an Andean provenance for these sediments. This interpretation is supported by other provenance indicators like Eu/Eu*, Zr/Sc, Th/Sc, and Cr/Th. Isotope ratios and trace elements from Los Chorros share similar values to younger, middle Miocene Pebas deposits near Iquitos, Peru (Roddaz et al., 2005), and suspended particulate matter (SPM) in the Solimões River (Viers et al., 2008). Two samples placed at upper part of the section (at 12 and 22 m) have anomalously low $\varepsilon_{Nd(0)}$ values (<-18), which we interpret to reflect a cratonic origin. The peaks in Sr ratios (0.709) at 7 m and 20 m (Fig. 10) we interpret as influence of marine water.

The $^{87}Sr/^{86}Sr$ values range between 0.70955 and 0.72004 (Fig. 10F) and show no trend with stratigraphic height. Nd-model ages of the sediments range from between 0.99 and 2.35 Ga with an average of 1.49 Ga. Overall, the $^{87}Sr/^{86}Sr$ isotopic ratio and the $\varepsilon_{Nd(0)}$ values do not significantly correlate ($P < 0.01$) with Eu/Eu*, Th/Sc, Al/Si, Cr/Th, Zr/Sc, nor CIA.

4.4.5. The effects of sorting and weathering

REE and Eu anomalies, Th/Sc and Cr/Th elemental ratios, and Nd—Sr isotopic compositions have proven useful tools for determining the composition sediment source areas (Taylor and McLennan, 1985; Basu et al., 1990; Condie and Wronkiewicz, 1990; McLennan et al., 1993; Fedo et al., 1996; Hassan et al., 1999; Cullers, 2000; Condie et al., 2001; Lee, 2002; Roddaz et al., 2005, 2006). However, before drawing conclusions on the provenance of sediments, the influence of sedimentary processes such as grain size sorting and chemical weathering on the chemical composition of sediments must be carefully evaluated.

Sedimentary sorting can preferentially concentrate heavy minerals like zircon and monazite that are usually associated with quartz dilution in the coarser fraction. This accumulation in turn can modify the concentrations of certain elements (REE, Th, Zr and Hf) and elemental ratios (Cr/Th, Th/Sc) that are classically used to determine sediment provenance (McLennan et al., 1993). For instance, enrichment in zircon will enrich the sediment in Zr, Hf and HREE, whereas enrichment in monazite will enrich the sediments in REE (McLennan et al., 1993). Enrichment in these elements is not found in Los Chorros samples, when compared with PAAS (Appendix 3c). Further, Al/Si ratios, which can be considered a proxy for Amazon sediment grain size (Bouchez et al., 2011) do not correlate with Zr, Hf, or Zr/Sc values, suggesting grain size sorting did not control sediment geochemistry of provenance indicators.

Post-depositional chemical weathering can also modify the geochemistry of the sediments, independent of changes in provenance. CIA is positively correlated with Th/Sc ($P = 0.008$, $R^2 = 0.79$) and negatively with Eu/Eu* ($P = 0.006$, $R^2 = 0.80$), but these correlations are solely due to the low-CIA outlier (CH 13, CIA = 48.6). When the outlier is removed, CIA is not significantly correlated with Th/Sc ($P = 0.25$; $R^2 = 0.31$) nor Eu/Eu* ($P = 0.50$, $R^2 = 0.12$). The absence of any correlation between CIA values and other provenance indicators ($^{87}Sr/^{86}Sr$, $\varepsilon_{Nd(0)}$) suggests that post-depositional chemical weathering did not control the chemical composition of the sediments. Instead, provenance indicators likely represent the chemical signature of the source area. As noted above, these correlations rely on a relatively small dataset ($n = 7$) and future work should test these results with improved data resolution.

5. Discussion

5.1. Paleoenvironments in western Amazonia

5.1.1. Palynomorphs as environmental indicators

Pollen and spores support the scenario of a local flora that formed in a transition from wetland shore to aquatic conditions, but also point at the presence of a forest in the periphery of the wetland (Hoorn, 1994a; Jaramillo et al., 2010; Nogueira et al., 2013; Leite et al., 2017; Bogotá-Ángel et al., 2021). Both the palynological data from the Los Chorros and Santa Sofia sites (this work and Hoorn, 1994a), suggest that *Grimsdalea* and other Mauritiinae palms were common on the wetland shores (see also Bogotá-Ángel et al., 2021). In the same manner as the present day (Urrego, 2018), these palm swamps were growing in areas isolated from fluvial influence, where the natural succession was interrupted by freshwater and nutrient-rich sediment pulses. These palms were part of an ecological succession that shifted towards Poaceae and *Azolla*-dominated aquatic vegetation. The lacustrine conditions, are supported by freshwater algae such as *Botryococcus* and *Pediastrum*, and floating ferns such as *Azolla* and *Ceratopteris,* and in agreement with biomarker and mollusc data (Hoorn, 1994a; Wesselingh et al., 2001; Vonhof et al., 2003; Wesselingh et al., 2006b).

Botryococcus is indicative for episodes of clear, oligotrophic waters (see also Hoorn, 1994a; Jaramillo et al., 2010, 2017; Sá et al., 2020), whereas *Azolla* is typical in tropical and temperate freshwaters, and an indicator of increased phosphorus and nitrogen levels (e.g. Temmink et al., 2018). As such, *Azolla* is a good indicator of eutrophication of the system, a process that is likely due to the input of nutrient-rich waters from the Andes but also related to the high production of organic waste from the many organisms inhabiting the aquatic system. Although *Azolla* occurs throughout the entire Los Chorros section, it is more common in zones 1–2 (Fig. 3, freshwater vegetation). Modern soil studies in Amazonia have shown that phosphorus generally decreases from west to east, and this gradient has an important influence on modern forest composition in the region (Quesada et al., 2010, 2012). Our palynological data suggest that significant phosphorus input into the sedimentary system date back at least to the middle Miocene.

When the algal signatures at Los Chorros are compared with signals from the vast mid-Cenozoic freshwater lakes of Southeast Asia (Morley and Morley, 2013), there are major differences. The main one being that although there is clear evidence from molluscs and sedimentology for lacustrine conditions, the representation of freshwater algae is a mere fraction of the algal records from lakes that filled the giant rift valleys of Sunda. In the mid-Oligocene lakes represented for instance by the Tra Tan Formation of the Cuu Long Basin to the south of the Mekong Delta, a combination of freshwater dinocysts, *Pediastrum* and *Botryococcus* typically contribute more than 95% of the total palynomorphs recorded during times of flood (Morley et al., 2019). On the other hand, in the North Belut field in the West Natuna Basin within the late Oligocene Barat and Udang Formations, studies of conventional cores show an inverse relationship between the representation of freshwater algal palynomorphs and the brackish foraminifer *Miliammina fusca* (Morley et al., 2007), and it may be that salinity fluctuations in the Miocene Amazonian wetland were in part responsible for the low representation of freshwater algal palynomorphs. Other possibilities are that the algal niche in the Miocene wetland was dominated by taxa that do not leave a palynological record, such as diatoms, or freshwater dinoflagellates that produced vegetatively, or produced cellulose-walled cysts.

Although a comparison between the vegetation in the Miocene Amazonian wetland with that of the modern *varzea* is tempting, there are major differences that confirm the Miocene wetland has no modern analogue. The modern *varzea* system is regulated by the annual flood

pulse (Junk, 2013), and common elements in the modern varzea floodplain forest include *Cecropia*, *Iriartea*, *Mauritia*, *Ilex*, *Pseudobombax*, *Acalypha*, *Luehea/Laetia*, and Poaceae. However, with the exception of *Mauritia* and the Poaceae, these taxa are rare or absent in the Miocene sediments (e.g. see Gomes et al., 2021; Akabane et al., 2020). Notably, Gomes et al. (2021) also observed that the Holocene environments in western Amazonia are much more heterogeneous in terms of species composition and vegetation types than the Miocene Amazonian wetland, which they considered to be more homogeneous.

5.1.2. *Geochemistry and molluscs as environmental indicators*

The organic matter in the sediments carries ample evidence for in situ swamp forest and swamp channels with reworked plant material, as well as lignite beds accumulating in situ, rather than through channel erosion (Hoorn, 1994a). The presence of *Amazoniconcha immanis* in such beds, a very large-sized terrestrial snail, further confirms this suggestion (Wesselingh and Gittenberger, 1999). In addition, the geochemical signatures of the organic carbon also point at a terrestrial source. GDGT distributions in lignite layers differ from the other sediments and show similarities with modern day soils as expressed by DC, MBT and BIT values (Fig. 10). These organic rich layers also contain high amounts of long-chain fatty acids, and friedelin was detected. Friedelin is a pentacyclic triterpene that is present in leaves, bark, and stem of a variety of terrestrial higher plants (Chandler and Hooper, 1979) and in fossil leaves of both angiosperms and conifers (Otto et al., 2005). The presence of friedelin, and the dominance of the long-chain fatty acids, along with GDGT distributions are known to occur in lowland soils and indicate that most of the organic matter in the lignite layers is derived from terrestrial plants (Zell et al., 2013a).

Geochemical signatures of terrestrial organic carbon do not, however, require that lignite layers exclusively represent ancient soil deposits. Instead, evidence points to these layers being preserved in oxygen-stressed, freshwater conditions and thus may reflect penecontemporaneous reworking. First, small amounts of tetrahymanol were detected in the lignite samples. Tetrahymanol is produced in the water column by ciliates when, due to anoxic conditions, their diet is deprived of sterols and they must feed on alternative food sources like green sulfur bacteria (Sinninghe Damsté et al., 1995). The presence of tetrahymanol thus points to a stratified water column where low oxygen levels likely helped preserve transported terrestrial organic carbon. In addition to tetrahymanol, shallow-burrowing molluscs adapted for dysoxic conditions have been identified in organic-rich lignite layers, providing further evidence for aquatic deposition (Wesselingh et al., 2001; Wesselingh et al., 2006b). Oxygen isotope ratios in these mollusc shells (~ −7‰ VPDB) are significantly lower than ocean water, providing strong evidence for a predominantly freshwater system with minimal marine influence (Wesselingh, 2006; Wesselingh et al., 2006a, 2006b), as was also shown by Sr ratios (Vonhof et al., 1998, 2003). It appears that most of the marine indicators occur in the deeper water facies of these cycles, suggesting possible salinity stratification, and that marine influence was most pronounced at higher base levels.

Although the deposits at Los Chorros mostly reflect freshwater conditions, molluscs such as *Nassarius* and *Melongena* (at 1 m in the section) point to transient brackish influence. Sr isotope data from other mollusc taxa, however, restrict Los Chorros salinities to oligohaline at most (Vonhof et al., 2003). The presence of marine palynomorphs (foraminifera and dinoflagellate cysts) in some intervals also suggests a connection with the marine environment albeit with low salinities between 0 and 10 psu (Hoorn, 1994a; Boonstra et al., 2015). Although mangrove pollen are relatively rare at Los Chorros, they are exceptionally rich in the lower Apaporis River area (Colombia), suggesting actual growth of mangroves in certain parts of Miocene Amazonia (Hoorn, 2006; Sciumbata et al., 2021). Other studies also report mangrove occurrences (Jaramillo et al., 2017; Linhares et al., 2017, 2019; Sá et al., 2020), but mangrove taxa at these sites are generally less common than at the lower Apaporis sites. Rare occurrences of calcareous microfossils support the hypothesis that episodic coastal conditions permitted different generations of foraminifera to coexist at the limit of their environmental tolerance (Boonstra et al., 2015).

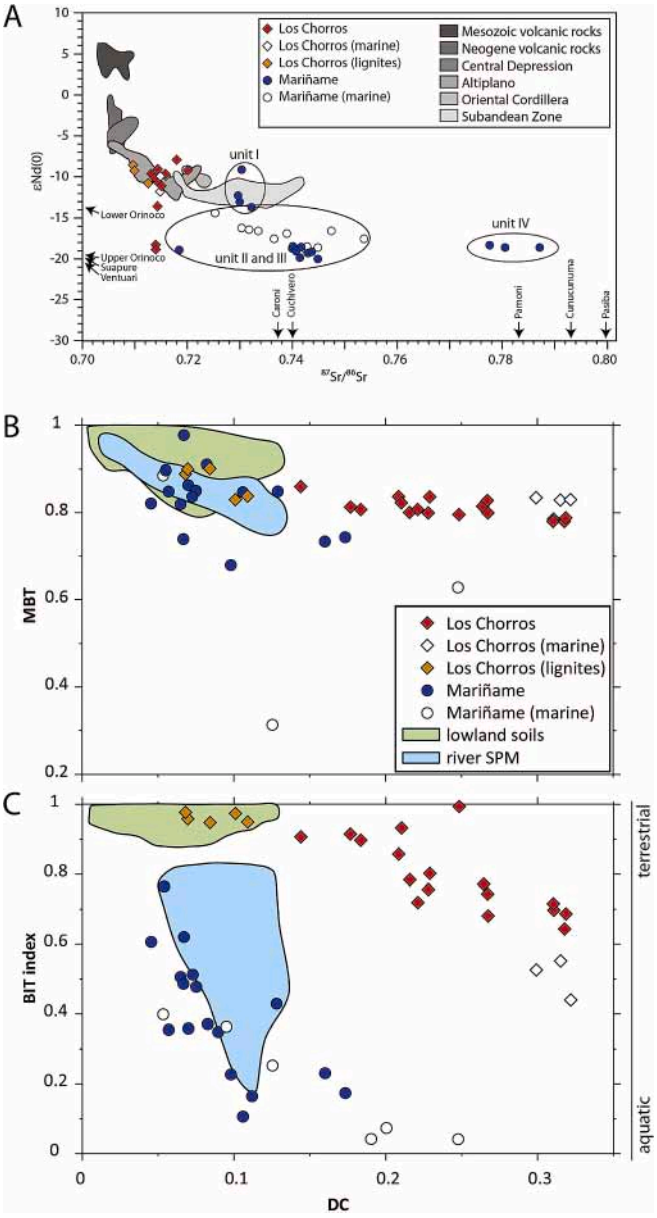

Fig. 11. Provenance reconstruction based on Sr and Nd analysis from middle Miocene Los Chorros site and comparison with a dataset from the latest early Miocene Mariñame site (Salamanca et al., 2016). **b)** crossplot of MBT and DC and **c)** BIT and DC with representative polygons for modern Amazon suspended particulate matter in rivers (SPM) (Zell et al., 2013a, 2013b) and lowland soils (Kim et al., 2012; Zell et al., 2013a).

Directly above some of the larger lignite layers, BIT index values are generally lower (Fig. 10). While a decrease in the BIT index may point to marine influence, the lowest BIT values in our study are consistent with branched GDGTs produced by in situ riverine production in Amazonia (Zell et al., 2013a, 2013b) and are higher than BIT values at the nearby Mariñame site (Salamanca Villegas et al., 2016; Fig. 11) and Saltarin site in Los Llanos, where there is further evidence of marine influence (Jaramillo et al., 2017). Each interval with a lower BIT index coincides with foraminiferal test linings. As mentioned above, Vonhof et al. (2003) showed that the Miocene Amazonian waters had episodes of oligohaline water conditions (see also Fig. 10h,i). This, in combination with the pollen and biomarker data, suggests that episodic shifts from oligohaline to freshwater conditions occurred in the Miocene wetland system.

5.2. Sediment provenance in western Amazonia

The modern Amazon drainage basin has an Andean provenance with $^{87}Sr/^{86}Sr$ ratios between 0.713 and 0.717 in river suspended particulate matter (Viers et al., 2008) and between 0.705 and 0.720 for dissolved Sr in river water (Palmer and Edmond, 1992; Santos et al., 2014). $\varepsilon_{Nd(0)}$ values in suspended sediments vary between −8.9 and − 9.9 (Viers et al., 2008). Samples from the middle Miocene Los Chorros site have a predominantly Andean signature, but with a craton-derived interval towards the top of the sedimentary succession. These data suggest that throughout the Miocene both the Andes and Amazon craton acted as sediment sources for the Miocene Amazonian wetland, as indicated also by pollen and spores (see above). Moreover, sediment successions observed in the periphery of the wetland, such as at Mariñame (early Miocene) and along the lower Apaporis River (middle Miocene) (Fig. 1), suggest that extensive, craton-derived fluvial environments existed here, and may have connected the craton with the wetland (Hoorn, 2006; Salamanca Villegas et al., 2016).

Sporomorphs from the Los Chorros site unmistakably point at a high montane sediment source. Pollen and spore taxa typical of the high Andean montane forest and open Andean vegetation are for instance Bruneliaceae?, *Cnemidaria horrida, Cyathea latevagans,* aff. *Thelypteris, Sambucus* and *Weinmannia,* which are representative of mountains reaching up to 3000–3200 m, whereas alpine taxa such as Brassicaceae? *Calceolaria*? *Clethra, Cystopteris-Hypolepis*, aff. *Cystopteris*, *Jamesonia*, *Huperzia, H. polycarpos, Polylepis-Acaena, Pteris,* and *Sphagnum* typically occur at altitudes above 3200–3500 m (Flantua et al., 2014; Bernal et al., 2015; www.gbif.org) (see Fig. 6 for elevational ranges). Together, these taxa all point to a hinterland with mountains reaching above 3 km elevation. We note that in the Miocene sediments of the 105-AM Well (Solimões Basin; D'Apolito 2016; Jaramillo et al., 2017) the mountain taxa *Polylepis* (*Byttneripollis rugulatus*) and *Daphnopsis* (*Thymelipollis amazonicus* sp. nov.) were also recorded, confirming the widespread presence of Andes-derived taxa in the Miocene infill of sedimentary basins in western Amazonia.

In 2014, Luebert and Weigend suggested that migration of cold-tolerant taxa along the tropical Andes started as early as 23 Ma (Luebert and Weigend, 2014). Our findings are consistent with the presence of high elevation taxa in the Andes from the middle Miocene onwards, identifying the first fossil evidence for protoparamo older than Pliocene age (c. <5 Ma). However, there are three lines of evidence that make us question the extent of high elevation vegetation types at the time: a) Martínez et al. (2020) indicate that prior to c. 5 Myr there was no Puna (alpine vegetation) on the Altiplano to the south of our study region (Peru) (Fig. 1, point 8), b), molecular data show that mid-elevation taxa such as the Campanulaceae diversified in the Andes only around 5 Myr (Lagomarsino et al., 2016) and c) the palynological record at the mouth of the Amazon River indicates that high-altitude Andean taxa did not reach the Atlantic until 5.6 Myr (Hoorn et al., 2017). This implies that high-elevation taxa only became uniformely distributed during the Pliocene (c. 5 Ma), when the Andes reached their modern elevation.. Furthermore, transcontinental Amazon River drainage was initiated in the late Miocene and only reached its modern catchment in the Pliocene (Figueiredo et al., 2009, 2010; Hoorn et al., 2017; Van Soelen et al., 2017). Therefore, organic debris sourced in the entire drainage basin could only reach the Atlantic depocenter by Pliocene times.

5.3. The Los Chorros succession in a sequence stratigraphic framework

5.3.1. Cyclic deposition in the Miocene wetland of western Amazonia

Our extended dataset from the Los Chorros site highlights that the Pebas wetland system hosted various sub-environments, including shallow to extensive and deep lakes that reached below storm wave base. We base the lake depth on in-situ occurrence of some mollusc taxa and their wide extent from pollen assemblages showing the Neves effect at the time of maximum flood. Other environments include fluvial channels, swamps, and lowland forests (see also Hoorn, 1994b; Wesselingh et al., 2006b; Hoorn et al., 2010a, 2010b; Latrubesse et al., 2010). Sediment deposition and paleoenvironments were regulated by orbital cyclicity (discussed below) that built successions ranging from palm-dominated swamps and lakes during flood phases (sensu Wesselingh et al., 2006b) to grass-rich swamps and soils during dry or regressive or fill phases. Based on our sequence biostratigraphy approach we determined that the onset of each sedimentary cycle began with peat deposition, as a transgressive lag deposit (see Hovikoski et al., 2010), followed by a tidally influenced transgression (which often resulted in reworking of the peat) with minor salinity elevations, allowing mangroves to expand into the region. This is followed by a succession of claystones and sandstones, variously bioturbated, and culminates in a shallowing upward succession with rootlets and evidence for weathering. The cycles closely parallel the upward-coarsening trends revealed by granulometric analysis (Fig. 12). The succession through an idealised cycle is shown in Fig. 13.

Within the lowermost part of the CU cycles, water conditions must have changed from eutrophic to oligotrophic. Within the fine-grained part of the cycles, conditions were aquatic, predominantly freshwater and occasionally oligohaline. The former was regulated by Andean sediment supply and productivity in the system, and the latter by the waxing and waning of the marine incursions.

The succession of eight, lithologically similar cycles of uniform-thickness suggest that they were driven by uniformly cyclical climatic fluctuations, but with the Cycle 7 flood being slightly more pronounced than the others. Depending on the periodicity of the climate oscillations, the succession could have formed over a period of about 200 kyr if the cycles were driven by precession (23 kyr cycles), 330 kyr if the cycles were due to obliquity fluctuations (41 kyr cycles) or 850 kyr if the cycles were due to eccentricity oscillations. As noted above, Vonhof and Kaandorp (2010) suggested that the Los Chorros cycles were either driven by precession or obliquity cycles. Such a succession of eight broadly similar cycles may have taken place only at specific periods in geological time.

The middle and late Miocene was characterized by many changes in global sea level, which have been revealed by detailed stable isotope studies, especially by Holbourn et al. (Holbourn et al., 2005; Holbourn et al., 2013). This time period is characterized by three trends, termed here long, medium and short term. At the broadest scale of the long-term trends, most of the middle Miocene coincides with the MMCO (17–14 Ma), a period of globally high sea levels when near ice-free conditions may have been present during the warmest periods (Miller et al., 2020). The period began with a sudden and dramatic rise in sea levels after 16.9 Myr (De Boer et al., 2010; Westerhold et al., 2020; Miller et al., 2020), remained relatively high for about 3 Myr, and then fell in an equally dramatic manner without subsequent rebound to MMCO levels after 13.8 Myr (De Boer et al., 2010; Holbourn et al., 2013; Westerhold et al., 2020) in the MMCT (14.7–13.8 Ma), see also Steinthorsdottir et al. (2020) for overview.

During the period from 13.8 Myr to the end of the late Miocene, sea levels were much lower (De Boer et al., 2010; Holbourn et al., 2013; Miller et al., 2020) reflecting a period of permanent development of the East Antarctic Ice Sheet (Miller et al., 2020). The main phases of sea level fall associated with the MMCT were at 13.8 Myr (Mi-3b) and 13.1 Myr (Mi-4) and the net fall in global sea levels after the MMCO was of the order of 60 m (Miller et al., 2020). These two periods of relatively stable sea levels were punctuated by short-lived phases of increased Antarctic glaciation (medium term trends), with the MMCO incurring glacial expansion with the Mi-2, Mi-2a and Mi-3a events, and the period after the MMCT by the Mi-3b, and Mi-4-7 events. These episodes were characterized by sea level oscillations of 30–40 m (Miller et al., 2020; Morley et al., 2021). Short term trends relate to the high frequency 106 kyr eccentricity or 41 kyr obliquity cycles, characterized by sea level oscillations of 20 m (Miller et al., 2020). Holbourn et al. (2013) show that prior to 14.6 Ma, and from 14.1 to 9.8 Ma, 106 kyr eccentricity cycles were dominant, whereas from 14.6–14.1 Ma, and immediately after 9.8 Ma, 41 kyr obliquity cycles predominated. With the availability of an approximate time framework, and knowledge of the likely cycle duration, whether 23, 41 or 106 kyr, the time window for the Los

Chorros succession can be suggested from the dominant cycle and sea level patterns as established by Holbourn et al. (2013).

5.3.2. Age of Los Chorros sediments and biostratigraphy

The first age model for the Los Chorros section was proposed by Hoorn (1994a) using the biostratigraphic scheme developed by Lorente (1986) for Venezuela. Based on the regular presence of *Grimsdalea magnaclavata* and *Crassoretitriletes vanraadshooveni* and the absence of *Alnipollenites verus* and *Fenestrites spinosus* (markers of younger ages) the age for these sediments was estimated at middle to late Miocene (15.9 to 7.1 Ma). Later, Boonstra et al. (2015) adjusted this age following the biostratigraphic scheme of Jaramillo et al. (2011) for Los Llanos and Llanos foothills of Colombia, providing an age of middle Miocene (T15; 14 to 12.7 Ma). The age of the marine incursions was estimated by Jaramillo et al. (2017) to be early and middle Miocene (confirming earlier estimates by Hoorn, 1993) and their presence was within a 200 kyr interval during the early Miocene and a 400 kyr interval during the middle Miocene.

The age boundaries for the T15 zone of Jaramillo et al. (2011) are based on reference to the first appearance datums of the sporomorphs *Crassoretitriletes vanraadshooveni* at 14.2 Myr *and Fenestrites spinosus* at 12.7 Myr with the dates determined by the graphic correlation method, using the ages of three formation boundaries from the Urumaco region of Colombia (6.8, 12.4 and 14.5 Myr) as tie points, where the succession is independently dated using foraminifera. Obtaining accurate biostratigraphic dates for the time interval from 14 Myr to 7 Myr is problematic even in open marine successions, since it is only with the more recent evaluations of planktonic foraminifera and nannofossils by reference to the astronomical timescale that a reliable correlation of planktonic foraminiferal and nannofossil zones across the middle to late Miocene boundary has been available (compare Berggren et al., 1995 with Gradstein et al., 2012; Gradstein and Ogg, 2020). This has led to major issues in dating successions where this time interval is well represented, such as offshore Malaysia (Morley et al., 2021), where a sequence biostratigraphic framework that applies to this time interval is dated by reference to 21 foraminiferal, nannofossil and palynomorph first and last appearance datums.

With respect to the evolutionary appearance of *C. vanraadshooveni*, Germeraad et al. (1968) interpreted the age of appearance to be the same in Venezuela and the Niger Delta. This species has its first appearance in Nigeria within foraminiferal zone N9 (Morley and Rosen, 1996, and Morley unpublished), the base of which was dated by Wade et al. (2011) at 15.1 Ma. It is possible that a similar age of about 15 Myr for the first appearance of *C. vanraadshooveni* may apply in Amazonia. Also, for the evolutionary appearance of *Fenestrites spinosus*, this species has a first appearance in the early Miocene according to Muller (1981) and so the event dated at 12.7 Myr in the Neotropics is likely to reflect a local climatic or migration event. In the Niger Delta, this event is poorly restrained, occurring at about 10 Myr within nannofossil zone NN9 (Morley and Rosen, 1996, and Morley unpublished). Due to the uncertainties with respect to the age of both the upper and lower zone T15 boundaries, the age of the succession is better evaluated by comparison to global trends in sea level, and by examining climate cyclicity patterns. A further issue is that first appearance datums may occur at different times in different areas, for instance, Leite et al. (2021) working in the Solimões Basin find that the oldest records of *C. vanraadshooveni* and *Grimsdalea magnaclavata* are inverted compared to the Llanos of Colombia. Clearly great care is needed in applying precise dates to palynomorph first appearance datums.

The Pebas depositional system is an inland sedimentary succession formed by the gradual and uniform subsidence of the Andean foreland basins. It has variously been brought to attention that the marine incursions observed in the Pebas/ Solimões Formation relate to the MMCO. It is highly unlikely that marine incursions could have occurred in Amazonia immediately outside this time window, and especially after the 13.8 Myr sea level fall, without recourse to a major tectonic change and greatly increased regional subsidence. In particular, since the Pebas/Solimões sedimentary succession is of very uniform thicknesses across the region in seismic profiles (Jaramillo et al., 2017). Nevertheless, after 13.8 Myr marine incursions might have occured as continued basinal subsidence could bring the Pebas wetland back to late Miocene sea levels, such as at the time of the late Miocene period of 'peak warmth' after 11 Myr (Holbourn et al., 2013) at which time accommodation space for marine deposition would again be present in Amazonia (e.g. see Espinosa et al., in press). If the Los Chorros succession was deposited after the MMCT, then open marine deposits would be expected for older Pebas deposits with water depths up to 50 m higher than those seen at Los Chorros. Since no such incursions are reported (Hoorn, 2006; Hoorn et al., 2010a); Jaramillo et al., 2017) this scenario is considered unlikely. Therefore, it is more probable that sedimentation took place entirely during the MMCO. To determine whether deposition took place during the earlier, or later part of the MMCO, a reassessment of the likely cycle duration of the Los Chorros cycles is required. This can be achieved by comparing cycle thicknesses with regional sedimentation rates. If the flood-fill cycles are driven by 106 kyr eccentricity cycles, sedimentation rates at Los Chorros would be about 3.5 m per 100 kyr, for obliquity cycles, sedimentation rates would be about 8.4 m per 100 kyr and for 23 kyr sedimentation rates of 15 m per 100 kyr would be expected (Fig. 14).

The regional sedimentation rate can be determined by reference to the ages applied to the palynological zone boundaries in well sections. For the 105-AM Well, evaluated by Jaramillo et al. (2017), by utilising tie points for the top of zones T13 and T14, but tying the top of zone T15 to the 13.8 Myr sea level fall, regional sedimentation rates compare closely to values for 41 kyr cycles, whereas using the 12.7 Myr date for the T15 termination, sedimentation rates would be more in line with 106 kyr cycles (Fig. 14). As discussed above, it is unlikely that these cycles were driven by 106 kyr eccentricity cycles. The Los Chorros cycles are therefore thought to reflect 41 kyr obliquity cycles, providing a new perspective on dating the Los Chorros sediments.

According to Holbourn et al. (2013), a succession of eight consecutive 41 kyr cycles during the MMCO is seen only within the time interval 14.6 to 14.1 Ma, immediately following a period with pronounced 106 kyr cycles. This succession also coincides with Cycle SEA54, established for the sedimentary succession seen offshore Malaysia by Morley et al. (2021), with boundaries tied to the isotope curves of De Boer et al. (2010) and Holbourn et al. (2013) and is thought to have global application. The Los Chorros succession is thus thought to correlate to the SEA54 cycle of Morley et al. (2021), between the Mi2a and Mi3a glaciations of Miller et al. (2011). It is thus possible that the most pronounced flooding event, the Cycle 7 flood, might tie to the SEA54 maximum flood at about 14.3 Ma.

5.3.3. The Los Chorros succession viewed in the regional and global stratigraphic context

The outcrops discussed in this paper fit well with a sequence biostratigraphic model with the Los Chorros sediments being representative for the 'Pebas' wetland phase (sensu Hoorn et al., 2010a, 2010b) with episodic marine incursions related to global sea level highstands during the MMCO. The Mariñame (early Miocene) and the Apaporis (middle Miocene) sites both represent fluvial tributaries with their source area on the Amazon craton (Fig. 11). Although salinity was low in most of the wetland system, at the Apaporis site brackish conditions and coastal vegetation occurred.

A time-equivalent analogue to the Miocene Amazonian depositional system was present during the middle Miocene across the Sunda Shelf in Southeast Asia. The exposed Sunda Shelf was much more extensive than today (Hall, 2002; Morley et al., 2016) but during the MMCO, shallow marine conditions prevailed at times of sea level highstand forming the Malay Sea (Morley et al., 2016). In its proximal extremities of this sea, extending to the North Malay Basin, very similar depositional settings to Pebas were present to those at Los Chorros, with sea level maxima reflected by pulses of mangrove pollen, marine dinoflagellate cysts and agglutinated foraminifera, with lacustrine conditions reflected by *Pediastrum* maxima —when sea levels were low— and with abundant peat swamp pollen suggesting the widespread development of peat swamps similar to those currently forming in Borneo (Anderson, 1964; Morley, 2013). These conditions persisted through cycles SEA53 to

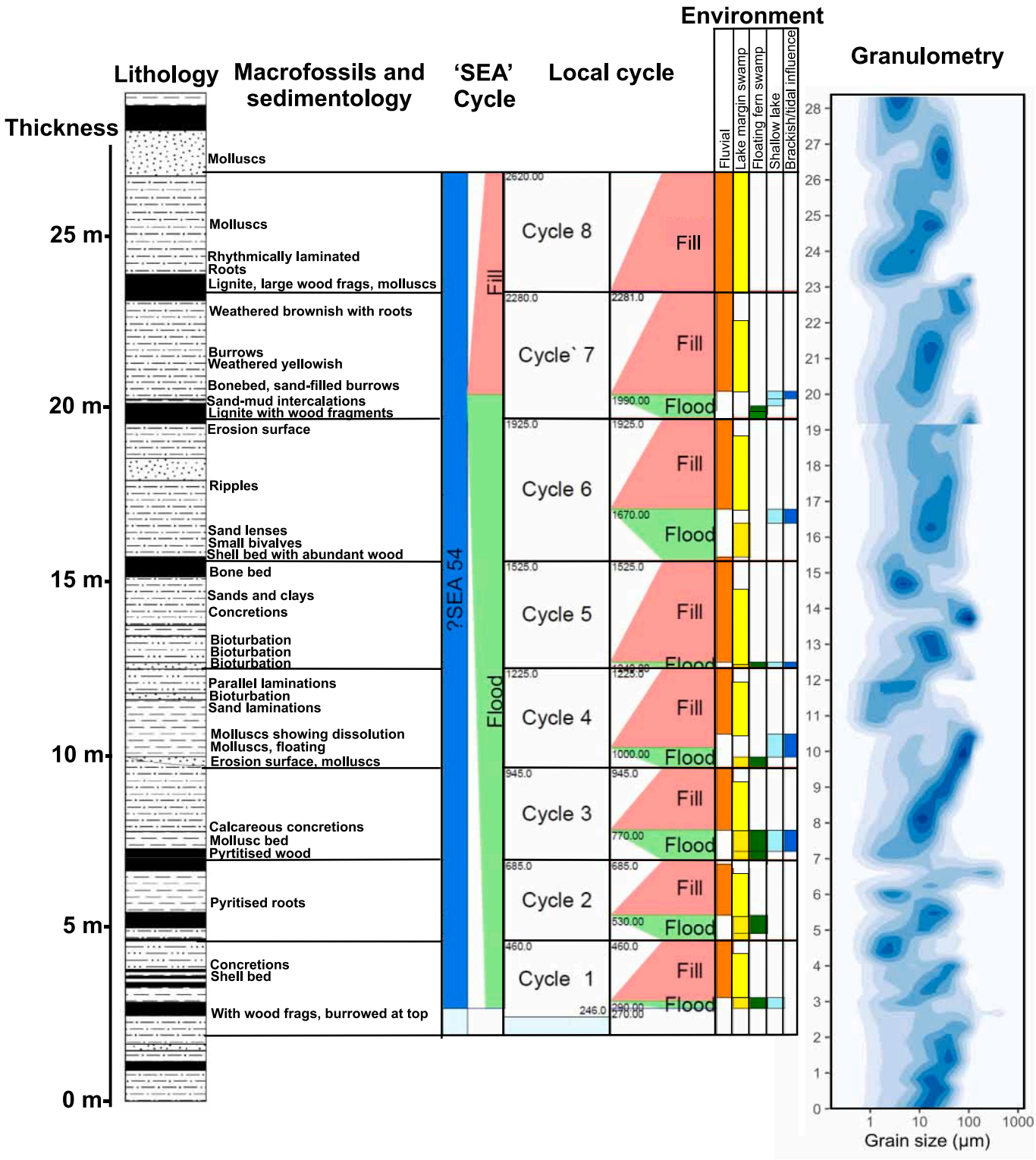

Fig. 12. Flood-fill cycles revealed from the sequence biostratigraphic evaluation and the relationship to lithologies, records of molluscs, depositional environments and a granulometric evaluation of the sediments.

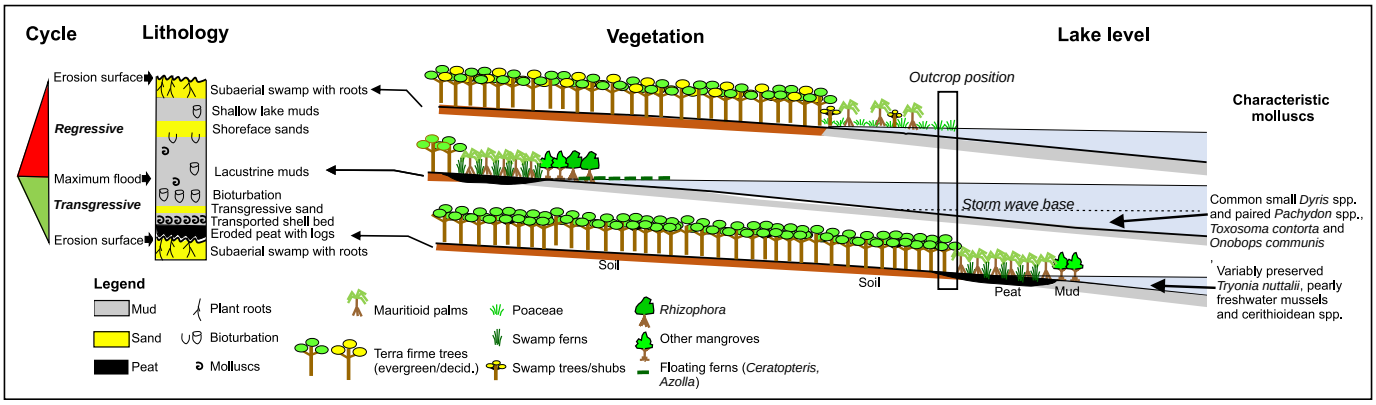

Fig. 13. Idealised succession of transgression and regression through a single flood-fill cycle.

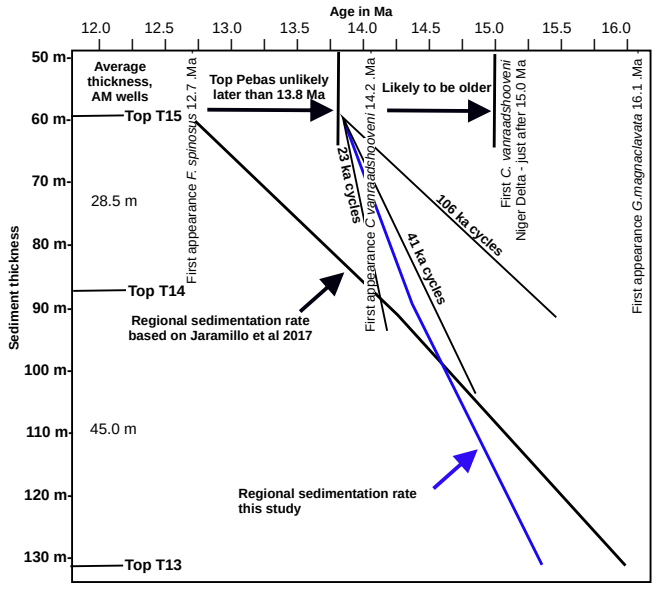

Fig. 14. Local sedimentation through the Los Chorros successions compared to regional rates based on the thickness of palynological zones T13 and T14 in AM wells that penetrate the Pebas succession. The thick black line is based on zone boundary ages according to Jaramillo et al. (2011), whereas the blue line shows the same events tied to the MMCO as discussed in the text. The thin black lines show the sedimentation rates for Los Chorros sediments depending on whether they relate to 23, 41 or 106 ka astronomical cycles. (For interpretation of the references to colour in this figure legend, the reader is referred to the web version of this article.)

SEA56, from 15.2 to 13.8 Myr (Morley et al., 2021). An example of the palynological response through the same time interval as for Los Chorros from the North Malay Basin is shown in cycle SEA54 of the Bergading Deep-3 well illustrated in Morley Morley et al. (2021).

6. Conclusions

In this paper we have revisited the Los Chorros site (Amazon River, Colombia), which is one of the classic outcrops of the Pebas Formation (and equivalent to the Solimões Formation), and representative for the Miocene wetland in western Amazonia. Our new palynological, paleontological and geochemical analyses, placed in a sequence biostratigraphic framework, suggest that the sediments at Los Chorros are most likely of middle Miocene age (c. 14.7 to 13.8 Ma), and were deposited in 8 sedimentary CU cycles during the latter part of the MMCO. These cycles were deposited as flood-fill packages which were most likely driven by 41 kyr obliquity cycles. The local environment for each cycle was predominantly shallow to deeper lacustrine, beginning with sudden transgressions and with water depths exceeding storm wave base at the time of the episodic marine incursions. During flood phases, the vegetation on the lake edges was mainly characterized by Mauritiinae palm swamps and ferns. Probable grass-rich swamps characterized the fill phase. The lakes were surrounded by unflooded *terra firme* forests of the Amazonian lowland, with adjacent montane forest in the Andes (reaching an altitude of >3 km). The aquatic intervals were characterized by algae and fern-allies indicating alternating oligotrophic and eutrophic conditions, whereas marine palynomorphs and sparse mangrove pollen point at marginal marine influence. Two mollusc assemblages characterize the shallow, clear lake water, and fluvio-deltaic conditions, whereas the rare occurrence of marine species signify low amounts of saltwater intrusion. The occurrence of the very-large terrestrial snail *Amazoniconcha immanis,* together with phytoliths belonging to forest taxa, further reaffirm the occasional presence of forest in the area. Biomarker data confirm the mixed environment ranging from aquatic (freshwater to oligohaline) to terrestrial. Lipid data for instance highlight the subdivision observed in the section with the first 20 m being characterized by predominantly aquatic and swamp taxa, and the top 5 m by floodplain and *terra firme* and montane taxa.

The stratigraphic interpretation presented here utilising a sequence biostratigraphic approach, by comparing flood-fill cycle patterns with high resolution stable isotope datasets must be considered as tentative, since it is the first time that such an approach has been used in Amazonia. However, we consider that the method has widespread application in the Pebas succession, since it is predictive. For instance, it suggests that depositional cycles in the immediately preceding (unsampled) succession should exhibit 106 kyr depositional cycles. We suggest that the approach should be applied more widely in Amazonia, especially with respect to establishing cycle durations by extrapolation of regional sedimentation rates, since models will become firmer with the availability of additional data in different stratigraphic intervals. The differentiation of 41 kyr from 106 kyr cycles and their comparison with the detailed isotope curves of Holbourn et al. (2013) and Westerhold et al. (2020) with ages restrained by confident events identified from age-restricted palynomorphs may provide a new stratigraphic framework for the evaluation of the whole Pebas succession.

In the broader context of the western Amazonia, the picture emerges that the Miocene wetland was affected by episodes of marine incursions, which coincide with repeated sea level highstands of the later part of the MMCO, as shown in Holbourn et al. (2013), Westerhold et al. (2020) and Miller et al. (2020).

Declaration of Competing Interest

The authors declare that they have no known competing financial interests or personal relationships that could have appeared to influence the work reported in this paper.

The authors declare the following financial interests/personal relationships which may be considered as potential competing interests.

Acknowledgements

This research was partly funded by the joint Brazilian-European facility for climate and geodynamic research on the Amazon River Basin sediment (CLIM-AMAZON) project. The research leading to these results has also received funding from the European Research Council under the European Union's Seventh Framework Program (FP7/2007-2013) / ERC grant agreement n° [226600]. Samples were collected in the framework of the Tropenbos International Program. We thank Jeane Grasyelle, Iris Dias, Rachel Bezerra and other analysts and students working at the Geochronology Laboratory of the University of Brasília for help with the Sr and Nd analyses. We also like to thank Denise Dorhout, Marianne Baas, Monique Veenstra, Angelique Mets, Jort Ossebaar, and Kevin Donkers for analytical assistance at the NIOZ. C.G.-A. acknowledges the support from the Programa de Investigaciones, Facultad de Ciencias (2021). We thank Annemarie Philip for processing the palynological samples at the University of Amsterdam.

Appendix A. Supplementary data

Supplementary data to this article can be found online at https://doi.org/10.1016/j.gloplacha.2021.103717.

References

Acton, F.S., 1959. Analysis of Straight-Line Data. Wiley, New York.
Akabane, T.K., Sawakuchi, A.O., Chiessi, C.M., Kern, A.K., Pinaya, J.L.D., Ceccantini, G. C.T., De Oliveira, P.E., 2020. Modern pollen signatures of Amazonian rivers and new insights for environmental reconstructions. Palaeogeogr. Palaeoclimatol. Palaeoecol. 554, 109802.
Alvim, A.M.V., Santos, R.V., Roddaz, M., Antoine, P.O., Ramos, M.I.F., do Carmo, D.A., Negri, F.R., 2021. Fossil isotopic constraints (C, O and 87Sr/86Sr) on Miocene shallow-marine incursions in Amazonia. Palaeogeogr. Palaeoclimatol. Palaeoecol. 573, 110422.
Anderson, J.A.R., 1964. The structure and development of the peat swamps of Sarawak and Brunei. J. Trop. Geogr. 18, 7ç16.
Armentrout, J.M., 1987. Integration of biostratigraphy and seismic stratigraphy: Pliocene–Pleistocene, Gulf of Mexico. In: Proceedings, Gulf Coast Section SEPM 8th Annual Research Conference, pp. 6–14.
Armentrout, J.M., 1991. Paleontologic constraints on depositional modelling: examples of integration of biostratigraphy and seismic stratigraphy, Gulf of Mexico. In: Weimer, P., Link, M.H. (Eds.), Seismic Facies and Sedimentary Processes of Submarine Fans and Turbidite Systems, Frontiers in Sedimentary Geology Series. Springer, New York, pp. 137–170.
Basu, A.R., Sharma, M., DeCelles, P.G., 1990. Nd, Sr-isotopic provenance and trace element geochemistry of Amazonian foreland basin fluvial sands, Bolivia and Peru: implications for ensialic Andean orogeny. Earth Planet. Sci. Lett. 100 (1–3), 1–17.
Bernal, R., Gradstein, R.S., Celis, M., 2015. Colombia Plant and Lichen Catalog. http://catalogoplantasdecolombia.unal.edu.co/es/.
Berggren, W.A., Kent, D.V., Swisher III, C.C., Aubry, M.P., 1995. A Revised Cenozoic Geochronology and Chronostratigraphy. SEPM Society for Sedimentary Geology.
Bernal, R., Bacon, C.D., Balslev, H., Hoorn, C., Bourlat, S.J., Tuomisto, H., Salamanca, S., van Manen, M.T., Romero, I., Sepulchre, P., Antonelli, A., 2019. Could coastal plants in western Amazonia be relicts of past marine incursions? J. Biogeogr. 46 (8), 1749–1759.
Bloom, D.D., Lovejoy, N.R., 2011. The biogeography of marine incursions in South America. In: James, S.A., Reis, R.E. (Eds.), Historical Biogeography of Neotropical Freshwater Fishes, pp. 137–144.
Bloom, D.D., Lovejoy, N.R., 2017. On the origins of marine-derived freshwater fishes in South America. J. Biogeogr. 44 (9), 1927–1938.
Bogotá, G., 2002. El polen de la Clase Asteridae en el Páramo de Monserrate. Unversidad Distrital Francisco Jose de Caldas, p. 128.
Bogotá, G., Lamprea, S., Rangel, J.O., 1996. Atlas palinológico de la Clase Magnoliopsida en el Páramo de Monserrate. El Páramo ecosistema a proteger. Serie Montañas Tropoandinas 2, 233.
Bogotá-Ángel, et al., 2021. Climate and geological change as drivers of Mauritiinae palm biogeography. J. Biogeogr. 48 (5), 1001–1022.
Boonstra, M., Ramos, M.I.F., Lammertsma, E.I., Antoine, P.-O., Hoorn, C., 2015. Marine connections of Amazonia: evidence from foraminifera and dinoflagellate cysts (early to middle Miocene, Colombia/Peru). Palaeogeogr. Palaeoclimatol. Palaeoecol. 417, 176–194.
Bouchez, J., Gaillardet, J., France-Lanord, C., Maurice, L., Dutra-Maia, P., 2011. Grain size control of river suspended sediment geochemistry: Clues from Amazon River depth profiles. Geochem. Geophys. Geosyst. 12 (3), Q03008.
Burn, M.J., Mayle, F.E., Killeen, T.J., 2010. Pollen-based differentiation of Amazonian rainforest communities and implications for lowland palaeoecology in tropical South America. Palaeogogr. Palaeoclimatol. Palaeoecol. 295, 1–18.
Caputo, M.V., Rodrigues, R., De Vasconcelos, D.N.N., 1971. Litoestratigrafia da bacia do rio Amazonas. In: Rel. Tec. Int. 641-A, Petrobras-Renor, Belem, pp. 35–46.
Chaloner, W.G., Muir, M., 1968. Spores and floras. In: Murchinson, D.G., Westall, T.S. (Eds.), Coal and Coal-Bearing Strata. Oliver and Boyd, Edinburgh, UK, pp. 127–146.
Chandler, R.F., Hooper, S.N., 1979. Friedelin and associated triterpenoids. Phytochemistry 18 (5), 711–724.
Chung, N.H., Morley, R.J., Dung, Bui Viet, Yen, Cao Dang Hoang, Nguyen Van, Su, 2021. Sequence biostratigraphy of the late Oligocene to Miocene succession in the northern Song Hong Basin, offshore Vietnam. Palaeogeogr. Palaeoclimatol. Palaeoecol. 569, 110322.
Condie, K.C., 1993. Chemical composition and evolution of the upper continental crust: Contrasting results from surface samples and shales. Chem. Geol. 104 (1–4), 1–37.
Condie, K.C., Wronkiewicz, D.J., 1990. The Cr/Th ratio in Precambrian pelites from the Kaapvaal Craton as an index of craton evolution. Earth Planet. Sci. Lett. 97 (3–4), 256–267.
Condie, K.C., Lee, D., Farmer, G.L., 2001. Tectonic setting and provenance of the Neoproterozoic Uinta Mountain and Big Cottonwood groups, northern Utah: constraints from geochemistry, Nd isotopes, and detrital modes. Sediment. Geol. 141–142, 443–464.
Conrad, T.A., 1871. Description of new fossil shells of the upper Amazon. Am. J. Conch. 4, 192–198.
Cooke, G.M., Chao, N.L., Beheregaray, L.B., 2012. Marine incursions, cryptic species and ecological diversification in Amazonia: the biogeographic history of the croaker genus Plagioscion (Sciaenidae). J. Biogeogr. 39 (4), 724–738.
Cullers, R.L., 2000. The geochemistry of shales, siltstones and sandstones of Pennsylvanian–Permian age, Colorado, USA: implications for provenance and metamorphic studies. Lithos. 51 (3), 181–203.
Da Silva-Caminha, S.A., Jaramillo, C.A., Absy, M.L., 2010. Neogene palynology of the Solimões basin, Brazilian Amazonia. Palaeontogr. Abt. B 284 (1–3), 13–79.
Da Silva-Caminha, S.A., D'Apolito, C., Jaramillo, C., Espinosa, B.S., Rueda, M., 2020. Palynostratigraphy of the Ramon and Solimões formations in the Acre Basin, Brazil. J. S. Am. Earth Sci. 103, 102720.
Dantas, E.L., de Alvarenga, C.J.S., Santos, R.V., Pimentel, M.M., 2009. Using Nd isotopes to understand the provenance of sedimentary rocks from a continental margin to a foreland basin in the Neoproterozoic Paraguay Belt, Central Brazil. Precambrian Res. 170 (1–2), 1–12.
D'Apolito, C., 2016. Landscape Evolution in Western Amazonia: Palynostratigraphy, Palaeoenvironments and Diversity of the Miocene Solimões Formation, Brazil, Doctoral dissertation. University of Birmingham.
D'Apolito, C., Jaramillo, C., Harrington, G., 2021. Miocene Palynology of the Solimões Formation (Well 1-AS-105-AM), Western Brazilian Amazonia. Smithsonian Contributions to Paleobiology, No. 105. Smithsonian Institution Scholarly Press, Washington, D.C.
De Boer, B., Van de Wal, R.S.W., Bintanja, R., Lourens, L.J., Tuenter, E., 2010. Cenozoic global ice-volume and temperature simulations with 1-D ice-sheet models forced by benthic δ18O records. Ann. Glaciol. 51 (55), 23–33.
De Silva, F.H.M., de Assis Ribeiro dos Santos, F., 2008. Pollen morphology of the shrub and arboreal flora of the mangroves of Northeastern Brazil. Wetl. Ecol. Manag. https://doi.org/10.1007/s11273-008-9118-2.
DePaolo, D.J., Wasserburg, G.J., 1976. Nd isotopic variations and petrogenetic models. Geophys. Res. Lett. 3 (5), 249–252.
Duivenvoorden, J.F., Lips, J.M., 1995. A Land-Ecological Study of Soils, Vegetation and Plan Diversity in Colombian Amazonia. Tropenbos Series, 12. The Tropenbos Foundation, Wageningen, The Netherlands, p. 438.
Eiras, J.F., Becker, C.R., Souza, E.M., Gonzaga, F.G., Silva, J.G.F., Daniel, L.M.F., Matsuda, N.S., Feijó, F.J., 1994. Bacia do Solimões. Boletim de Geociências da Petrobras 8 (1), 17–22.
Espinosa, B.S., D'Apolito, C., Silva-Caminha, S.A.F., 2021. Marine influence in western Amazonia during the late Miocene. Glob. Planet. Chang.
Fedo, C.M., Eriksson, K.A., Krogstad, E.J., 1996. Geochemistry of shales from the Archean (~3.0 Ga) Buhwa Greenstone Belt, Zimbabwe: Implications for provenance and source-area weathering. Geochim. Cosmochim. Acta 60 (10), 1751–1763.
Figueiredo, J., Hoorn, C., van der Ven, P., Soares, E., 2009. Late Miocene onset of the Amazon River and the Amazon deep-sea fan: evidence from the Foz do Amazonas Basin. Geology 37 (7), 619–622.
Figueiredo, J.J.J.P., Hoorn, C., Van der Ven, P., Soares, E., 2010. Late Miocene onset of the Amazon River and the Amazon deep-sea fan: evidence from the Foz do Amazonas Basin: Reply. Geology 38 (7), e213.
Flantua, S.G.A., Hooghiemstra, H., van Boxel, J.H., Cabrera, M., González-Carranza, Z., Gonzalez-Arango, C., 2014. Connectivity dynamics since the Last Glacial Maximum in the northern Andes: a pollen-driven framework to assess potential migration. In: Stevens, W.D., Montiel, O.M., Raven, P.H. (Eds.), Paleobotany and Biogeography: A festschrift for Alan Graham in his 80th year. Monographs in systematic botany from the Missouri Botanical Garden 128. Missouri Botanical Garden Press, St. Louis, pp. 98–123.
Fontenelle, J.P., Marques, Portella Luna, Kolmann, M.A., Lovejoy, N.R., 2021. Biogeography of the neotropical freshwater stingrays (Myliobatiformes: Potamotrygoninae) reveals effects of continent-scale paleogeographic change and drainage evolution. J. Biogeogr. https://doi.org/10.1111/jbi.14086.
Fontes, D., Jaramillo, C., Moreno, J.E., 2019. Pollen morphology of the Amacayacu Forest dynamics plot, Western Amazon, Colombia. Palynology 44 (1), 32–79. https://doi.org/10.1080/01916122.2018.1538024.

Gabb, W.M., 1869. Descriptions of fossils from the clay deposits of the upper Amazon. Am. J. Conch. 4, 197–200.
Germeraad, J.H., Hopping, C.A., Muller, J., 1968. Palynology of Tertiary sediments from tropical areas. Rev. Palaeobot. Palynol. 6, 189–348.
Gill, D., Shomrony, A., Fligelman, H., 1993. Numerical zonation of the log suites and logofacies recognition by multivariate clustering. The Am. Associat. Petrol Geol. Bull. 77, 1781–1791.
Gingras, M.K., Räsänen, M.E., Pemberton, S.G., Romero, L.P., 2002. Ichnology and sedimentology reveal depositional characteristics of bay-margin parasequences in the Miocene Amazonian foreland basin. J. Sediment. Res. 72 (6), 871–883.
Gioia, S.M.C.L., Pimentel, M.M., 2000. The Sm-Nd isotopic method in the geochronology laboratory of the University of Brasília. An. Acad. Bras. Ciênc. 72 (2), 219–245.
Giraldo-Cañas, D., 2013. Las gramíneas en Colombia. Riqueza, distribución, endemismo, invasión, migración, usos y taxonomías populares. Instituto de Ciencias Naturales, Universidad Nacional de Colombia.
Gomes, B.T., Absy, M.L., D'Apolito, C., Jaramillo, C., Almeida, R., 2021. Compositional and diversity comparisons between the palynological records of the Neogene (Solimões Formation) and Holocene sediments of Western Amazonia. Palynology 45 (1), 3–14.
González, C., Dupont, L.M., Behling, H., Wefer, G., 2008. Neotropical vegetation response to rapid climate changes during the last glacial period: palynological evidence from the Cariaco Basin. Quat. Res. 69 (2), 217–230.
Gradstein, F.M., Ogg, J.G., 2020. The chronostratigraphic scale. In: Geologic Time Scale 2020. Elsevier, pp. 21–32.
Gradstein, F.M., Ogg, J.G., Schmitz, M.D., Ogg, G.M., 2012. The Geologic Time Scale 2012. Elsevier.
Grimm, E.C., 1987. CONISS: a FORTRAN 77 program for stratigraphically constrained cluster analyses by the method of incremental sum of squares. Comput. Geosci. 13, 13–15.
Grimm, E.C., 1991. Tilia and Tiliagraph. Illinois State Museum, Springfield. Hartley.
Gross, M., Piller, W.E., 2020. Saline waters in Miocene Western Amazonia–an alternative view. Front. Earth Sci. 8, 116.
Wesselingh, F.P., Guerrero, J., Räsänen, M., Romero Pitmann, L., Vonhof, H., 2006. Landscape evolution and depositional processes in the Miocene Amazonian Pebas lake/wetland system: evidence from exploratory boreholes in northeastern Peru. Scr. Geol. 133, 323–361.
Guzmán, -R.A., 2012. Plantas de los humedales de Bogotá y del Valle Ubaté. In: Ana Guzmán Ruiz. Fundación Humedales/Instituto de Investigación de Recursos Biológicos. Alexander von Humboldt/Fondo Hugo de Vries, Amsterdam.
Hall, R., 2002. Cenozoic geological and plate tectonic evolution of SE Asia and the SW Pacific: computer-based reconstructions, model and animations. J. Asian Earth Sci. 20, 353–431.
Hammer, Ø., Harper, D.A.T., Ryan, P.D., 2001. PAST: paleontological statistics software package for education and data analysis. Palaeontol. Electron. 4, 9. http://palaeo-electronica.org/2001_1/past/issue1_01.htm.
Hassan, S., Ishiga, H., Roser, B.P., Dozen, K., Naka, T., 1999. Geochemistry of Permian–Triassic shales in the Salt Range, Pakistan: implications for provenance and tectonism at the Gondwana margin. Chem. Geol. 158 (3–4), 293–314.
Hermoza, W., 2004. D.ynamique tectono-sedimentaire et restauration sequentielle du retro-bassin d'avant-pays des Andes Centrales. University Paul Sabatier, Toulouse, 196 p.
Hernani, L.A.R., 2012. The Sedimentology, Ichnology and Hydrogeochemistry of the Late Miocene, Marginal Marine, Upper Pebas and Nauta Formations, Amazonian Foreland Basin, Peru. Yliopisto. University of Turku, Finland.
Higgins, M.A., Ruokolainen, K., Tuomisto, H., Llerena, N., Cardenas, G., Phillips, O.L., Vásquez, R., Räsänen, M., 2011. Geological control of floristic composition in Amazonian forests. J. Biogeogr. 38 (11), 2136–2149.
Holbourn, A., Kuhnt, W., Frank, M., Martin, J., Haley, B., 2013. Changes in Pacific Ocean circulation following the Miocene onset of permanent Antarctic ice cover. Earth Planet. Sci. Lett. 365, 38–50.
Holbourn, A., Kuhnt, W., Schulz, M., Erlenkeuser, H., 2005. Impacts of orbital forcing and atmospheric carbon dioxide on Miocene ice-sheet expansion. Nature 438 (7067), 483–487.
Hooghiemstra, H., 1984. Vegetational and climatic history of the high plain of Bogotá, Colombia. J. Cramer (Dissertationes botanicae, Bd. 79), 368.
Hoorn, C., 1993. Marine incursions and the influence of Andean tectonics on the Miocene depositional history of northwestern Amazonia: results of a palynostratigraphic study. Palaeogeogr. Palaeoclimatol. Palaeoecol. 105 (3–4), 267–309.
Hoorn, C., 1994a. An environmental reconstruction of the palaeo-Amazon River system (Middle–late Miocene, NW Amazonia). Palaeogeogr. Palaeoclimatol. Palaeoecol. 112 (3–4), 187–238.
Hoorn, C., 1994b. Fluvial palaeoenvironments in the intracratonic Amazonas Basin (early Miocene-early Middle Miocene, Colombia). Palaeogeogr. Palaeoclimatol. Palaeoecol. 109 (1), 1–54.
Hoorn, C., 2006. Mangrove forests and marine incursions in Neogene Amazonia (lower Apaporis River, Colombia). Palaios. 21 (2), 197–209.
Hoorn, C., Paxton, C.G., Crampton, W.G., Burgess, P., Marshall, L.G., Lundberg, J.G., Linna, A.M., 1996. Miocene deposits in the Amazonian foreland basin. Science 273 (5271), 122–125.
Hoorn, C., Wesselingh, F.P., Hovikoski, J., Guerrero, J., 2010a. The development of the Amazonian mega-wetland (Miocene; Brazil, Colombia, Peru, Bolivia). In: Hoorn, C., Wesselingh, F.P. (Eds.), Amazonia: Landscape and Species Evolution, a look into the past. Wiley-Blackwell Publishing Ltd, pp. 123–142.
Hoorn, C., Wesselingh, F.P., Ter Steege, H., Bermudez, M.A., Mora, A., Sevink, J., Antonelli, A., 2010b. Amazonia through time: Andean uplift, climate change, landscape evolution, and biodiversity. Science 330 (6006), 927–931.
Hoorn, C., Bogotá-A, G.R., Romero-Baez, M., Lammertsma, E.I., Flantua, S.G., Dantas, E. L., Chemale Jr., F., 2017. The Amazon at sea: Onset and stages of the Amazon River from a marine record, with special reference to Neogene plant turnover in the drainage basin. Glob. Planet. Chang. 153, 51–65.
Hoorn, C., Boschman, L.M., Kukla, T., Sciumbata, M., Val, P., 2021. The Miocene wetland of western Amazonia and its role in Neotropical biogeography. Bot. J. Linn. Soc. https://doi.org/10.1093/botlinnean/boab098.
Hopmans, E.C., Schouten, S., Pancost, R.D., van der Meer, M.T.J., Sinninghe Damsté, J. S., 2000. Analysis of intact tetraether lipids in archaeal cell material and sediments by high performance liquid chromatography/atmospheric pressure chemical ionization mass spectrometry. Rapid Commun. Mass Spectrom. 14 (7), 585–589.
Hopmans, E.C., Weijers, J.W.H., Schefuß, E., Herfort, L., Sinninghe Damsté, J.S., Schouten, S., 2004. A novel proxy for terrestrial organic matter in sediments based on branched and isoprenoid tetraether lipids. Earth Planet. Sci. Lett. 224 (1–2), 107–116.
Horbe, A.M.C., Roddaz, M., Gomes, L.B., Castro, Tokuta, Dantas, E.L., Do Carmo, D.A., 2019. Provenance of the Neogene sediments from the Solimões Formation (Solimões and Acre Basins), Brazil. J. S. Am. Earth Sci. 93, 232–241.
Hovikoski, J., Wesselingh, F.P., Räsänen, M., Gingras, M., Vonhof, H.B., 2010. Marine influence in Amazonia: Evidence from the geological record. In: Hoorn, C., Wesselingh, F.P. (Eds.), Amazonia: Landscape and Species Evolution, a Look into the Past. Wiley-Blackwell Publishing Ltd., pp. 143–161
Huguet, C., Hopmans, E.C., Febo-Ayala, W., Thompson, D.H., Sinninghe Damsté, J.S., Schouten, S., 2006. An improved method to determine the absolute abundance of glycerol dibiphytanyl glycerol tetraether lipids. Org. Geochem. 37 (9), 1036–1041.
Jaramillo, C., Rueda, M., De la Parra, F., 2008. A Morphological Electronic Database of Cretaceous-Tertiary Fossil Pollen and Spores from Northern South America. Colombian Petroleum Institute & Smithsonian Tropical Research Institute.
Jaramillo, C., Hoorn, C., Silva, S.A., Leite, F., Herrera, F., Quiroz, L., Dino, R., Antonioli, L., 2010. The origin of the modern Amazon rainforest: Implications of the palynological and palaeobotanical record. In: Amazonia: Landscape and Species Evolution, a Look into the Past, vol. 317. Wiley-Blackwell Publishing, p. 334.
Jaramillo, C.A., Rueda, M., Torres, V., 2011. A palynological zonation for the Cenozoic of the Llanos and Llanos Foothills of Colombia. Palynology 35 (1), 46–84.
Jaramillo, C.A., Moreno, E., Ramírez, V., da Silva-Caminha, S.A., de la Barrera, A., de la Barrera, A., Hoyos, N., 2014. Palynological record of the last 20 million years in Panama. In: Stevens, W.D., Montiel, O.M., Raven, P. (Eds.), Paleobotany and Biogeography: A Festschrift for Alan Graham in his 80th Year. Missouri Botanical Garden Press, St. Louis, pp. 134–253.
Jaramillo, C., Romero, I., D'Apolito, C., Bayona, G., Duarte, E., Louwye, S., Escobar, J., Luque, J., Carrillo-Briceño, J.D., Zapata, V., Mora, A., 2017. Miocene flooding events of western Amazonia. Sci. Adv. 3 (5), e1601693.
Jiménez, L.C., Bogotá, R.G., Rangel, J.O., 2008. Atlas palinológico de la Amazonía Colombiana - las familias mas ricas en especies. In: Rangel, J.O. (Ed.), Colombia Diversidad Biótica VII: Vegetación, Palinología y Paleoecología de la Amazonia Colombiana. Universidad Nacional de Colombia, Instituto de Ciencias Naturales, pp. 217–416.
Junk, W.J., 2013. The Central Amazon Floodplain: Ecology of a Pulsing System, vol. 126. Springer Science & Business Media.
Kern, A.K., Gross, M., Galeazzi, C.P., Pupim, F.N., Sawakuchi, A.O., Almeida, R.P., Piller, W.E., Kuhlmann, G.G., Basei, M.A., 2020. Re-investigating Miocene age control and paleoenvironmental reconstructions in western Amazonia (northwestern Solimões Basin, Brazil). Palaeogeogr. Palaeoclimatol. Palaeoecol. 545, 109652.
Kim, J.-H., Zell, C., Moreira-Turcq, P.M.A., Pérez, P., Abril, G., Mortillaro, J.-M., Weijers, T. Meziane, Sinninghe Damsté, J.S., 2012. Tracing soil organic carbon in the lower Amazon River and its tributaries using GDGT distributions and bulk organic matter properties. Geochim. Cosmochim. Acta 90, 163–180.
Kirschner, J.A., Hoorn, C., 2020. The onset of grasses in the Amazon drainage basin, evidence from the fossil record. Front. Biogeogr. 12 (2).
Lacerda, L.D., Conde, J.E., Kjerfve, B., Álvarez-León, R., Alarcón, C., Polanía, J., 2001. American Mangroves. In: Lacerda, L.D. (Ed.), Mangrove Ecosystem, Function and Management. Springer, Berlín, Alemania, pp. 1–62.
Lagomarsino, L.P., Condamine, F.L., Antonelli, A., Mulch, A., Davis, C.C., 2016. The abiotic and biotic drivers of rapid diversification in A ndean bellflowers (Campanulaceae). New Phytol. 210 (4), 1430–1442.
Latrubesse, E.M., Cozzuol, M., da Silva-Caminha, S.A., Rigsby, C.A., Absy, M.L., Jaramillo, C., 2010. The late Miocene paleogeography of the Amazon Basin and the evolution of the Amazon River system. Earth Sci. Rev. 99 (3–4), 99–124.
Leal, A., Berrio, J.C., Raimúndez, E., Bilbao, B., 2011. A pollen atlas of premontane woody and herbaceous communities from upland savannas of Guyana, Venezuela. Palynology 35 (2), 226–266.
Lee, Y.I., 2002. Provenance derived from the geochemistry of late Paleozoic–early Mesozoic mudrocks of the Pyeongan Supergroup., Korea. Sediment. Geol. 149 (4), 219–235.
Leite, F.P., Paz, J., do Carmo, D.A., Silva-Caminha, S.A., 2017. The effects of the inception of Amazonian transcontinental drainage during the Neogene on the landscape and vegetation of the Solimões Basin, Brazil. Palynology. 41 (3), 412–422.
Leite, F.P.R., Silva-Caminha, S.A.F., D'Apolito, C., 2021. New Noegene index pollen and spore taxa from the Solimões Basin (Western Amazonia), Brazil. Palynology. 45 (1), 115–141.
Lindeman, J.C., 1953. The vegetation of the coastal region of Surinam. Results of the scientific expedition to Suriname 1948-'49. Botanical series No. 1 (Doctoral dissertation, Thesis, Utrecht, x+ 135 pp., figs, iv, 17 pis).
Linhares, A.P., Ramos, M.I.F., 2011. Evidence for marine influx during the Miocene in southwestern Amazonia, Brazil-Evidencias de influencia marina durante el Mioceno

en el Sudoeste de la Amazonia (Brasil). Geología Colombiana. Vol. 36, www.revistas.unal.edu.co/index.php/geocol/.
Linhares, A.P., de Souza Gaia, V.D.C., Ramos, M.I.F., 2017. The significance of marine microfossils for paleoenvironmental reconstruction of the Solimões Formation (Miocene), western Amazonia, Brazil. J. S. Am. Earth Sci. 79, 57–66.
Linhares, A.P., Ramos, M.I., Gaia, V.C., Friaes, Y.S., 2019. Integrated biozonation based on palynology and ostracods from the Neogene of Solimões Basin, Brazil. J. S. Am. Earth Sci. 91, 57–70.
Lorente, M.A., 1986. Palynology and palynofacies of the Upper Tertiary in Venezuela. Dissertationes Botanicae, Band 99. ISBN 978-3-443-64011-8.
Louterbach, M., Roddaz, M., Bailleul, J., Antoine, P.-O., Adnet, S., Kim, J.H., van Soelen, E., Parra, F., Gérard, J., Calderon, Y., Gagnaison, C., Sinninghe Damsté, J.S., Baby, P., 2014. Evidences for a Paleocene marine incursion in southern Amazonia (Madre de Dios Sub-Andean Zone, Peru). Palaeogeogr. Palaeoclimatol. Palaeoecol. 414, 451–471.
Lovejoy, N.R., Bermingham, E., Martin, A.P., 1998. Marine incursion into South America. Nature 396, 421–422.
Luebert, F., Weigend, M., 2014. Phylogenetic insights into Andean plant diversification. Front. Ecol. Evol. 2, 27.
Lundberg, J.G., Marshall, L.G., Guerrero, J., Horton, B., Malabarba, M.C.S.L., Wesselingh, F., 1998. The stage for Neotropical fish diversification: a history of tropical South American rivers. Phylogeny Classif. Neotropical Fishes, Part 1 - Fossils and Geological Evidence. 13–48.
Lundberg, J.G., Sabaj Pérez, M.H., Dahdul, W.M., Aguilera, O.A., 2010. The Amazonian Neogene fish fauna. In: Hoorn, C., Wesselingh, F.P. (Eds.), Amazonia: Landscape and Species Evolution, a Look into the Past. Wiley-Blackwell Publishing Ltd., pp. 281–301
Madella, M., Alexandre, A., Ball, T., 2005. International code of phytolith nomenclature 1.0. Ann. Bot. 96, 253–260.
Maia, R.G., Godoy, H.K., Yamaguti, H.S., De Moura, P.A., Da Costa, F.S., De Holanda, M. A., Costa, J., 1977. Projeto de Carvão no Alto Solimões. Relatorio Final. CPRM-DNPM, p. 137.
Marchant, R., Almeida, L., Behling, H., Berrio, J.C., Bush, M., Cleef, A., Salgado-Labouriau, M.L., 2002. Distribution and ecology of parent taxa of pollen lodged within the Latin American Pollen Database. Rev. Palaeobot. Palynol. 121 (1), 1–75.
Martínez, C., Jaramillo, C., Correa-Metrío, A., Crepet, W., Moreno, J.E., Aliaga, A., Bush, M.B., 2020. Neogene precipitation, vegetation, and elevation history of the Central Andean Plateau. Sci. Adv. 6 (35), eaaz4724.
McLennan, S.M., 2001. Relationships between the trace element composition of sedimentary rocks and upper continental crust. Geochem. Geophys. Geosyst. 2 (4), 1021.
McLennan, S.M., Hemming, S., McDaniel, D.K., Hanson, G.N., 1993. Geochemical approaches to sedimentation, provenance, and tectonics. Geol. Soc. Am. Spec. Pap. 284, 21–40.
Miller, K.G., Mountain, G.S., Wright, J.D., Browning, J.V., 2011. A 180-million-year record of sea level and ice volume variations from continental margin and deep-sea isotopic records. Oceanography 24, 40–53.
Miller, K.G., Browning, J.V., Schmelz, W.J., Kopp, R.E., Mountain, G.S., Wright, J.D., 2020. Cenozoic sea-level and cryospheric evolution from deep-sea geochemical and continental margin records. Sci. Adv. 6 (20), eaaz1346.
Mommersteeg, H.J.P.M., 1998. Vegetation development and cyclic and abrupt climatic change during the late quaternary: palynological evidence from the Colombian EasternCordillera, PhD.. University of Amsterdam.
Monsch, K.A., 1998. Miocene fish faunas from the northwestern Amazonia basin (Colombia, Peru, Brazil) with evidence of marine incursions. Palaeogeogr. Palaeoclimatol. Palaeoecol. 143 (1–3), 31–50.
Moraes Rego, L.F., 1930. Notas sobre a Geologia do territorio de Acre e da bacia do Javari. Cezar and Cavalcante, Manaus, p. 45.
Morcote-Ríos, G., Giraldo-Cañas, D., Raz, L., 2015. Illustrated Catalogue of Contemporary Phytoliths for Archaeological and Paleoecology. I. Amazonian Grasses of Colombia. Instituto de Ciencias Naturales, Universidad Nacional de Colombia, Bogotá.
Morcote-Ríos, G., Bernal, R., Raz, L., 2016. Phytoliths as a tool for archaeobotanical, palaeobotanical and palaeoecological studies in Amazonian palms. Bot. J. Linn. Soc. 182 (2), 348–360.
Morley, R.J., 1996. Biostratigraphic characterisation of systems tracts in Tertiary sedimentary basins. In: Proceedings of the International Symposium on Sequence Stratigraphy in SE Asia, IPA Jakarta, pp. 49–71.
Morley, R.J., 2013. Cenozoic ecological history of South East Asian peat mires based on the comparison of coals with present day and Late Quaternary peats peat swamps. J. Limnol. 72, 36.
Morley, R.J., Morley, H.P., 2013. Mid Cenozoic freshwater wetlands of the Sunda region. J. Limnol. 72 (s2), 18–35.
Morley, R.J., Rosen, R.S., 1996. High resolution biostratigraphic zonation for the offshore Niger Delta region. In: IX International Palynology Congress, Houston, June 1996, p. 32.
Morley, R.J., Salvador, P., Challis, M.L., Morris, W.R., Adyaksawan, I.R., 2007. Sequence biostratigraphic evaluation of the North Belut Field, West Natuna Basin. In: Proceedings of the Indonesian Petroleum Association 31st Annual Convention, IPA07-G-120.t.
Morley, R.J., Swiecicki, T., Pham, D.T.T., 2011. A sequence stratigraphic framework for the Sunda Region, based on integration of biostratigraphic, lithological and seismic data from Nam Con Son Basin, Vietnam Proceedings. In: Indonesian Petroleum Association 35th Annual Convention & Exhibition, May 2011.
Morley, R.J., Morley, H.P., Swiecicki, T., 2016. Mio-Pliocene palaeogeography, uplands and river systems of the Sunda region based on mapping within a framework of VIM depositional cycles. In: IPA Fortieth Annual Convention & Exhibition, Jakarta, IPA16-506-G.
Morley, R.J., Dung, B.V., Tung, N.T., Kullman, A.J., Bird, R.T., Van Kieu, N., Chung, N. H., 2019. High-resolution Palaeogene sequence stratigraphic framework for the Cuu Long Basin, offshore Vietnam, driven by climate change and tectonics, established from sequence biostratigraphy. Palaeogeogr. Palaeoclimatol. Palaeoecol. 530, 113–135.
Morley, R.J., Morley, H.P., Zaim, Y., Huffman, O.H., 2020. Palaeoenvironmental setting of Mojokerto *Homo erectus*, the palynological expressions of Pleistocene marine deltas, open grasslands and volcanic mountains in East Java. J. Biogeogr. 47, 566–583.
Morley, R.J., Hasan, Sanatul Salwa, Morley, H.P., Jais, Jaizan Hardi, Mansor, Amiruddin, Aripin, M. Raziken, Nordin, M. Hafiz, Rohaizar, M. Helmi, 2021. Sequence biostratigraphic framework for the Oligocene to Pliocene of Malaysia: polar glaciation and δ13C climate oscillations drive high frequency depositional cycles. Palaeogeogr. Palaeoclimatol. Palaeoecol. 561, 110058.
Muller, J., 1981. Fossil pollen records of extant angiosperms. Botan. Rev. 47 (1), 1–142.
Nesbitt, H.W., Young, G.M., 1982. Early Proterozoic climates and plate motions inferred from major element chemistry of lutites. Nature 299 (5885), 715–717.
Nogueira, A.C.R., Silveira, R., Guimarães, J.T.F., 2013. Neogene-Quaternary sedimentary and paleovegetation history of the eastern Solimões Basin, Central Amazon region. J. S. Am. Earth Sci. 46, 89–99.
Oberdorff, T., Dias, M.S., Jézéquel, C., Albert, J.S., Arantes, C.C., Bigorne, R., Zuanon, J., 2019. Unexpected fish diversity gradients in the Amazon basin. Sci. Adv. 5 (9), eaav8681.
Otto, A., Simoneit, B.R.T., Rember, W.C., 2005. Conifer and angiosperm biomarkers in clay sediments and fossil plants from the Miocene Clarkia Formation, Idaho, USA. Org. Geochem. 36 (6), 907–922.
Palmer, M.R., Edmond, J.M., 1992. Controls over the strontium isotope composition of river water. Geochim. Cosmochim. Acta 56 (5), 2099–2111.
Parra, F.J., Navarrete, R.E., di Pasquo, M.M., Roddaz, M., Calderón, Y., Baby, P., 2020. Neogene palynostratigraphic zonation of the Maranon Basin, Western Amazonia, Peru. Palynology 44 (4), 675–695.
Piedade, M.T.F., Junk, W., D'ÂngeloWittmanm, S.A.F., Schöngart, J., Barbosa, K.M.N., Lopes, A., 2010. Aquatic herbaceous plants of the Amazon floodplains: state of the art and research needed. Acta Limnologica Brasiliensia 22 (2), 165–178.
Pinto, L., 2003. Traçage de l'érosion Cénozoïque des Andes Centrales à l'aide dela minéralogie et de la géochmie des sédiements (Nord du Chili et Nord-Ouest de la Bolivie). University Paul Sabatier, Toulouse.
Piperno, D., 2006. Phytoliths. A Comprehensive Guide for Archaeologists and Paleoecologists. Altamira Press.
Quesada, C.A., Lloyd, J., Schwarz, M., Patiño, S., Baker, T.R., Czimczik, C., Paiva, R., 2010. Variations in chemical and physical properties of Amazon forest soils in relation to their genesis. Biogeosciences 7 (5), 1515–1541.
Quesada, C.A., Phillips, O.L., Schwarz, M., Czimczik, C.I., Baker, T.R., Patiño, S., Lloyd, J., 2012. Basin-wide variations in Amazon forest structure and function are mediated by both soils and climate. Biogeosciences. 9 (6), 2203–2246.
Rangel-Ch, J.O., 2010. Vegetación acuática -caracterización inicial. In: Rangel-Ch, J.O. (Ed.), Colombia Diversidad Biótica IX. Cienagas de Córdoba: Biodiversidad Ecología y manejo ambiental, 325-339. Corporación Autónoma Regional de los valles del Sinú y del San Jorge-CVS. Universidad Nacional de Colombia, Instituto de Ciencias Naturales, Bogota Colombia.
Räsänen, M., et al., 1998. Geología y geoformas de la zona de Iquitos. In: Kalliola, R., Flores, S. (Eds.), Geoecología y desarrollo amazónico: estudio integrado en la zona de Iquitos, Perú. Turun, Turku, 114. Annales Universitatis Turkuensis, Ser. A-II, pp. 59–137.
Riff, D., Romano, P.S.R., Oliveira, G.R., Aguilera, O.A., 2010. Neogene crocodile and turtle fauna in northern South America. In: Hoorn, C., Wesselingh, F.P. (Eds.), Amazonia: Landscape and Species Evolution, a Look into the Past. Wiley-Blackwell Publishing Ltd, pp. 259–280.
Roddaz, M., Viers, J., Brusset, S., Baby, P., Hérail, G., 2005. Sediment provenances and drainage evolution of the Neogene Amazonian foreland basin. Earth Planet. Sci. Lett. 239 (1–2), 57–78.
Roddaz, M., Viers, J., Brusset, S., Baby, P., Boucayrand, C., Hérail, G., 2006. Controls on weathering and provenance in the Amazonian foreland basin: Insights from major and trace element geochemistry of Neogene Amazonian sediments. Chem. Geol. 226 (1–2), 31–65.
Roddaz, M., Hermoza, W., Mora, A., Baby, P., Parra, M., Christophoul, F., Brusset, S., Espurt, N., 2010. Cenozoic sedimentary evolution of the Amazonian foreland basin system. In: Hoorn, C., Wesselingh, F.P. (Eds.), Amazonia: Landscape and Species Evolution, a Look into the Past. Wiley-Blackwell Publishing Ltd., pp. 61–88
Romero-Ruiz, M.H., Flantua, S.G.A., Tansey, K., Berrio, J.C., 2012. Landscape transformation in savannas of northern South America: land use/cover changes since 1987 in the llanos Orientales of Colombia. Appl. Geogr. 32 (2), 766–776.
Roubik, D.W., Moreno, P., 1991. Pollen and Spores of Barro Colorado Island. Monographs in Systematic Botany 36. Missouri Botanical Garden Press, St. Louis, 268 pp.
Sá, N.P., Carvalho, M.A., Correia, G.C., 2020. Miocene paleoenvironmental changes in the Solimões Basin, western Amazon, Brazil: A reconstruction based on palynofacies analysis. Palaeogeogr. Palaeoclimatol. Palaeoecol. 537, 109450.
Salamanca Villegas, S., van Soelen, E.E., Teunissen van Manen, M.L., Flantua, S.G., Santos, R.V., Roddaz, M., Dantas, E.L., van Loon, E., Sinninghe Damsté, J.S., Kim, J. H., Hoorn, C., 2016. Amazon forest dynamics under changing abiotic conditions in the early Miocene (Colombian Amazonia). J. Biogeogr. 43 (12), 2424–2437.
Salas-Gismondi, R., Flynn, J.J., Baby, P., Tejada-Lara, J.V., Wesselingh, F.P., Antoine, P. O., 2015. A Miocene hyperdiverse crocodylian community reveals peculiar trophic

dynamics in proto-Amazonian mega-wetlands. Proc. R. Soc. B Biol. Sci. 282 (1804), 20142490.
Sánchez Fernández, A.W., De la Cruz Wetzell, J.S., Monge Miguel, R.W., Chira Fernández, J.E., Herrera Tufino, I., Valencia Muñoz, M.M., Romero Fernández, D., Cervantes Gárate, J., Cuba Manrique, A., 1999. Geología de los cuadrángulos de Puerto Arturo, Flor de Agosto, San Antonio del Estrecho, Nuevo Perú, San Felipe, Río Algodón, Quebrada Airambo, Mazán, Francisco de Orellana, Huanta, Iquitos, Río Maniti, Yanashi, Tamshiyacu, Río Tamshiyacu, Buenjardín, Ramón Castilla, Río Yavarí-Mirín y Buenavista 4-p, 5-p, 5-q, 5-r, 6-p, 6-q, 6-r, 7-p, 7-q, 7-r, 8-p, 8-q, 8-r, 9-p, 9-q, 9-r, 10–9, 10-q y 10-r. INGEMMET. Boletín, Serie A: Carta Geológica Nacional 132 (310 p).
Santos, C., Jaramillo, C., Bayona, G., Rueda, M., Torres, V., 2008. Late Eocene marine incursion in north-western South America. Palaeogeogr. Palaeoclimatol. Palaeoecol. 264 (1–2), 140–146.
Santos, R.V., Sondag, F., Cochonneau, G., Lagane, C., Brunet, P., Hattingh, K., Chaves, J. G.S., 2014. Source area and seasonal 87Sr/86Sr variations in rivers of the Amazon basin. Hydrol. Process. 1–11. https://doi.org/10.1002/hyp.10131.
Scheyer, T.M., Aguilera, O.A., Delfino, M., Fortier, D.C., Carlini, A.A., Sánchez, R., Sánchez-Villagra, M.R., 2013. Crocodylian diversity peak and extinction in the late Cenozoic of the northern Neotropics. Nat. Commun. 4 (1), 1–9.
Sciumbata, M., Weedon, J.T., Bogota-Angel, G., Hoorn, H., 2021. Linking modern-day relicts to a Miocene mangrove community of western Amazonia. Palaeobiodiver. Palaeoenviron. 101 (1), 123–140.
Seminario, F., Guizado, J., 1976. Síntesis bioestratigráfica de la región de la Selva del Perú. In: Congreso Latinoamericano de Geología, 2, Caracas, 1973, Memoria, Ed. Sucre, Caracas, 2, pp. 881–898.
Shaffer, B.L., 1987. The potential of calcareous nannofossils for recognizing Plio–Pleistocene climatic cycles and sequence boundaries on the shelf. In: Proceedings, Gulf Coast Section SEPM 8th Annual Research Conference, pp. 142–145.
Shaffer, B.L., 1990. The nature and significance of condensed secrtions in Gulf coast Late Neogene sequence stratigraphy. In: Trans. Gulf Coast Association of Geological Societies, 40, pp. 767–776.
Sinninghe Damsté, J.S., Kenig, F., Koopmans, M.P., Köster, J., Schouten, S., Hayes, J.M., de Leeuw, J.W., 1995. Evidence for gammacerane as an indicator of water column stratification. Geochim. Cosmochim. Acta 59 (9), 1895–1900.
Sinninghe Damsté, J.S., Ossebaar, J., Abbas, B., Schouten, S., Verschuren, D., 2009. Fluxes and distribution of tetraether lipids in an equatorial African lake: Constraints on the application of the TEX_{86} palaeothermometer and BIT index in lacustrine settings. Geochim. Cosmochim. Acta 73 (14), 4232–4249.
Steinthorsdottir, M., Coxall, H.K., de Boer, A.M., Huber, M., Barbolini, N., Bradshaw, C. D., et al., 2020. The Miocene: the future of the past. Palaeogeogr. Palaeocl. e2020PA004037.
Taylor, S.R., McLennan, S.M., 1985. The Continental Crust: Its Composition and Evolution. Blackwell Scientific Publications, Oxford Boston.
Temmink, R.J., Harpenslager, S.F., Smolders, A.J., van Dijk, G., Peters, R.C., Lamers, L. P., van Kempen, M.M., 2018. Azolla along a phosphorus gradient: biphasic growth response linked to diazotroph traits and phosphorus-induced iron chlorosis. Sci. Rep. 8 (1), 1–8.
Tuomisto, H., Van Doninck, J., Ruokolainen, K., Moulatlet, G.M., Figueiredo, F.O., Sirén, A., Cárdenas, G., Lehtonen, S., Zuquim, G., 2019. Discovering floristic and geoecological gradients across Amazonia. J. Biogeogr. 46 (8), 1734–1748.
Urrego, L.E., 2018. Cananguchales y manglares: humedales forestales de las zonas bajas tropicales, tan semejantes como contrastantes. Revista de la Academia Colombiana de Ciencias Exactas, Fisicas y Naturales 42 (162), 80–95.
Van Soelen, E.E., Kim, J.H., Santos, R.V., Dantas, E.L., de Almeida, F.V., Pires, J.P., Roddaz, M., Sinninghe Damsté, J.S., 2017. A 30 Ma history of the Amazon River inferred from terrigenous sediments and organic matter on the Ceará rise. Earth Planet. Sci. Lett. 474, 40–48.
Van't Veer, R., Hooghiemstra, H., 2000. Montane forest evolution during the last 650.000 yr in Colombia: a multivariate approach based on pollen records Funza-I. J. Quat. Sci. 15, 329–346.
Velásquez, C., 1990. Atlas palinologico de la flora vascular de Colombia: Angiospermae. UNAL-Medellin- Facultad de Ciencias. Colciencias, Medellin 173p.
Velásquez, C., 1999. Atlas palinológico de la flora vascular de Colombia: Angiospermae. UNAL-Medellín Facultad de Ciencias, Colciencias, Medellín, p. 173.
Viers, J., Roddaz, M., Filizola, N., Guyot, J.-L., Sondag, F., Brunet, P., Zouiten, C., Boucayrand, C., Martin, F., Boaventura, G.R., 2008. Seasonal and provenance controls on Nd–Sr isotopic compositions of Amazon rivers suspended sediments and implications for Nd and Sr fluxes exported to the Atlantic Ocean. Earth Planet. Sci. Lett. 274 (3–4), 511–523.
Vonhof, H.B., Kaandorp, R.J.G., 2010. Climate variation in Amazonia during the Neogene and the Quaternary. In: Hoorn, C., Wesselingh, F.P. (Eds.), Amazonia: Landscape and Species Evolution, a Look into the Past. Wiley-Blackwell Publishing Ltd, pp. 201–210.
Vonhof, H.B., Wesselingh, F.P., Ganssen, G.M., 1998. Reconstruction of the Miocene western Amazonian aquatic system using molluscan isotopic signatures. Palaeogeogr. Palaeoclimatol. Palaeoecol. 141 (1–2), 85–93.
Vonhof, H.B., Wesselingh, F.P., Kaandorp, R.J.G., Davies, G.R., van Hinte, J.E., Guerrero, J., Räsänen, M., Romero-Pittman, L., Ranzi, A., 2003. Paleogeography of Miocene western Amazonia: isotopic composition of molluscan shells constrains the influence of marine incursions. Geol. Soc. Am. Bull. 115 (8), 983–993.
Wade, B.S., Pearson, P.N., Berggren, W.A., Palike, H., 2011. Review and revision of Cenozoic tropical planktonic foraminiferal biostratigraphy and calibration to the geomagnetic polarity and astronomical time scale. Earth Sci. Rev. 104, 111–142.
Watson, L., Dallwitz, M.J., 1992. Onwards. Grass Genera of the World: Descriptions, Illustrations, Identification, and Information Retrieval; Including Synonyms, Morphology, Anatomy, Physiology, Phytochemistry, Cytology, Classification, Pathogens. World and Local Distribution.
Weijers, J.W.H., Schouten, S., van den Donker, J.C., Hopmans, E.C., Sinninghe Damsté, J. S., 2007. Environmental controls on bacterial tetraether membrane lipid distribution in soils. Geochim. Cosmochim. Acta 71 (3), 703–713.
Wesselingh, F.P., 1993. On the Systematics of Miocene Aquatic Molluscs from Los Chorros (dept. Amazonas, Colombia) and Nuevo Horizonte (dept. Loreto, Peru) with Comments on Palaeoenvironment and Palaeogeography. M.Sc. Thesis. Free University, Amsterdam, 123 pp.
Wesselingh, F.P., 2006. Miocene long-lived lake Pebas as a stage of mollusc radiations, with implications for landscape evolution in western Amazonia. Scr. Geol. 133, 1–17.
Wesselingh, F.P., Gittenberger, E., 1999. The giant Amazonian snail (Pulmonata: Acavidae) beats them all. The Veliger. 42 (1), 67–71.
Wesselingh, F.P., Ramos, M.I.F., 2010. Amazonian aquatic invertebrate faunas (Mollusca, Ostracoda) and their development over the past 30 million years. In: Hoorn, C., Wesselingh, F.P. (Eds.), Amazonia: Landscape and Species Evolution, a Look into the Past. Wiley-Blackwell Publishing Ltd, pp. 302–316.
Wesselingh, F.P., Räsänen, M.E., Irion, G., Vonhof, H.B., Kaandorp, R., Renema, W., Gingras, M., 2001. Lake Pebas: a palaeoecological reconstruction of a Miocene, long-lived lake complex in western Amazonia. Cainozoic Res. 1 (1/2), 35–68.
Wesselingh, F.P., Kaandorp, R.J.G., Vonhof, H.B., Räsänen, M.E., Renema, W., Gingras, M., 2006. The nature of aquatic landscapes in the Miocene of western Amazonia: an integrated palaeontological and geochemical approach. Scr. Geol. 133, 363–393.
Westerhold, T., Marwan, N., Drury, A.J., Liebrand, D., Agnini, C., Anagnostou, E., Zachos, J.C., 2020. An astronomically dated record of Earth's climate and its predictability over the last 66 million years. Science 369 (6509), 1383–1387.
Willard, D.A., Bernhardt, C.E., Weimer, L., Cooper, S.R., Gamez, D., Jensen, J., 2004. Atlas of pollen and spores of the Florida Everglades. Palynology 28 (1), 175–227.
Zavala Carrión, B.L., Guzmán Martínez, A., Valenzuela Ortíz, G., De la Cruz Matos, O., Núñez Juárez, S., Rosas Casusol, M., Quispe Aranda, L.A., 1999. Geología de los cuadrángulos de Punchana, Remanso, San Martín de Soledad, Quebrada Esperanza, Río Yahuillo, Quebrada Lupuna, Río Yahuas, Primavera, Pebas, Río Atacuari, Río Cotuhé, Quebrada Chontadero, San Francisco, Chambira, Caballococha, San Juan de Cacao, Carolina, San Pablo de Loreto, San Pedro, Islandia, Isla Chinería y Lagogrande 5-s, 5-t, 5-u, 5-v, 6-s, 6-t, 6-u, 6-v, 7-s, 7-t, 7-u, 7-v, 8-s, 8-t, 8-u, 8-v, 9-s, 9-t, 9-u, 9-v, 9-x, 10-s–[Boletín A 133], pp. 0257–1641.
Zell, C., Kim, J.-H., Moreira-Turcq, P., Abril, G., Hopmans, E.C., Bonnet, M.-P., Sobrinho, R.L., Damste, J.S.S., 2013a. Disentangling the origins of branched tetraether lipids and crenarchaeol in the lower Amazon River: Implications for GDGT-based proxies. Limnol. Oceanogr. 58 (1), 343–353.
Zell, C., Kim, J.-H., Abril, G., Sobrinho, R.L., Dorhout, D., Moreira-Turcq, P., Sinninghe Damste, J.S., 2013b. Impact of seasonal hydrological variation on the distributions of tetraether lipids along the Amazon River in the central Amazon basin: implications for the MBT/CBT paleothermometer and the BIT index. Front. Microbiol. 4.